

STATUS OF THESIS

Title of thesis

VOLUME DETERMINATION OF LEG ULCER USING
REVERSE ENGINEERING METHOD

I, CHONG KIAN KIONG

(CAPITAL LETTERS)

hereby allow my thesis to be placed at the Information Resource Center (IRC) of Universiti Teknologi PETRONAS (UTP) with the following conditions:

1. The thesis becomes the property of UTP
2. The IRC of UTP may make copies of the thesis for academic purposes only.
3. This thesis is classified as

Confidential

Non-confidential

If this thesis is confidential, please state the reason:

The contents of the thesis will remain confidential for _____ years.

Remarks on disclosure:

Endorsed by

Signature of Author

Signature of Supervisor

Permanent address: No. 2374

Taman Gaya, Jalan Kuhara,

91000 Tawau, Sabah,

Malaysia.

Name of Supervisor

Assoc. Prof. Dr. Ahmad Majdi

Abdul Rani

Date : _____

Date : _____

UNIVERSITI TEKNOLOGI PETRONAS
VOLUME DETERMINATION OF LEG ULCER USING REVERSE
ENGINEERING METHOD

by

CHONG KIAN KIONG

The undersigned certify that they have read, and recommend to the Postgraduate Studies Programme for acceptance this thesis for the fulfilment of the requirements for the degree stated.

Signature:

Main Supervisor:

Assoc. Prof. Dr. Ahmad Majdi Abdul Rani

Signature:

Co-Supervisor:

Prof. Ir. Dr. Ahmad Fadzil Mohamad Hani

Signature:

Head of Department:

Assoc. Prof. Ir. Dr. Masri Baharom

Date:

VOLUME DETERMINATION OF LEG ULCER USING REVERSE
ENGINEERING METHOD

by

CHONG KIAN KIONG

A Thesis

Submitted to the Postgraduate Studies Programme

as a Requirement for the Degree of

MASTER OF SCIENCE

MECHANICAL ENGINEERING

UNIVERSITI TEKNOLOGI PETRONAS

BANDAR SERI ISKANDAR,

PERAK

AUGUST 2014

DECLARATION OF THESIS

Title of thesis

VOLUME DETERMINATION OF LEG ULCER USING
REVERSE ENGINEERING METHOD

I, _____ CHONG KIAN KIONG _____
(CAPITAL LETTERS)

hereby declare that the thesis is based on my original work except for quotations and citations which have been duly acknowledged. I also declare that it has not been previously or concurrently submitted for any other degree at UTP or other institutions.

Witnessed by

Signature of Author

Signature of Supervisor

Permanent address: No. 2374
Taman Gaya, Jalan Kuhara,
91000 Tawau, Sabah,
Malaysia.

Name of Supervisor
Assoc. Prof. Dr. Ahmad Majdi
Abdul Rani

Date : _____

Date : _____

To My Beloved Parents

ACKNOWLEDGEMENTS

First and foremost, I am thankful to God, for his encouragement and timely blessings to complete my work.

Special thanks to my supervisor, Associate Professor Dr. Ahmad Majdi Abdul Rani, for his excellent guidance and patience throughout the duration of my master degree. My appreciation goes out to Professor Ir. Dr. Ahmad Fadzil Mohamad Hani, co-supervisor, for his priceless advice on my project.

I would like to express my gratitude to Dr. Roshidah Baba, Dr. Asmah Johar, and Dr. Haji Yusoff Ahmad from Department of Dermatology and Outpatient Department, Hospital Kuala Lumpur, for granting me permission to collect the ulcer data in their department. The doctors in both departments were exceptionally helpful namely, Dr. Felix Yap Boon Bin and Dr. Adawiyah Jamil.

I would like to thank my colleagues from the Intelligent Imaging Lab (Hermawan, Esa, Hanung, Fitri, Leena, Dileep) for their support, discussion and contribution in the data collection. I would like also to thank Mr. Khurram Altaf for offering the training on rapid prototyping machine. In addition, my deepest gratitude also goes to Universiti Teknologi PETRONAS for providing financial assistance for my research project.

My unending thanks go to my parents and family members for their support and encouragement throughout my studies. Last but not least, I would like to thank all people involved in assisting me either directly or indirectly in my work.

Kian Kiong

ABSTRACT

Reverse Engineering is defined as the process of obtaining a geometric CAD model by digitizing the existing objects. In medical application, it is applied to obtain the CAD model of human skin surface. Chronic leg ulcer refers to the wound which does not heal in the predictable period. Approximately 1% of the world population will develop leg ulcers in their lifespan. Volume assessment is the most important criterion as the first indicator of wound healing is changes in wound volume. Some dressing and treatment might not suitable to some particular due to their unique body structure. Current ulcer assessment methods are subjective and depend on visual inspection of the ulcer appearance. The faster changes in wound parameters are observed, the faster the doctors can make clinical decisions on suitable treatments needed for wound healing. Hence, quantitative volume measurement is crucial to shorten the treatment period. In this work, 17 various wound attribute models with known volume were built for the validation process on how the wound attributes, data acquisition methods and volume computation techniques will affect the accuracy of volume measurement. Wound attribute are being classified into four categories, which were the boundary, edge, base and depth. Two types of data acquisition method (laser triangulation and structured light) were being used to acquire 3D surface scan of the models. Midpoint projection and convex hull approximation are the two methods used for the volume computation. Same methodology is then applied on 26 ulcer wound model. The study revealed that structured-light-based 3D technique produces better accuracy compared to laser triangulation data acquisition method to retrieve 3D surface information. Both techniques show the incapability to retrieve the CAD accurately for models with punched out base and 5 mm total depth due to the shadow effect. Midpoint projection is more accurate than convex hull approximation method in volume measurement. Convex hull is suitable only for the wound without elevated base and it require dense of points to produce accurate results. Although the conventional method of volume measurement is accurate, it is invasive and hence not suited for clinical practice.

ABSTRAK

Kejuruteraan Balikan ditakrifkan sebagai proses mendapatkan model CAD geometri dengan mendigitkan objek yang sedia ada. Untuk aplikasi dalam bidang perubatan, ia digunakan untuk mendapat model CAD pada permukaan kulit manusia. Ulser kaki kronik merujuk kepada luka yang tidak sembuh dalam tempoh yang diramalkan. Kira-kira 1% daripada penduduk dunia akan dijangkiti ulser kaki sepanjang jangka hayat mereka. Penilaian isipadu merupakan kriteria yang paling penting disebabkan indikator pertama ialah perubahan isipadu luka. Sesetengah pembalutan dan rawatan mungkin tidak sesuai untuk pesakit tertentu disebabkan kepada struktur badan yang unik. Kaedah penilaian ulser kini adalah subjektif dan bergantung kepada pemeriksaan visual penampilan ulser. Doktor dapat membuat keputusan klinikal mengenai rawatan yang sesuai untuk menyembuhkan luka pesakit tersebut sekiranya perubahan luka dapat dikesan dengan lebih awal. Oleh itu, pengukuran isipadu kuantitatif adalah penting untuk memendekkan tempoh rawatan. Dalam penyelidikan ini, 17 model sifat atribut yang berbeza yang telah diketahui mengenai isipadu telah dibina untuk proses pengesanan tentang sifat-sifat luka, pemerolehan kaedah mengenai data dan teknik-teknik pengiraan isipadu akan menjejaskan ketepatan pengukuran isipadu. Sifat luka telah diklasifikasi kepada empat kategori, iaitu sempadan, pinggir, dasar dan kedalaman. Dua jenis kaedah perolehan data (Triangulasi laser dan cahaya berstruktur) telah digunakan untuk memperoleh imbasan permukaan 3D model. Unjuran titik tengah dan anggaran badan cembong ialah dua algoritma yang digunakan untuk pengiraan isipadu. Metodologi yang sama kemudian dikenakan pada 26 luka model ulser. Kajian ini menunjukkan bahawa teknik 3D berasaskan cahaya berstruktur menghasilkan ketepatan yang lebih baik berbanding dengan kaedah laser triangulasi untuk mendapatkan maklumat permukaan 3D. Kedua-dua teknik menunjukkan ketidakupayaan untuk mendapatkan CAD dengan tepat untuk model bersifat penimbulan dengan ketinggian 5 mm yang disebabkan oleh kesan bayang-bayang. Unjuran titik tengah lebih tepat daripada

anggaran badan cembong algoritma dalam pengukuran isipadu. Anggaran badan cembong hanya sesuai untuk luka yang tidak bersifat berasaskan elevated dan ia memerlukan titik yang padat untuk menghasilkan keputusan yang tepat. Walaupun kaedah konvensional ukuran isipadu adalah tepat, tetapi ia adalah invasif. Oleh itu kaedah ini tidak sesuai untuk pengukuran isipadu dalam aplikasi klinikal. Anggaran badan cembong sesuai hanya untuk luka yang tidak bersifat elevated untuk asa dan ia memerlukan titik yang padat untuk menghasilkan keputusan yang tepat.

In compliance with the terms of the Copyright Act 1987 and the IP Policy of the university, the copyright of this thesis has been reassigned by the author to the legal entity of the university,

Institute of Technology PETRONAS Sdn Bhd.

Due acknowledgement shall always be made of the use of any material contained in, or derived from, this thesis.

© Chong Kian Kiong, 2014
Institute of Technology PETRONAS Sdn Bhd
All rights reserved.

TABLE OF CONTENTS

| | |
|----------------------------|-----|
| LIST OF TABLES | xiv |
| LIST OF FIGURES | xv |
| LIST OF ABBREVIATIONS..... | xix |

CHAPTER

| | |
|---|----|
| 1. INTRODUCTION | 1 |
| 1.1 Overview | 1 |
| 1.2 Problem Statement..... | 2 |
| 1.3 Research Objective and Scope | 3 |
| 1.4 Thesis Organisation | 4 |
| 2. LITERATURE REVIEW | 5 |
| 2.1 Reverse Engineering..... | 5 |
| 2.1.1 Three Phase of Reverse Engineering..... | 7 |
| 2.1.1.1 Data Acquisition | 8 |
| 2.1.1.1.1 Triangulation..... | 11 |
| 2.1.1.1.2 Structured Light | 13 |
| 2.1.1.1.3 Interferometry | 17 |
| 2.1.1.1.4 Time of Flight | 18 |
| 2.1.1.2 Data Processing | 19 |
| 2.1.1.3 CAD Regeneration | 20 |
| 2.2 Ulcer | 20 |
| 2.2.1 Venous Ulcer | 24 |
| 2.2.2 Arterial Ulcer | 25 |
| 2.2.3 Mix Ulcer..... | 26 |
| 2.2.4 Neuropathic Ulcer..... | 27 |
| 2.2.5 Differential Diagnosis..... | 28 |
| 2.3 Assessment of Leg Ulcer..... | 29 |

| | | |
|---------|---|----|
| 2.3.1 | Measurement Tools Used in Assessment of Leg Ulcer..... | 30 |
| 2.3.1.1 | Surface Area Measurement | 31 |
| 2.3.1.2 | Volume Measurement..... | 34 |
| 2.4 | Wound Assessment Using Digital Imaging Technique..... | 37 |
| 2.4.1 | Structured Light | 38 |
| 2.4.2 | Laser Triangulation..... | 39 |
| 2.4.3 | Photogrammetric..... | 40 |
| 2.5 | Surface Reconstruction and Volume Computation | 43 |
| 2.5.1 | Midpoint Projection | 44 |
| 2.5.2 | Convex Hull Approximation | 47 |
| 2.6 | Archimedes Principle in Volume Determination | 51 |
| 2.6.1 | Level Method | 52 |
| 2.6.2 | Overflow Method | 52 |
| 2.7 | Common Error in 3D Wound Measurement | 52 |
| 2.8 | Prototyping of 3D Objects..... | 53 |
| 2.9 | Coefficient of Determination..... | 56 |
| 2.10 | Summary..... | 56 |
| 3. | METHODOLOGY..... | 58 |
| 3.1 | Validation of Various Wound Attribute Models with Known Volume and Volume Measurement of Ulcer Wound Model | 58 |
| 3.1.1 | CAD Modeling of Ulcer Attribute..... | 60 |
| 3.1.2 | Prototyping of the 17 Wound Attribute Models | 64 |
| 3.1.3 | Volume Computation and Data Analyzing..... | 65 |
| 3.1.3.1 | Conventional Method | 66 |
| 3.1.3.2 | Reverse Engineering Method | 68 |
| 3.1.4 | Volume measurement of Ulcer Wound Model | 77 |
| 3.1.5 | Leg Ulcer Wound and Data Acquisition of Leg ulcer | 78 |
| 3.1.6 | Image Processing and STL Format Conversion | 79 |
| 3.1.7 | Prototyping of Ulcer Wound Model..... | 80 |
| 3.1.8 | Volume Computation and Data Analyzing..... | 80 |
| 3.2 | Summary..... | 81 |

| | | |
|-------|--|-----|
| 4. | RESULTS AND DISCUSSION | 83 |
| 4.1 | Volume Computation of Various Wound Attribute Models With Known Volume | 83 |
| 4.1.1 | Comparison of Laser Triangulation And Structured Light Data Acquisition Technique Using Midpoint Projection Method | 84 |
| 4.1.2 | Comparison of Laser Triangulation And Structured Light Data Acquisition Technique Using Convex Hull Approximation Method | 87 |
| 4.1.3 | Comparison of Midpoint Projection, Convex Hull Approximation Method And Conventional Volume Computation Mehtod | 94 |
| 4.2 | Volume Computation of Ulcer Wound Model | 100 |
| 4.3 | Summary | 104 |
| 5. | CONCLUSIONS AND RECOMMENDATIONS | 106 |
| 5.1 | Conclusion | 106 |
| 5.2 | Recommendations | 107 |

LIST OF TABLES

| | |
|--|-----|
| Table 2.1: Differential diagnosis of three major types of leg ulcers | 29 |
| Table 3.1: Common wound attributes, descriptor and their schematic diagram | 61 |
| Table 3.2: Seventeen models based with different wound attributes..... | 63 |
| Table 3.3: Volume measurement process using mould material | 67 |
| Table 3.4: Steps of data processing..... | 74 |
| Table 3.5: Surface reconstruction prior to volume computation | 76 |
| Table 4.1: Volume computation using midpoint projection | 85 |
| Table 4.2: Example of 20 surface division for 5 models | 89 |
| Table 4.3: Volume computation using convex hull approximation..... | 90 |
| Table 4.4: Volume measurement using midpoint projection method..... | 95 |
| Table 4.5: Volume measurement using convex hull approximation method | 96 |
| Table 4.6: Volume computation using midpoint projection. | 101 |

LIST OF FIGURES

| | |
|--|----|
| Figure 2.1: (a) & (b) Sequence of manufacture engineering products | 6 |
| Figure 2.2: Three phase of reverse engineering | 8 |
| Figure 2.3: Classifications of reverse engineering | 9 |
| Figure 2.4: Triangulation methods: (a) single and (b) double camera arrangement ... | 11 |
| Figure 2.5: Optical triangulation | 12 |
| Figure 2.6: Various light patterns in structured light technique | 13 |
| Figure 2.7: Working principle of fringe (stripe) projection | 13 |
| Figure 2.8: Work flow in fringe projection profilometry | 15 |
| Figure 2.9: Optical setup for structured light technique | 16 |
| Figure 2.10: Michelson arrangement | 18 |
| Figure 2.11: Working principle of time of flight | 19 |
| Figure 2.12: Four common types of ulcer..... | 21 |
| Figure 2.13: Management strategy for treatment of chronic wounds | 23 |
| Figure 2.14: Venous insufficiency | 25 |
| Figure 2.15: Squamous cell carcinoma in chronic venous ulcer | 25 |
| Figure 2.16: Chronic arterial insufficiency with punched out edge and irregular outlines | 26 |
| Figure 2.17: Chronic combined arterial and venous ulcers | 27 |
| Figure 2.18: Diabetic, neuropathic ulcer on the sole | 28 |
| Figure 2.19: Strip of paper ruler to measure length and width of the wound | 31 |
| Figure 2.20: Area measurement based on maximal length and longest width | 32 |
| Figure 2.21: Acetate sheet | 33 |
| Figure 2.22: Technique for tracing the ulcer margin | 33 |
| Figure 2.23: Visitrak digital planimetry..... | 34 |
| Figure 2.24: Technique for tracing the ulcer margin | 35 |
| Figure 2.25: Kundin guage | 35 |
| Figure 2.26: Technique for injecting saline | 36 |
| Figure 2.27: Trolley mounted MAVIS equipment | 38 |
| Figure 2.28: Wound covered with thin layer of healthy skin surface (green colour) for volume measurement | 39 |

| | |
|--|----|
| Figure 2.29: Tissue segmentation for area percentage measurement (necrotic, slough and granulation) | 40 |
| Figure 2.30: Stereo-photogrammetry operating principle | 41 |
| Figure 2.31: Camera configuration | 41 |
| Figure 2.32: Camera photogrammetry system (MEDPHOS hardware) | 42 |
| Figure 2.33: ESCALE wound assessment tool | 43 |
| Figure 2.34: Midpoint generation by the points from the edges..... | 44 |
| Figure 2.35: Tetrahedral form by connecting the triangular faces to the generated midpoint..... | 45 |
| Figure 2.36: Midpoint generation by the points from the edges..... | 45 |
| Figure 2.37: Process flow chart of surface reconstruction and volume computation using midpoint projection | 46 |
| Figure 2.38: L shape border with midpoint lies outside the border | 47 |
| Figure 2.39: Working principle of Delaunay | 48 |
| Figure 2.40: 3D model enclosed with smallest convex shape | 49 |
| Figure 2.41: Example of convex hull approximation with surface division | 49 |
| Figure 2.42: Process flow chart of surface reconstruction and volume computation using convex hull approximation | 50 |
| Figure 2.43: Schematic diagram of level and overflow methods of measuring volume | 51 |
| Figure 2.44: Schematic diagram of MultiJet Modeling process | 54 |
| Figure 2.45: Fine mesh characteristic (a) and mesh characteristic which cause failure in generating accurate prototype objects (b-e) | 55 |
| Figure 3.1: Ulcer Wound Attribute and Real Ulcer Wound Determination | 59 |
| Figure 3.2: Schematic diagram of ulcer attributes | 60 |
| Figure 3.3: Model with regular boundary, sloped edge, 3 mm depth and 2 mm elevated base | 62 |
| Figure 3.4: Arrangement of 3D model in solid object printer. | 64 |
| Figure 3.5: Prototype produced by solid object printer | 65 |
| Figure 3.6: Securing the exact level of the balance | 66 |
| Figure 3.7: The reading of empty model | 67 |
| Figure 3.8: Model filled with mould material..... | 67 |
| Figure 3.9: The reading of model which filled with mould material..... | 67 |

| | |
|---|-----|
| Figure 3.10: The mould material placed into the measuring cylinder which filled with 2ml distilled water | 68 |
| Figure 3.11: Working principle of noncontact 3D laser scanner | 69 |
| Figure 3.12: Illuminance meter..... | 69 |
| Figure 3.13: Setup for noncontact 3D laser scanner | 70 |
| Figure 3.14: Setup of optical scanner | 71 |
| Figure 3.15: Schematic of optical scanner | 71 |
| Figure 3.16: Working principle of optical scanner | 72 |
| Figure 3.17: Fringe pattern on targeted object..... | 72 |
| Figure 3.18: The correct position for the object being focused | 73 |
| Figure 3.19: Operating system and image focusing to perform surface scan | 73 |
| Figure 3.20: Points cloud | 74 |
| Figure 3.21: Triangulation mesh..... | 74 |
| Figure 3.22: Boundary selection | 74 |
| Figure 3.23: Zigzag boundary shape..... | 75 |
| Figure 3.24: Fit boundary to curves | 75 |
| Figure 3.25: Prototype model RSD3D1 | 76 |
| Figure 3.26: Surface reconstruction using midpoint projection..... | 76 |
| Figure 3.27: Surface reconstruction using convex hull approximation | 76 |
| Figure 3.28: Real Wound Case Study Flow..... | 77 |
| Figure 3.29: Equipment set-up in HKL | 79 |
| Figure 3.30: Extrusion operation to form a leg ulcer solid model | 80 |
| Figure 4.1: Absolute error of volume computed using midpoint projection method .. | 86 |
| Figure 4.2: Visual inspection on RPO5H model | 87 |
| Figure 4.3: Absolute error of volume computed using convex hull method | 91 |
| Figure 4.4: Multiple view of the estimated RSD3E2 solid cavity | 92 |
| Figure 4.5: Reconstructed RSD3E2 solid cavity using convex hull approximation ... | 93 |
| Figure 4.6: Model IRSD1H with surface division prior to convex hull | 94 |
| Figure 4.7: Optical scanner with midpoint projection and convex hull approximation method..... | 97 |
| Figure 4.8: Laser scanner with midpoint projection and convex hull approximation method | 98 |
| Figure 4.9: Gaps introduced from surface division | 100 |

Figure 4.10: Absolute error for models using midpoint projection 102
Figure 4.11: Multiple view of ulcer wound model 26 103
Figure 4.12: Deviation of the 3D surface scanned of wound model 104

LIST OF ABBREVIATIONS

| | |
|----------------|--|
| 3D | Three Dimensional |
| CAD | Computer Aided Design |
| CCD | Charge-Coupled Device |
| CMM | Coordinate Measuring Machine |
| CNC | Computer Numerical Control |
| CT | Computed Tomography |
| CVI | Chronic Venous Insufficient |
| DSM | Digital Surface Model |
| DVT | Deep Vein Thrombosis |
| HSV | Herpes Simplex Virus |
| LUMT | Leg Ulcer Measurement Tools |
| MAVIS | Measurement of Area and Volume Instrument System |
| MEDPHOS | MEDical PHOtogrammetric System |
| MRI | Magnetic Resonance Imaging |
| MJM | Multi Jet Modelling |
| R ² | Coefficient of Determination |
| RE | Reverse Engineering |
| SCC | Squamous Cell Carcinoma |
| STL | Standard Triangulation Language |

CHAPTER 1

INTRODUCTION

1.1 Overview

Reverse engineering (RE) is defined as the process of reproducing an existing object or part, sub assemble or product, which does not have the drawing and documentation or computer model [1]. It is a process of “reversing” forward engineering and is also known as the bottom up approach. It creates 3D virtual models from existing physical parts. The RE process can be divided into three stages, which are data acquisition, data processing, and prototype generation. Data acquisition involves the equipment and the method used to obtain the 3D data of an object. Second step of RE is to process the obtained scanned data into a fine 3D model without defect and noise. Building the prototype is the last step of RE process which normally used for testing.

RE is widely applied in various industries such as automotive, manufacturing and industrial design, and now making inroads into medical field. Basic RE tools that are used in the medical field are Computed Tomography (CT), Magnetic Resonance Imaging (MRI) and also 3D scanner to enable a more efficient process of diagnosis. CT and MRI are used to visualize internal structure of human whereas 3D scanner is used to obtain 3D geometrical shape of human skin surface in digital form which could be stored in any computer system. It is useful to monitor the treatment given by dermatologist in more accurate and quantitative way. The data accuracy is dependent on the type of data acquisition technique such as laser triangulation method or structured light method. Time taken to complete the scanning of patient is also an important factor to ensure accuracy of the data. Due to human nature, it is impossible for a human to stay still for a long period. Pain, discomfort, and even breathing can cause slight movement which affect the reliable and accuracy of the scanned data.

Ulcer is a skin disease that refers to the discontinuity of skin exhibiting complete loss of the epidermis which is not short lived. The duration of the ulcer could last from a few weeks to even few years. Patients suffering from such chronic skin have faced a huge loss in quality of life. The patient not only has to endure pain but also time consuming outpatient treatment and cost. Leg ulcer is very common and based on the statistics, 3.5% of all adults in the USA suffer from venous leg ulcers [2]. Chronic ulcerative skin lesions interest around 1.5% of the European population and represent an important medical and social problem [3]. There is no analytical statistic for the leg ulcer population in Malaysia for the past few years.

1.2 Problem Statement

Currently, dermatologists do not have any quantitative tool to assess the severity and the healing rate for the leg ulcer [4]. The clinical evaluation of the leg ulcers depend heavily on the skills of the dermatologist with the help of predetermined assessment criteria such as the Leg Ulcer Measurement Tools [5], which are mainly qualitative. The examination process is very time consuming. With the huge number of patients suffering from this disease, a quantitative method needs to be researched and developed. The main issues are reliability, repeatability and accuracy of the current ulcer assessment and reduction in time spent on ulcer examination. Normally, the dermatologists will evaluate leg ulcers based on four main criteria, which are volume, area, percentage of the granulation tissue and percentage of the necrotic tissue of the wound. The first indicator of a healing wound is the growth of granulation tissue which reflects changes in ulcer cavity volume followed by a gradual decrease in perimeter and area [6].

Every evaluation has therapeutic consequences which differ depending on the treating dermatologist [7]. It is generally accepted that good clinical assessment normally leads to good treatment. There exists more than 200 possible dressing material and treatment in market. The visual observation method might not result in the best treatment for the patient due to the subjective nature of the assessment. Different levels of ulcer severity require different dressing and treatment remedies which will

best promote the healing process of the ulcer. In contrast, unsuitable dressing and remedies may not worsen the condition. Hence, efficacy on the leg ulcer assessment is very important in determining the treatment approach and the healing process in order to shorten the treatment period.

1.3 Research Objectives and Scopes

This research is a collaboration research between Universiti Teknologi PETRONAS (UTP), Department of Dermatology Hospital Kuala Lumpur (HKL) and Outpatient Department Hospital Kuala Lumpur (HKL). These centres were chosen as Hospital Kuala Lumpur is a referral centre for Kuala Lumpur and Selangor, and is also the tertiary referral centre for dermatology in Malaysia. Hospital Kuala Lumpur is well-resourced with trained personnel and investigative tools essential in the fields of Dermatology, Laboratory and Radiology. The Clinical Study Proposal (NMRR-11-39-7990) was approved by the Clinical Research Centre, Ministry of Health Malaysia.

From the literature, research initiatives were carried out in attempt to provide dermatologists with a more objective and quantitative assessment that would contribute in monitoring and improving the treatment efficacy. This research is conducted to determine the accuracy of conventional contact measurement method in contrast with the non-contact methods.

Objectives

1. To establish the accuracy of contact and non-contact measurement methods, which are Archimedes method, laser triangulation (laser scanner), structured light (optical scanner) data acquisition techniques in capturing 3D information of ulcer wounds.
2. To assess the suitability of the methods for surface reconstruction and volume computation of ulcer cavity.

Scopes

1. Modeling of ulcer wound using was based on 4 wound attributes, which are boundary, edge, base and depth. Undermined type ulcer was not considered.
2. Producing prototypes were based on the 4 wound attributes and ulcer wound.
3. 3D geometrical data acquisitions using were limited to laser triangulation and structured light techniques. Rapidform software was used for the data processing.
4. Volume computation techniques were limited to midpoint projection and convex hull approximation methods.

1.4 Thesis Organisation

Chapter 1 presents an overview of work completed in this project. It includes the objectives and research scope of which is focused on the accuracy of laser triangulation and structured light technique in generating 3D images of ulcer wounds.

Chapter 2 covers the literature review and is focused on the different types of leg ulcers and diagnostic methods. This section also highlights the principle of the active scanning method, which are commonly used in the industry. This chapter also specifies how reverse engineering can contribute towards the volume assessment of the ulcer wound.

Chapter 3 reports the methodology for this research. It contains of two stages, which are the validation process where volume measurement are performed on various wound attribute models with known volume. The second section is covering the volume measurement of ulcer wound model.

Chapter 4 presents the critical analysis of the performance of data acquisition techniques and volume computation method. It also shows the details of the results from the two different models.

Chapter 5 concludes the work in this project and introduces future work that can be carried out.

CHAPTER 2

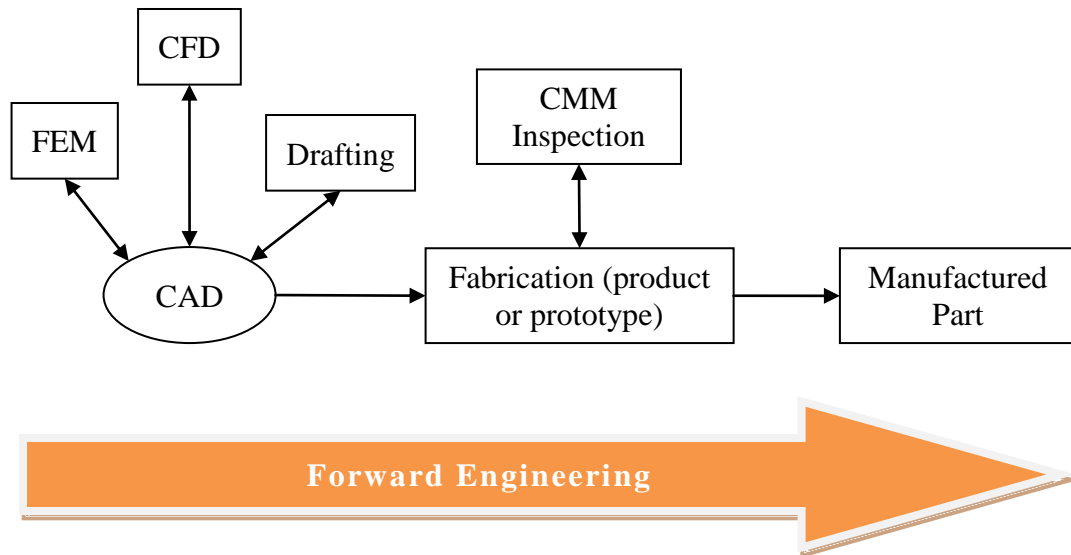
LITERATURE REVIEW

This chapter covers two different aspects. The first part discusses on the definition of ulcer wound and the assessment of ulcer. 3D imaging techniques were used to assist in ulcer assessment in a more objective way. The second part demonstrates how the reverse engineering, surface reconstruction and rapid prototyping can assist in determining the accuracy of the proposed data acquisition technique and surface reconstruction method.

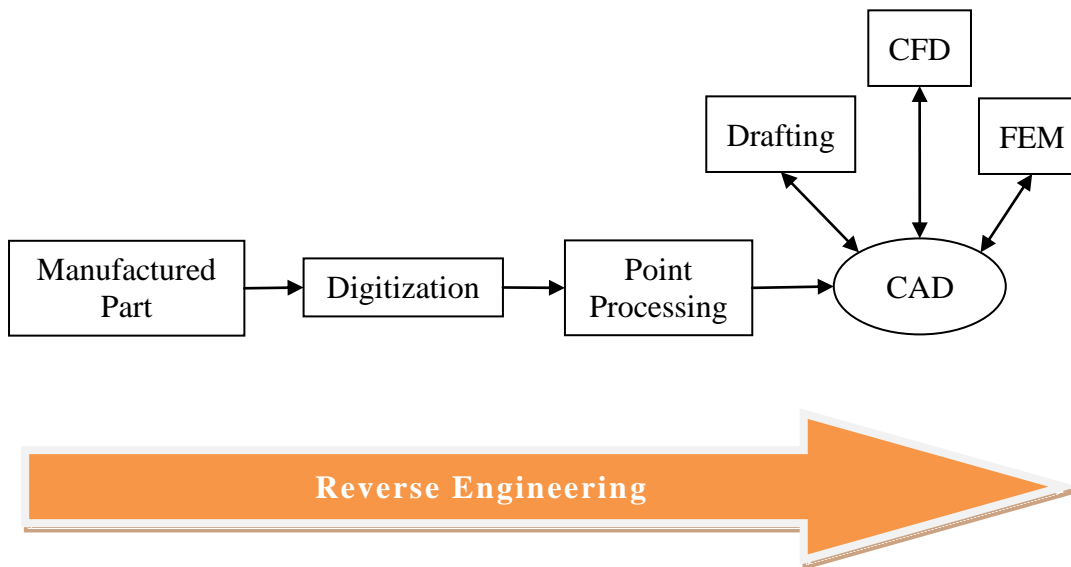
2.1 Reverse Engineering

Engineering is defined as the process of designing, manufacturing, assembling and maintaining the parts, products and systems [1]. There are two types of engineering, which are forward engineering and reverse engineering. Forward engineering is the conventional engineering that creates CAD models based on the engineering concept and functional specification. The process is continued with transforming the CAD models into real parts. In some situation, there might be the objects or parts that do not have any documentation, technical details or engineering drawing. In this scenario, reverse engineering is the only solution for the situation. Reverse engineering (RE) is defined as the process of creating a geometric CAD model from 3D points cloud that generated by scanning or digitizing an existing physical part or object [8-13]. Fig. 2.1 (a) and (b) shows that RE is widely used in numerous applications, such as automotive, industrial, cultural heritage reconstruction, manufacturing, industrial design, jewellery design, entertainment industry or even in the medical field. For example, RE is applied in the process of protecting cultural heritage sites.

Cultural heritage sites are invaluable and might be damaged due to the friction of wind over certain time period. Reverse engineering can be applied with the aim of capturing the geometry CAD of cultural heritage and provides a reference for similar subject. Besides that, it helps to interpret and fitting fragments of broken artefacts together.



(a) Forward Engineering



(b) Reverse Engineering

Figure 2.1: (a) & (b) Sequence of manufacture engineering products [13]

Other applications of reverse engineering are listed below:

- The manufacturer has stopped the production due the original product becoming obsolete and the accessories and spare parts are still needed for the daily usage.
- The manufacturer does not exist anymore, but the product's spare parts are still needed for some minor repairing of the product. For example, automobile spare parts are needed in the event of a breakdown.
- Creating the manufactured part when there are no CAD data or the data was lost.
- Architectural and construction measurement and documentation.
- Creating 3D models and sculptures for animation (games or movies).
- Inspection and comparing the quality of the fabricated parts to its CAD description.
- Eliminate bad features of a product.
- Strengthen the good features of a product.
- Examining the features of competitors' products (good and bad features).
- Generating the geometrical 3D CAD of humans, models or sculptures, scale and reproduce artwork.
- Generating 3D data to create dental and surgical prosthetics, surgical planning or tissue engineered body parts.

2.1.1 Three Phases of Reverse Engineering

Reverse engineering process can be divided into three phases, which are scanning, point processing and application of the generated CAD model. The generic process of reverse engineering is depicted in Fig. 2.2.

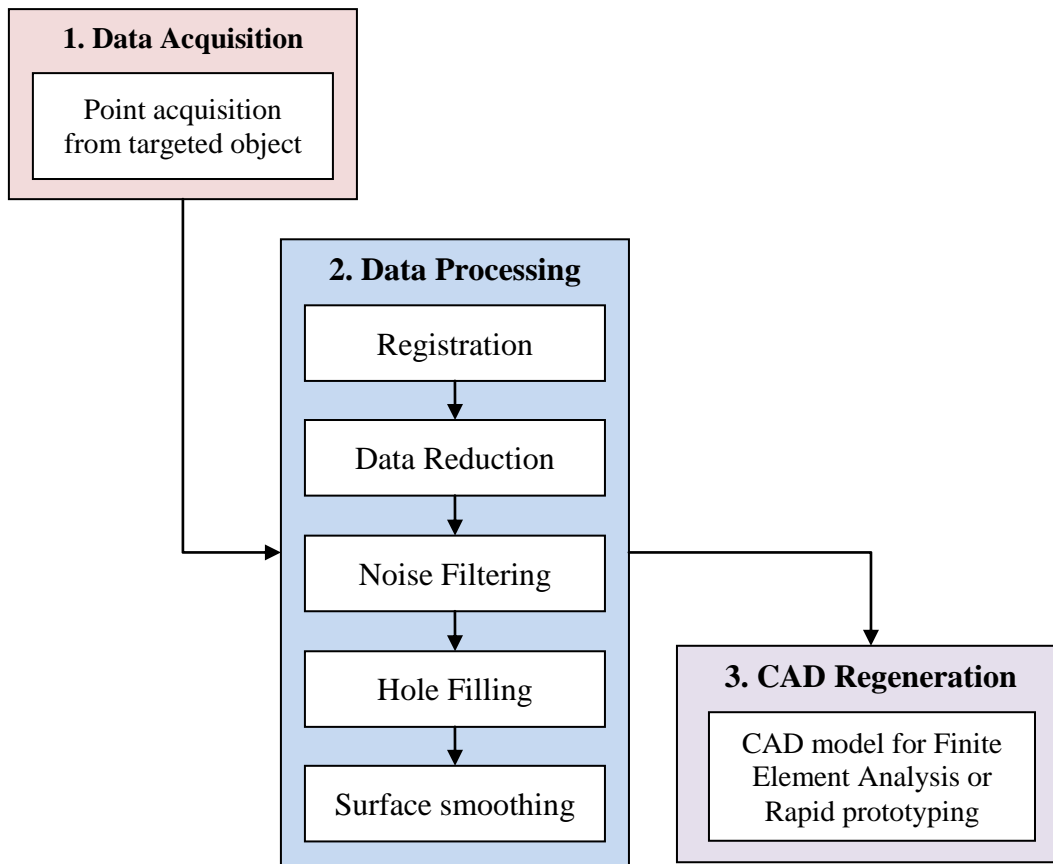


Figure 2.2: Three phase of reverse engineering [1]

2.1.1.1 Data Acquisition

Data acquisition is the most crucial part in the reverse engineering [9]. Three dimensional scanners such as coordinate measuring machine (CMM), laser-based range finders and optic-based scanners are used to scan the features of the object geometry in three dimensions [14]. The outcome of the data acquisition will be in the form of point clouds, which defines the surface geometry of the object. Suitable data acquisition techniques must be selected earlier in order to get the accuracy that the user demands. There are two different types of scanners, the contact and noncontact scanner. The classification of reverse engineering systems is shown in Fig. 2.3.

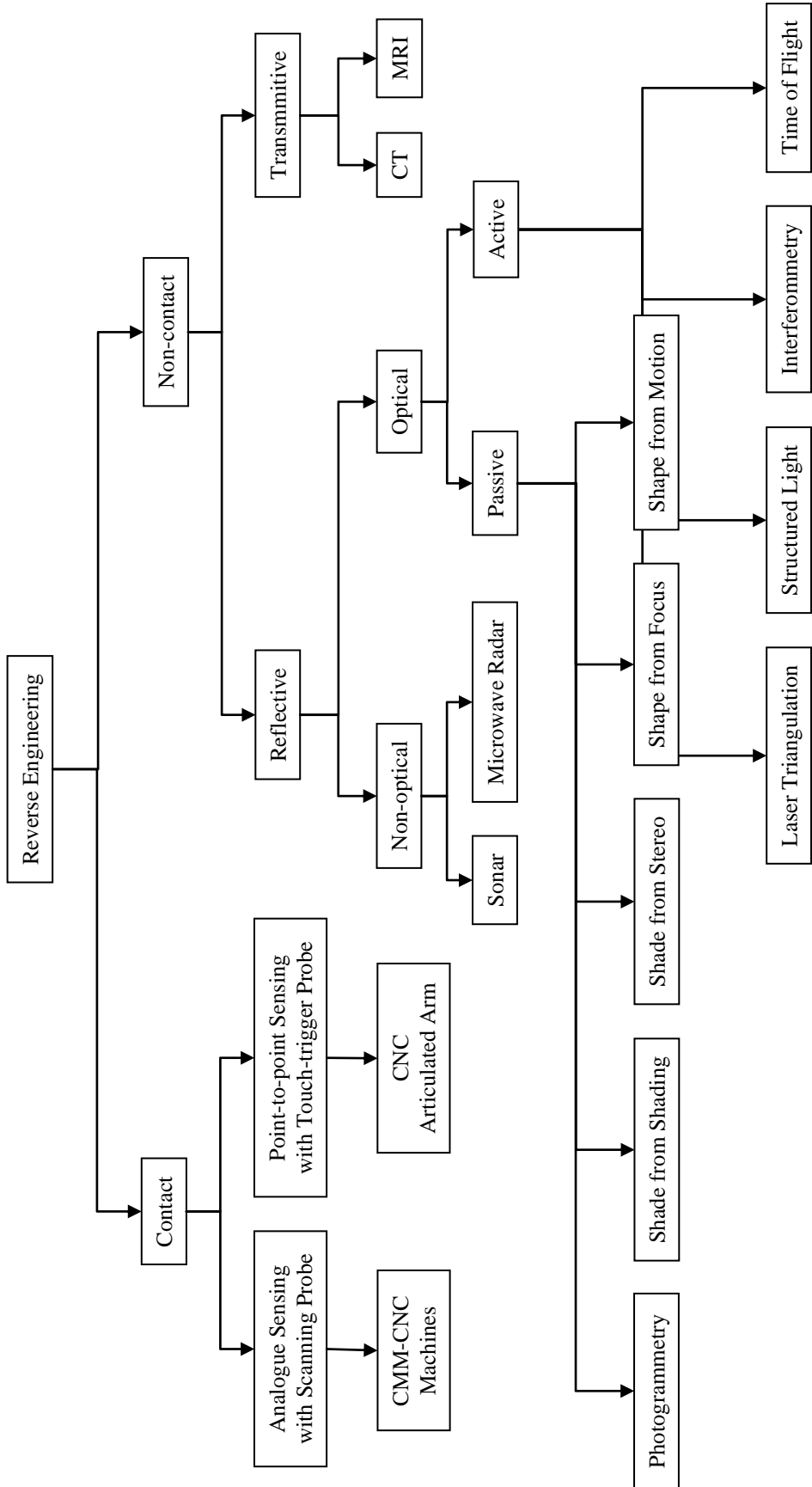


Figure 2.3: Classifications of reverse engineering [1]

Contact methods are used to digitize an object surface with a touching probe. It uses the sensing device with mechanical arms, CMM, and computer numerical control (CNC) machines. In general, there are two types of the contact methods for digitizing surfaces: i) Analogue sensing with scanning probes, ii) Point-to-point sensing with touch-trigger probes.

CMM is the most common 3D contact scanner. It employs a contact probe that move according to the contour of a physical surface. Each point is generated in a consecutive manner at the tip of the probe and it is a very slow process of scanning. The contact pressure is maintained at the same degree throughout the scanning process. However, this might cause inaccurate scanning on soft and tactile material such as rubber.

Various noncontact scanners are available in the market that captures the data without any physical contact to the object. Basically, noncontact data acquisition method can be divided into two categories, which are active and passive noncontact acquisition methods.

In active noncontact method, the object's geometry is obtained by projecting energy onto the object surface. Either the transmitted or reflected energy is observed to determine the position of an object. These devices normally use laser, light, optical and charge-coupled device (CCD) sensors to capture data. Although these devices can capture numerous points within a short space of time, there are few issues related to the scanning technology. The issues are (a) contact system having problems in generating surface data which are parallel to the laser axis (b) reflection of the light might not be accurate on shining surfaces, hence, temporary coating of fine powder is needed before scanning. Triangulation, structured light, interferometry, moiré effect and time of flight are the basic components classified under the active noncontact data acquisition method.

2.1.1.1.1 Triangulation

Triangulation is commonly used in laser scanners to establish the surface location or coordinate of an object. Light was emitted from the light source towards the object and lastly reflected to the photosensitive devices to calculate coordinates of the object surface. The arrangement of the light source, object and the photosensitive devices form the triangulation shape to obtain the geometrical shape and coordinates of the object [15-17] .

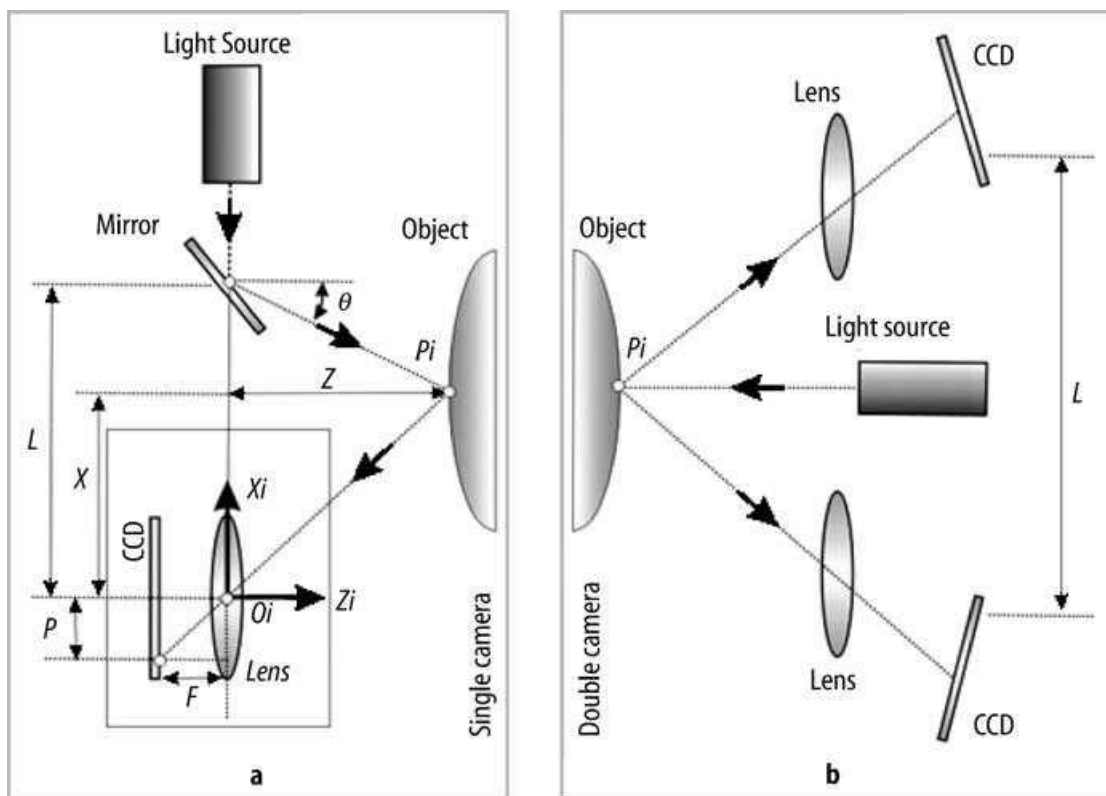


Figure 2.4: Triangulation methods: (a) single and (b) double camera arrangement [1]

Two types of the triangulation system using single and double camera arrangement are shown in Fig. 2.4. In single camera system, the light source emitting slight spot, stripe or line toward the object with a fix angle. The photosensitive devices are used to detect the reflected points to determine the location of the object. Two photosensitive devices are used in the double camera system. Light projector/source is not involved in the measuring task but creates the light, moving light spot and stripe pattern.

Fig. 2.5 shows the basic principles of optical triangulation. This system involves three principle axes labeled as X, Y, and Z. Focal length of the camera, image coordinates of the illuminated point and baseline are represented with f , p and b .

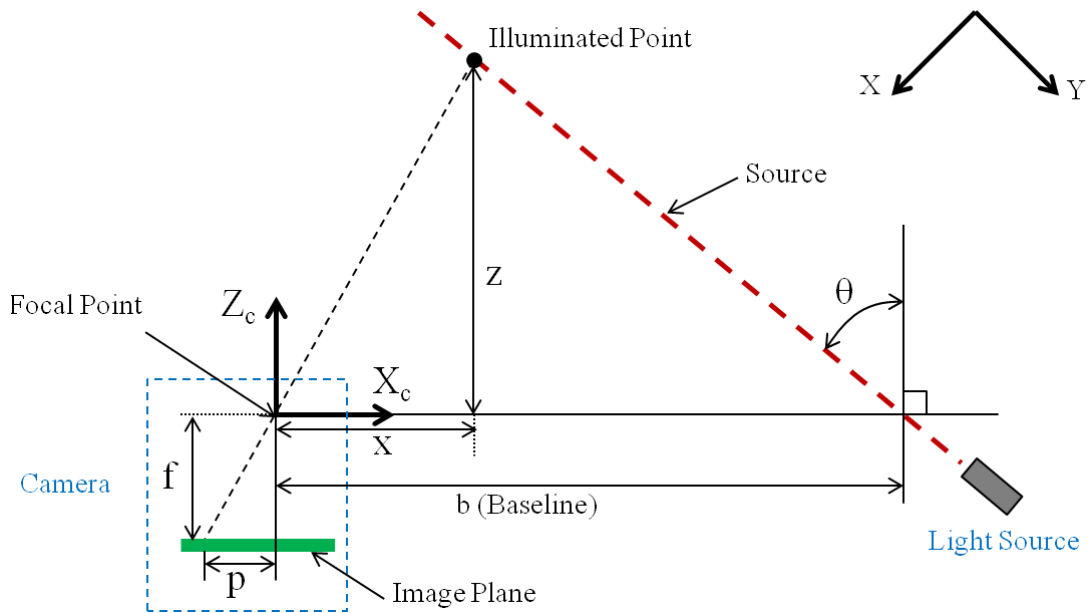


Figure 2.5: Optical triangulation [18]

By using similar triangles theory, the value of z can be obtained with the following equation.

$$\frac{z}{f} = \frac{b}{p + f \tan \theta} \quad (2.1)$$

$$z = \frac{bf}{p + f \tan \theta} \quad (2.2)$$

The value of x can be measured using the trigonometric function.

$$x = b - z \tan \theta \quad (2.3)$$

2.1.1.1.2 Structured Light

Structured light is another technique under the active optical approach to obtain the information of the object. A light pattern is projected at the pre-specified angle onto the object surface and the reflected image is captured by a camera. Light patterns vary in many forms, such as strip, grid or more complex coded light which are shown in Fig. 2.6.

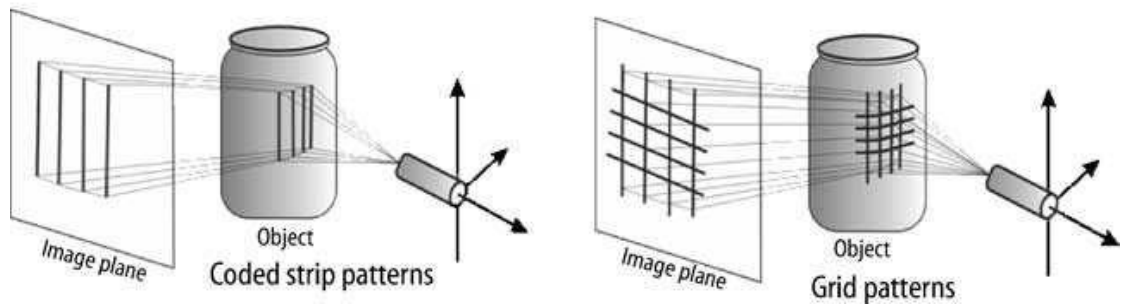


Figure 2.6: Various light patterns in structured light technique [1]

Fig. 2.7 shows how the fringe projection is generated. The light projecting onto the object surface and the illumination that appears is being captured by the camera to extract and reconstruct the three dimensional geometry shape of the object.

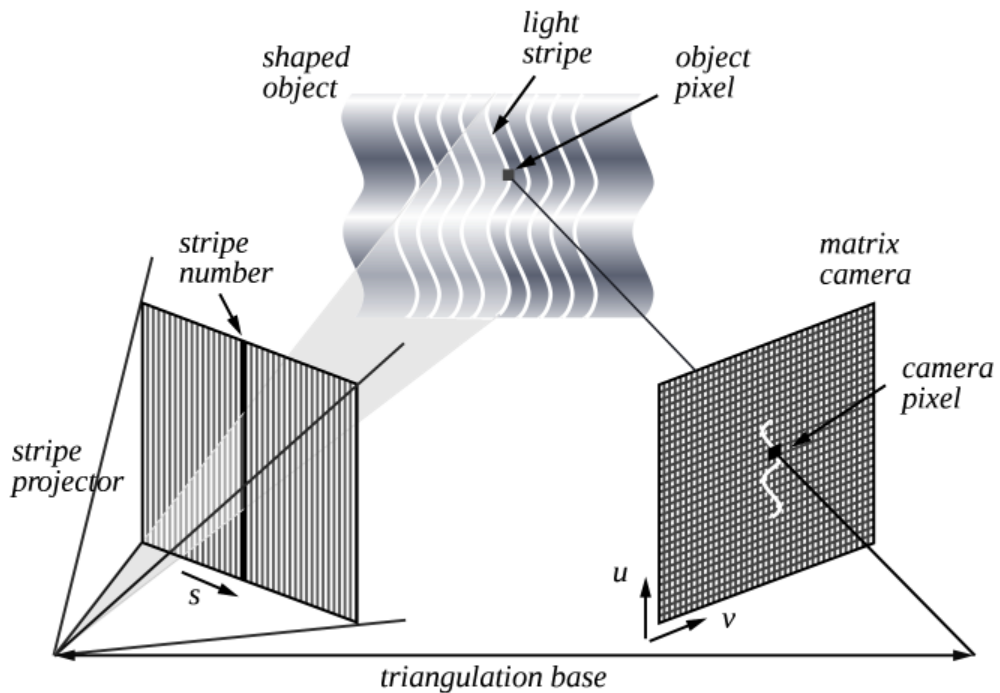


Figure 2.7: Working principle of fringe (stripe) projection [19]

Fringe projection technique is one of the promising research areas to generate 3D surface information [20]. The object measurement using fringe projection techniques involves 4 stages [21] ; (a) The fringe pattern is generated using projection onto an object and phase shifting is viewed by the camera from a fixed position (b) the underlying phase distribution of the acquired fringe image is calculated using some fringe analysis techniques, such as Fourier transform, wavelet transform or phase-shifting method (c) most of the fringe analysis techniques generate wrapped phase distribution and phase unwrapping (to obtain the continuous phase distribution for the wrapped phase map) (d) lastly, the system is calibrated for mapping the unwrapped phase distribution to real world 3-D coordinates. A more details pictorial representation of the measuring process is shown in Fig. 2.8.

The measurement of an object starts with the projection of fringe pattern and ends with the mapping process. Some equations are involved to provide information such as phase map and height [22-23]. The intensity distribution of the projected pattern on reference plane can be written as

$$I_R = a(\eta) + b(\eta)\cos(2\pi \cdot n + \Phi_R(\eta)) \quad (2.4)$$

From the equation, $a(\eta)$ represents the background intensity, $b(\eta)$ is the fringe contrast, $\Phi_R(\eta)$ is the phase map range from 0 to 2π whereas n is an integer. Meanwhile, the intensity distribution on the structured surface is expressed as

$$I(\eta) = r(\eta) \cdot [a(\eta) + b(\eta)\cos(2\pi \cdot n + \Phi(\eta))] \quad (2.5)$$

The symbol of object reflectivity and changed phase map are $r(\eta)$ and $\Phi(\eta)$, respectively. For the calculation of phase map, the equations above are used. The projected pattern is shifted M times with a phase increment of $2\pi/M$ throughout the measurement process. Intensity of each pattern is recorded and the phase map of the measured surface is expressed in the equation below.

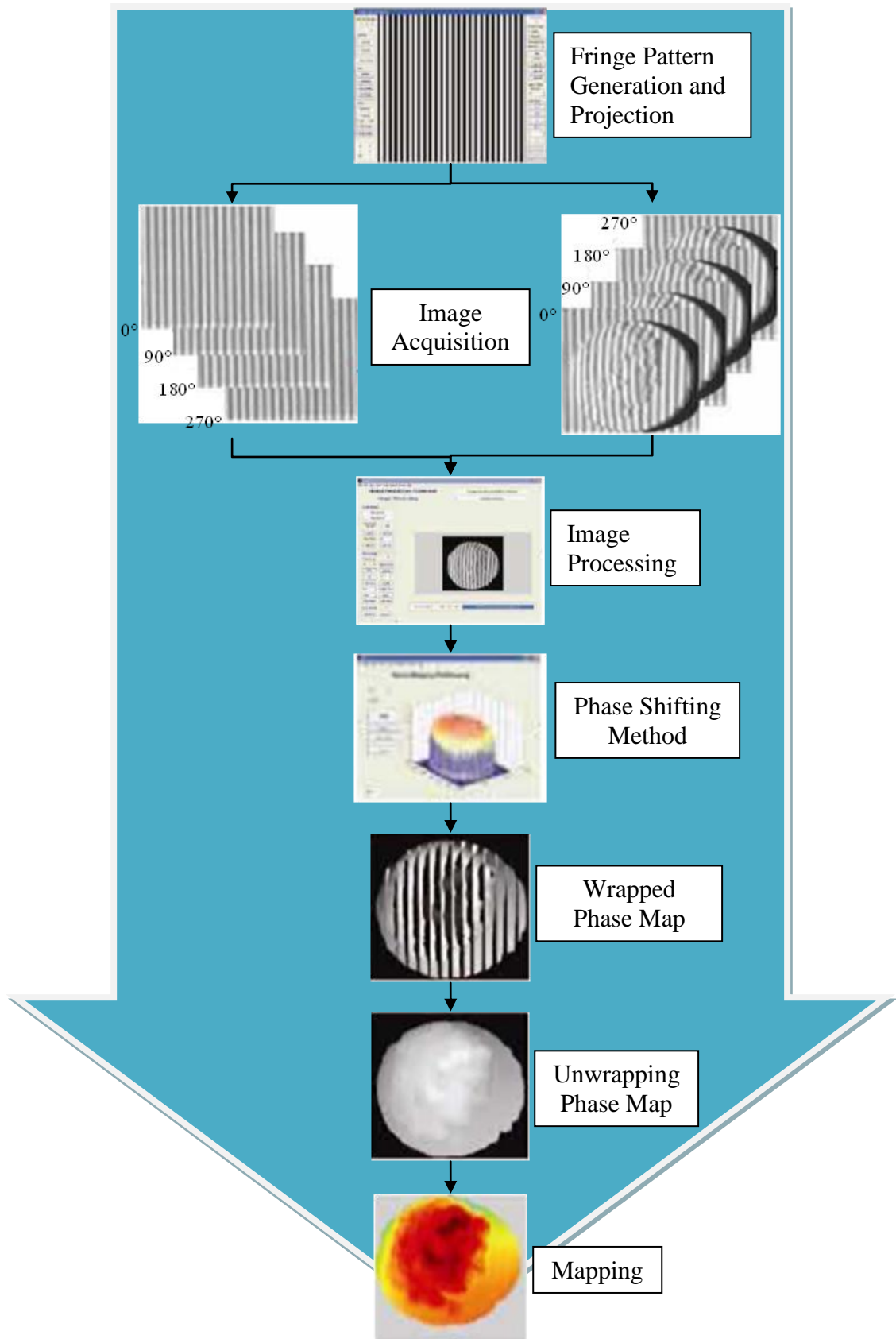


Figure 2.8: Work flow in fringe projection profilometry [21]

$$\tan \left[\Phi(\eta) \right] = \frac{\sum_{k=1}^M I_k \cdot \sin\left(\frac{2\pi k}{M}\right)}{\sum_{k=1}^M I_k \cdot \cos\left(\frac{2\pi k}{M}\right)} \quad (2.6)$$

The same method is used in the calibration process and the phase map of the reference plane is obtained. The phase changes due to the topography of the surface can be obtained by

$$\Delta\Phi(\eta) = \Phi_R(\eta) - \Phi(\eta) \quad (2.7)$$

The optical setup of phase shift profilometry is shown in Fig. 2.9. The position of camera and projector are on the same plane [24-26].

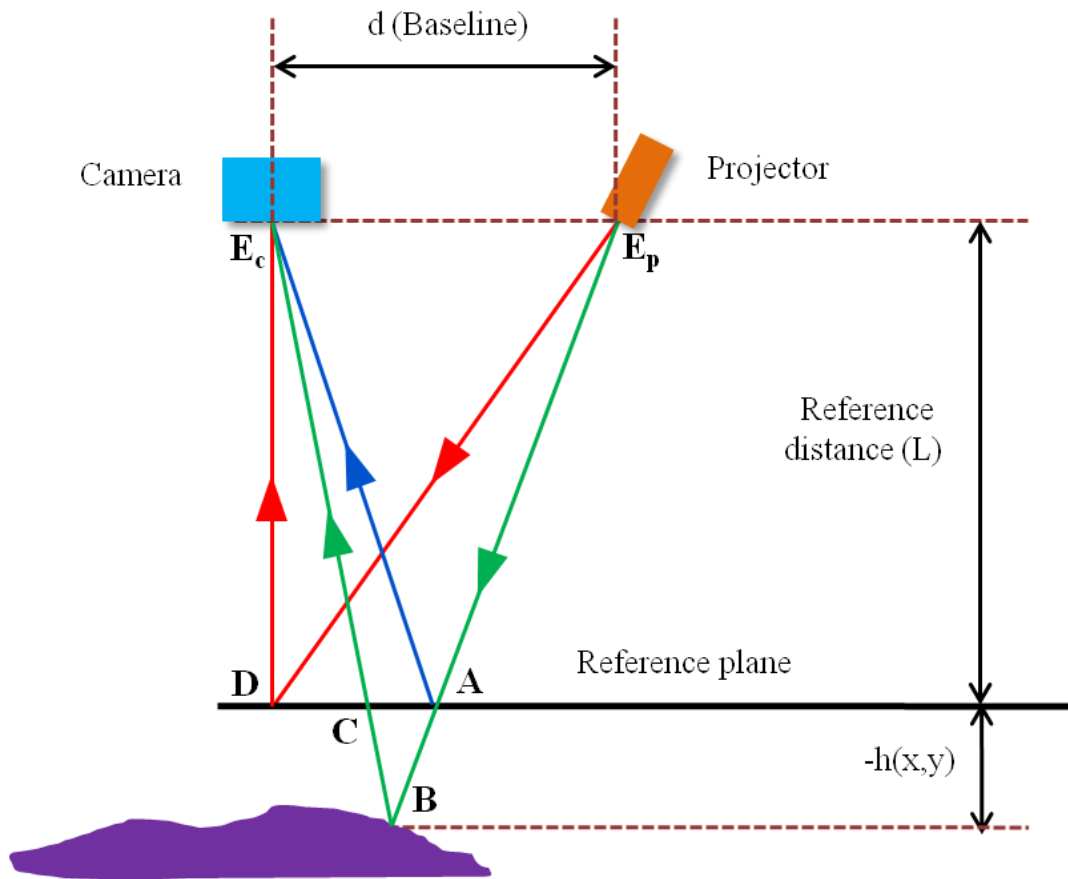


Figure 2.9: Optical setup for structured light technique [22]

The changes in phase map can also be expressed as

$$\Delta\Phi(\eta) = \Phi_r(\eta) - \Phi(\eta) = 2\pi f_0 \overline{AC} \quad (2.8)$$

By using the similar triangles principle (E_pBE_c and ABC), an equation in terms of height is obtained

$$\frac{-h(x, y) + L}{-h(x, y)} = \frac{d}{AC} \quad (2.9)$$

By substitute equation... to equation....., $h(x, y)$ can expressed as a function of $\Delta\Phi(\eta)$

$$h(x, y) = \frac{L\Delta\Phi(\eta)}{\Delta\Phi(\eta) - 2\pi f_0 d} \quad (2.10)$$

Structured light technique has its own advantages compared to the laser system, leading it to be used for digitizing images of human beings. The advantages are (i) fast data acquisition time, which can obtain up to a few million points per second; (ii) colour texture information of the object is obtainable; and (iii) structured-light systems do not use laser.

2.1.1.1.3 Interferometry

Interferometry is produced from mutually coherent waves for interference based on the amplitude division method [27]. It is commonly used for length measurement. The most frequently used interference arrangement is based on the Michelson principle which is depicted in Fig. 2.10. Beam splitter is used to separate the reference and object wave and eventually recombine them after being reflected from mirror 1 and 2. Fringe analysis such as phase shifting technique is used for direct measurement of phase difference in the interferometry.

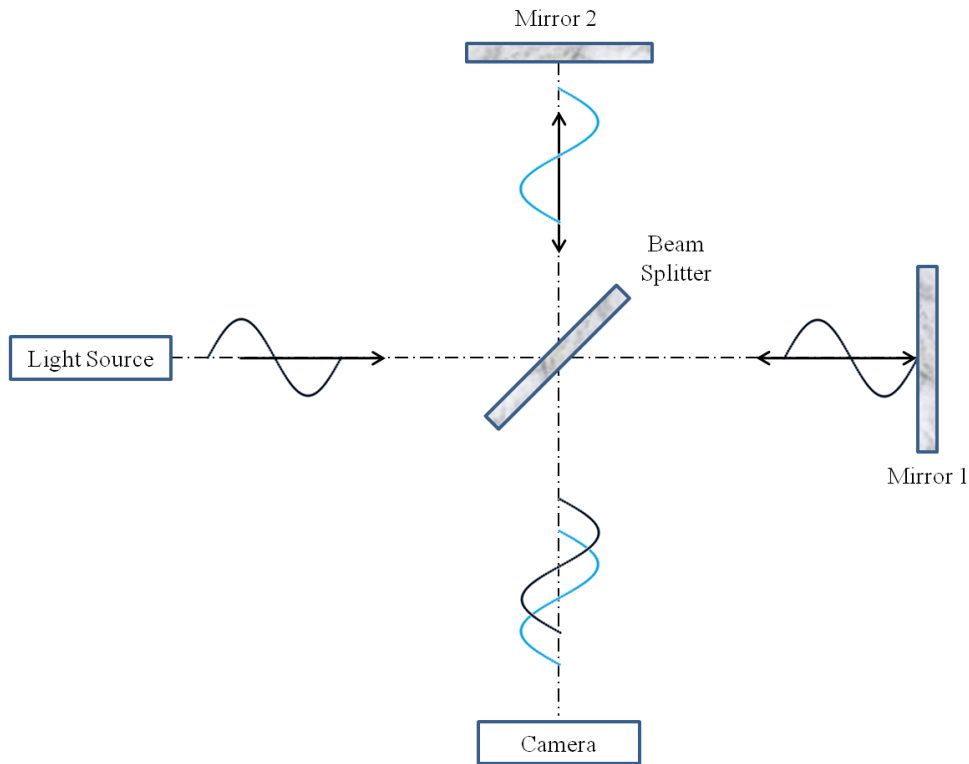


Figure 2.10: Michelson arrangement [27]

2.1.1.1.4 Time of Flight

Time of flight technique is often used in capturing large objects. Time of flight used to measure the total time taken for the light pulse to travel and return from the object. Fig. 2.11 shows the block diagram for the time of flight principle. Light pulse is emitted onto the object. The receiver will measure and record the time taken for the pulse to travel. Speed of light is exactly equal to 299,792,458 metres per second. Hence, it is possible to determine the distance travelled since the speed of light is known (with the condition that the angle θ is very small).

The distance of the object can be calculated with:

$$\text{Distance, } D = \text{Speed of Light } (C) \times \frac{t}{2} \quad (2.11)$$

In order to achieve a high accuracy in measurement, the pulse width of the laser has to be short while the speed of the detector has to be fast.

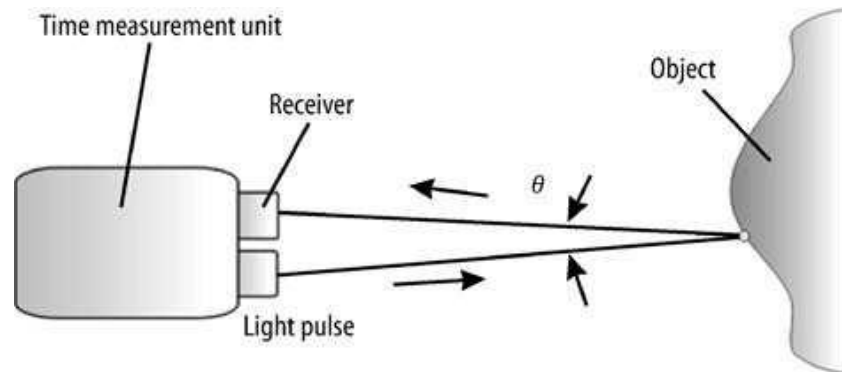


Figure 2.11: Working principle of time of flight [1]

There are some of the advantages and disadvantages of the time of flight techniques.

Advantages

- (i) High velocity of light enables thousands of measurement to be done every second.
- (ii) Able to digitize large, distant object such as bridges and buildings.

Disadvantages

- (i) Scanner size is huge.
- (ii) Cannot capture the object's texture, only its geometry.
- (iii) Not suitable for fast digitizing of small and medium size objects. (a long time is taken for the object to be swept during scanning process)

2.1.1.2 Data Processing

The second phase of the reverse engineering is point processing. Registration is the process of merging multiple scanned images to a single image if the object could not be obtained in a single scan. Point processing also allows post processing work such as sampling, triangulating, holes filling and smoothing. It is to ensure the output of the point processing phase is in a clean and merged format with minimal noise.

2.1.1.3 CAD Regeneration

Eventually, the processed points cloud will be transformed into a CAD format. The generated CAD format can be used for many purposes and is streamlined according to desired output. For example, if the application of reverse engineering is to replace the broken part, the output of the reverse engineering is the replacement part. If reverse engineering is used for inspection purposes, the output should be the comparison of the manufactured parts and the designed parts.

The application of reverse engineering is not limited to the automotive and aerospace industries, but also contributes in assisting the medical diagnosis and assessment in the medical field. Computed Tomography (CT), Magnetic Resonance Imaging (MRI) and 3D laser scanner are most commonly used in the medical industry. CT and MRI are used for internal part visualization based on transmissive approach. CT reconstructs images by projecting an X-ray beam through an object from many angles and measuring the amount of radiation that passes through it whereas MRI uses magnetic fields and radio wave to visualize internal structure detail of human body. 3D scanner uses the reflective approach instead of the transmissive approach.

2.2 Ulcer

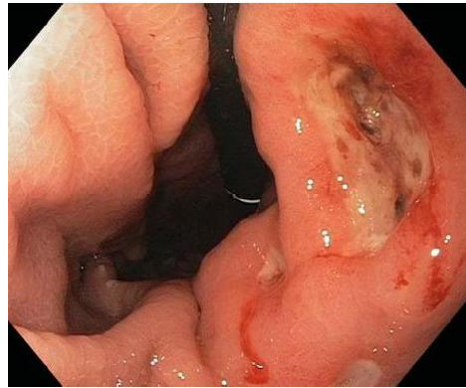
Ulceration is defined as discontinuity of skin that exhibits complete loss of epidermis and is most commonly seen at lower extremities of humans. [28]

Ulcers generally occur in several areas in the human body such as mouth, gastrointestinal tract, skin and corneal. Oral ulcer, also known as canker sore is an open sore inside the mouth. Oral ulcer occurs when the oral epithelium exposes the nerve ending in the underlying lamina propria which could result in pain or soreness. Peptic ulcer is located in the gastrointestinal tract which is typically acidic. Gastric ulcer and duodenal ulcer are the two common types of the peptic ulcer. Ulcers that are found in the stomach are gastric ulcers whereas ulcers that located in the duodenum are called duodenal ulcers. A person can be suffering from both gastric and duodenal ulcers at the same time [29]. Another type of ulcer located at the corneal is called

corneal ulcer. Corneal ulcer occurs when the outer layer of cornea is damaged. It is usually caused by infection with bacteria, viruses or fungus. Corneal ulcer should be treated as early as possible to avoid the poor visual prognosis. In dermatology, ulcer refers to any discontinuity of skin which appears as an inflamed tissue with reddened skin. This kind of the ulcer could be occurring anywhere on the body surface or limb. Four types of common ulcers are depicted in Fig. 2.12.



(a) Minor aphthous ulcer (oral ulcer) [30]



(b) Peptic ulcer [31]



(c) Irregular ulcer with severe corneal vascularisation [32]



(d) Neuropathic ulcer (leg ulcer) [33]

Figure 2.12: Four common types of ulcer

An increase in the number of patients with chronic wound has been recorded with the population advancing in age, increasing in weight, and with the resultant comorbidities of diabetes and venous insufficiency. According to the estimation, approximately 1% of the population will develop leg ulceration during their life [34]. In United State alone, chronic wound affect three million to six million patients and treating these wounds costs estimation five billion to ten billion each year. Chronic

wounds are wounds that fail to heal within the estimation period. Process of wound healing is divided into three stages, which are inflammation, tissue formation and tissue remodeling phase.

Inflammation is the first phase of the wound healing right after the wounding. Under the normal condition, it usually last for 4-6 days. The main processes of inflammation are vasoconstriction, haemostasis, vascular dilatation with increased capillary permeability, chemotactic growth factor and phagocytosis. Second phase of wound healing begins about 4-5 days after the wounding and last for few weeks under healthy healing process. It is the most important event in the process of wound healing. The main processes in this phase are angiogenesis, granulation tissue formation, re-epithelisation, and extracellular matrix formation. Tissue formation phase also known as proliferative phase. Eventually, a continuous process of dynamic equilibrium between the synthesis of new stable collagen and the lysis of old collagen is taken place. The process is called tissue remodelling phase and can take up to two years.

Lower limb ulceration tends to be recurrent and becomes a chronic wound if the wound does not heal in an orderly stage and the estimated period. Since the chronic ulcers are hard to heal, monitoring wound healing progress becomes crucial. Fig. 2.13 shows the management strategy for the wound treatment.

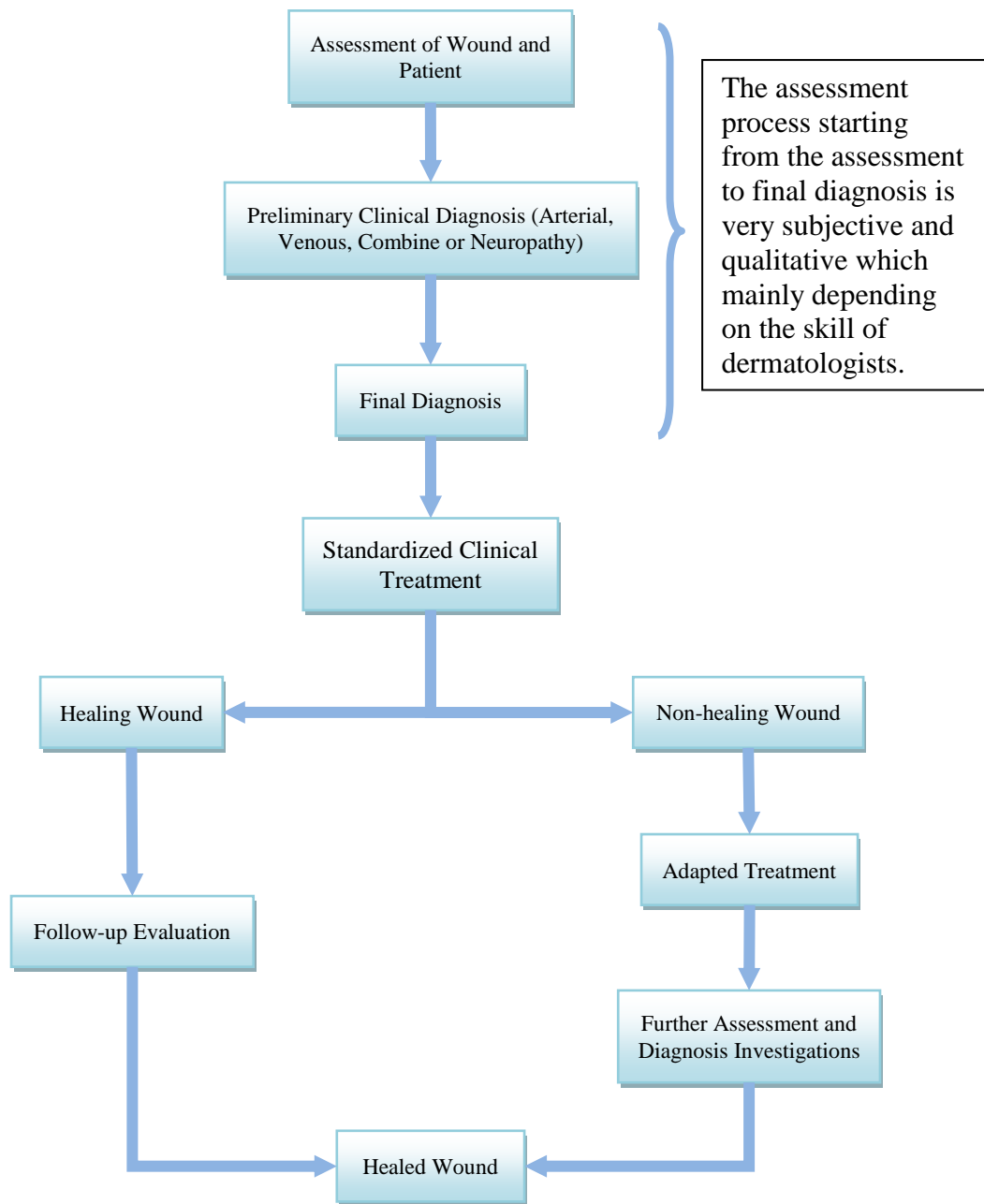


Figure 2.13: Management strategy for treatment of chronic wounds [34]

Ulcers that are located at the lower extremities of humans are also known as leg ulcers. Leg ulcer commonly occurs during late middle or old age due to the chronic venous insufficiency (CVI), chronic arterial insufficiency or peripheral sensory neuropathy or combination of these factors. Leg ulcer results in long term morbidity and often do not heal unless the underlying cause is corrected.

Leg ulcers were classified into four types, which are venous ulcer, arterial ulcer, combined venous and arterial ulcer, and neuropathy ulcer. Each type of the ulcer has its own symptoms, causes, lesion shape, and locations.

There are more than 200 possible dressing materials and treatments available and new products are continuously promoted to dermatologists. Different dressing and treatment remedies are applied based on ulcer severity. However, visual observation from dermatologist requires skills and experiment, and it is very subjective as it may differ from one dermatologist to the other. In addition, the dressing material and treatment might not be suitable to some particular due to their unique body structure. The faster changes in wound parameters are observed, the faster the doctors can make clinical decisions on suitable treatments needed for wound healing.

2.2.1 Venous Ulcer

The rise in patient age, obesity, previous leg injury (fractures), Deep Vein Thrombosis (DVT), and phlebitis have been associated with the increase in the prevalence of venous ulcers, which is approximately 1%. Among the symptoms that occur are limb heaviness, swelling associated with standing, which worsens in the evening and pain. Usually patient with venous ulcers are associated with at least one of the symptoms of chronic venous Insufficiency (CVI) and it can be shown in Fig. 2.14. The venous ulcers may be single or multiple. Venous ulcers are usually found in the area supplied by an incompetent perforating vein such as on the medial lower aspect of the calf, especially over the malleolus (medial > lateral) and often can be as large as the circumference of the entire lower leg. The ulcers are usually painful with well-defined, irregular shaped, relatively shallow with a sloping border and the base covered by fibrin and necrotic material, which are always secondary bacterial colonization. A massively obese individual has a risk of developing stasis ulcer in the most dependent parts of a pendulous abdominal panniculus. Longstanding venous ulcer is associated with the risk of developing squamous cell carcinoma (SCC), which shown in Fig. 2.15.



(a) Two coalescing ulcers with a necrotic base



(b) A giant ulcer with scalloped borders and a beefy red base

Figure 2.14: Venous insufficiency [35]



Figure 2.15: Squamous cell carcinoma in chronic venous ulcer [35]

2.2.2 Arterial Ulcer

Arterial ulcer has an age-adjusted prevalence of 12% and is usually seen in patients with peripheral arterial disease. Patients commonly suffer from symptoms of intermittent claudication and pain, even at rest. As the disease progresses, they tend to have a characteristically painful leg at night, which is often severe. The pain may worsen as the legs are elevated. The common locations for arterial ulcers to appear are

over sites of pressure and trauma such as pretibial supramalleolar and toes. Arterial ulcers are painful and have a punched out appearance with sharply demarcated borders. An example of chronic arterial insufficiency is shown in Fig. 2.16. Sometimes tendons can be seen under the base of the ulcers and are covered by slough tissues. However it has minimal amount of exudation. Common findings in a patient with arterial ulcers are loss of hair on feet and lower legs, shiny atrophic skin and diminished or absence of pulses. In contrast to venous ulcers, arterial ulcers do not have stasis pigmentation and lipodermatosclerosis.

Martorell's ulcer is a special type of arterial ulcer which is associated with labile hypertension and lacks signs of atherosclerosis obliterans. This is a very painful ulcer located on the anterior lateral lower leg, which usually starts with black eschar with erythematous surrounding. It has a punched out appearance with sharply demarcated borders and erythematous surrounding after sloughing of necrotic tissue.



Figure 2.16: Chronic arterial insufficiency with punched out edge and irregular outlines [35]

2.2.3 Mix Ulcer

These ulcers have a combination of signs and symptoms of both venous and arterial insufficiency and ulceration as the patients usually have both CVI and atherosclerosis obliterans. Among the symptoms are intermittent claudication, pain when elevated or

put in when the leg put in dependent position, both pallor and cyanosis of the foot, stasis dermatitis, and lipodermatosclerosis. The ulcers have both sloped and punched out appearance that reached down to tendons. It can be shown in Fig. 2.17.



Figure 2.17: Chronic combined arterial and venous ulcers [35]

2.2.4 Neuropathic Ulcer

This type of ulcers are usually found at soles, toes and heels and are commonly associated with prolonged period of having diabetes. Fig. 2.18 shows a neuropathy ulcer on the sole. Among the symptoms are paresthesia, pain, anesthesia of leg and foot. Patients usually are unaware of the getting the ulcers as they have lost of sensation over their feet.

“Diabetic foot” is a common term associated with peripheral neuropathy. However, other conditions that can contribute to diabetic foots are angiopathy, atherosclerosis, and infection. Usually they occur together to cause diabetic foot. Diabetic neuropathy results from the combination of motor and sensory deficit that caused patient unable to feel any pain even if they had injured their legs. Weakness and distal muscle wasting are due to motor neuropathy. Meanwhile, neurotropic ulcers over bony prominences of feet, usually on the great toe and sole are the result of sensory neuropathy. Osteomyelitis is one of the complications that may arise as the ulcers are surrounded by a ring of callus and which could extend into interlying joint and bone.



Figure 2.18: Diabetic, neuropathic ulcer on the sole [35]

2.2.5 Differential Diagnosis

Differential diagnosis of the three main types of leg/foot ulcer is listed in Table 2.1. Other differential diagnosis that can be considered are ulcerated Squamous Cell Carcinoma (SCC) as it may arise in a longstanding venous ulcer, basal cell carcinoma, injection drug use (skin popping), and pressure ulcer, due to prolonged compression of bony prominence of the foot. Ulcerations also occur in vasculitis (particularly polyarteritis nodosa), erythema induratum, calciphylaxis and various infections (ecthyma, Buruli ulcer, Mycobacterium marinum infection, gumma, leprosy, invasive fungal infection, chronic herpes simplex virus (HSV) ulcer) and in sickle cell anemia, polycythemia vera, pyoderma gangrenosum, necrobiosis lipoidica with ulceration, factitia [35].

Even though there are many dressing materials and treatments are used in the clinical practice, but the dressing and treatment also depending on the ulcer types. Three major types of leg ulcers have been classified. This classification categorizes the available dressing and treatment. However, there is a need to identify the best dressing treatment among hundreds types in each category to give the higher efficiency of ulcer treatment. In addition, certain dressing are not suitable to

particular patients due to their unique body structure. Hence, assessments of ulcers not only depend on those parameters, but also depending on severity of the ulcer and some other parameters which were introduced to help in assessment of leg ulcer.

Table 2.1: Differential diagnosis of three major types of leg ulcers [35]

| | Lesion | Site | Surrounding Skin | General Examination |
|-------------|----------------|--|--|--------------------------------|
| Venous | Irregular | Malleolar and supramalleolar (medial) | Lipodermatosclerosis | Varicose vein |
| | Sloped Borders | | Stasis dermatitis | Pain, worse in dependent state |
| | Necrotic base | | Atrophie blanche | |
| | Fibrin | | Pigmentation | |
| | | | Lymphedema | |
| Arterial | Punched Out | Pressure sites: distal (toes), pretibial, supramalleolar (lateral) | Hair loss | Pallor on elevation of leg |
| | | | Pallor or reactive hyperaemia | Pain worse on elevation of leg |
| Neuropathic | Punched Out | Pressure Site | Callus before ulceration and surrounding ulcer | Peripheral neuropathy |
| | | Plantar | | Decreased sensation |
| | | | | No Pain |

2.3 Assessment of Leg Ulcer

In common clinical practice, the evaluation of leg ulcers depending on the skill of the dermatologist as the assessments are based on the observation and rough

measurement of the ulcer wound geometrical shape. Assessment form such as Leg Ulcer Measurement Tools (LUMT) [5] is served as a guideline to monitor and response to the treatment whether healing or worsening. It is time consuming for dermatologist to perform all assessment parameters which are inside the LUMT. Hence, 4 main criteria of evaluation were introduced in clinical practice, which are volume measurement, area measurement, percentage of granulation tissue and percentage of necrotic tissue. The first indicator of the wound healing is changes in wound volume and followed by a slow decrease in perimeter and area [6].

Assessments are very subjective as it may differ from one dermatologist to other. Reproducibility of the assessment might not be same as the first assessment. Hence, quantitative and objective measurement is crucial for the assessment in order to give the accurate prediction and monitoring the progress of healing. Knowing which ulcer that fails to follow the normal healing path will enable a dermatologist to choose an alternative treatment and dressing.

2.3.1 Measurement Tools Used in Assessment of Leg Ulcer

Besides observation from the dermatologist, some of the measurement tools such as ruler, acetate sheet, swab and saline also help dermatologists to achieve slightly better assessment.

Generally, there are four main criteria for the assessment of leg ulcer, which are volume, area, percentage of the granulation tissue and percentage of the necrotic tissue. Each criterion needed different measurement tools for the assessment. A standardized method of measurement which is objective and quantitative is important to determine the amount of healing that has occurred in response to various treatments, medications, and disease processes.

2.3.1.1 Surface Area Measurement

There is no quantitative method in determine the surface area of an ulcer wound. However, certain measurement techniques are introduced to overcome inaccurate result based on observation. Three methods of measurement used to measure surface area of ulcer are introduced in daily clinical practice. The measurement methods are using the measuring tape or ruler technique, acetate sheet technique and planimetry.

Fig. 2.19 shows the measurement tape made from a strip of paper or plastic. It is used to measure the length and width of the ulcer. For the safety purposes, a transparent film is placed on the top of the wound to avoid direct contact to the wound.



Figure 2.19: Strip of paper ruler to measure length and width of the wound [36]

The easiest method to measuring the surface area is based on the maximal length and the longest width that is perpendicular to the length as shown in Fig. 2.20. The area is calculated by multiplying length and width of the ulcer. The ulcer here represents a rectangular shape instead of its original shape. It is difficult to measure the healing progress over a period even if the greatest length and width remain unchanged. Multiplying wound greatest width with length gives the estimated wound size but should not considered as accurate wound area. It has the limited sensitivity to the changes of the wound size and limited information of the wound shape [37]. Besides that, this method has no standard description of the ulcer margin. Repeat measurement

either from one dermatologist or different dermatologist may give different result as different reference points may be chosen. In addition, this method also does not document the curvature of the wound. Although it gives less accurate measurements compares to other methods, it can be used as a parameter for therapeutic effectiveness [36].

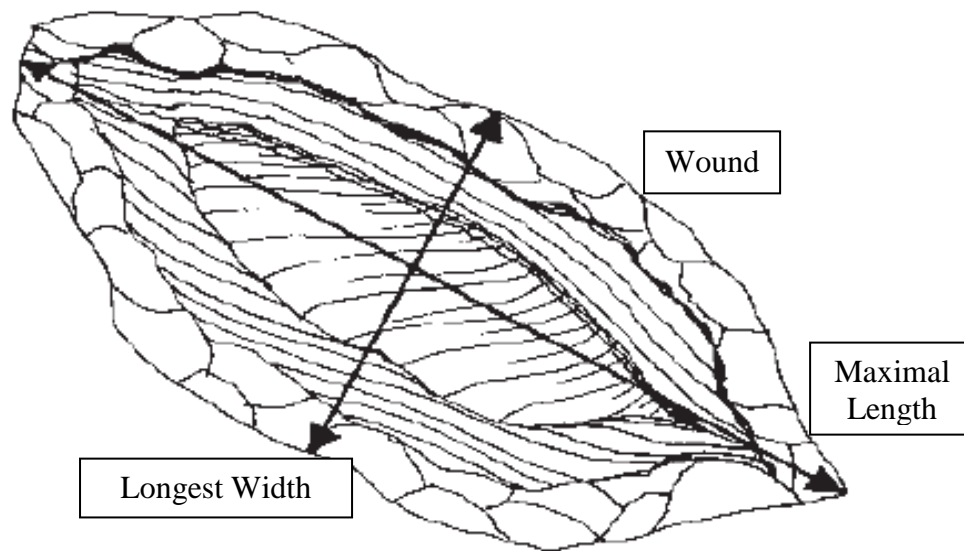


Figure 2.20: Area measurement based on maximal length and longest width [38]

Another method to measure the surface area is using acetate sheet which is shown in Fig. 2.21. The acetate sheet is placed onto the ulcer wound and the margin of wound is traced. Then, the acetate sheet will place onto graph paper and the number of squares will be counted to determine the area of the wound [39]. The technique for tracing the ulcer margin is shown in Fig. 2.22. However, there are some difficulties with the tracing. Difficulties including subjective in wound border determination, too much of the pressure on the wound can change the wound outline and thick marker could lead to confusion and error in counting the squares. Area is calculated manually with the number of squares inside the wound border and those with more than half of the squares are counted as one unit of squares. Some graph paper was pre-printed with 1 cm^2 measure and some was pre-printed with 1 mm^2 measure. Some considerations need to be taken when choosing the suitable graph paper. For instance, the square measure that pre-printed with small scale could take long time to count whereas if the square measure with large scale, there might be the possibility in gaining and losing

of surface area. This method is more accurate and precise compared to the measurement by ruler. It is sensitive to the early changes in wound size. However, it will bring uncomfortable and probably infection to the ulcer.

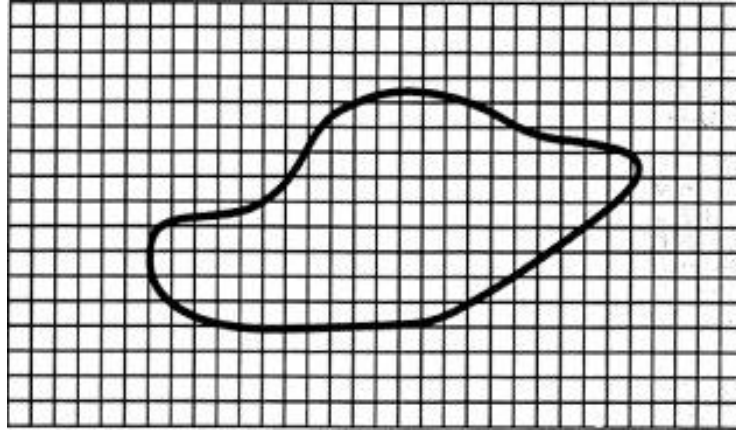


Figure 2.21: Acetate sheet [39]



Figure 2.22: Technique for tracing the ulcer margin [36]

Third measurement method is using the digital planimetry which shown in Fig. 2.23. The use the digital planimetry is same as the acetate sheet. Instead of counting the squares, digital planimetry measure the area by placing the tracing on the digital tablet and the border is re-trace by using the stylus. The underlying sensor will automatically calculate the area of the wound.

Acetate sheet and digital planimetry are used to measure the area of the wound. At the same time, it can be used to record the area of the granulation and necrotic tissue for the wound.



Figure 2.23: Visitrak digital planimetry

2.3.1.2 Volume Measurement

Among the four parameters of wound assessment, volume measurement is the most important variable to be measured. The first indicator of the wound healing is changes in wound volume and followed by a slower decrease in perimeter and area [6]. Basically, volume measurement is not an easy process and the most common measurement is done by multiplying area with wound depth.

For the depth measurement, a sterile swab is inserted into the deepest area of ulcer to measure the depth of ulcer. The height parallel to the external margin is observed and marked in order to determine the ulcer depth. The process of marking the height could cause error due to parallax error from observer. In addition, the head of swab might not point to the deepest wound bed which leads to wrong measurements. Fig. 2.24 shows the technique for tracing the wound margin using a sterile swab.

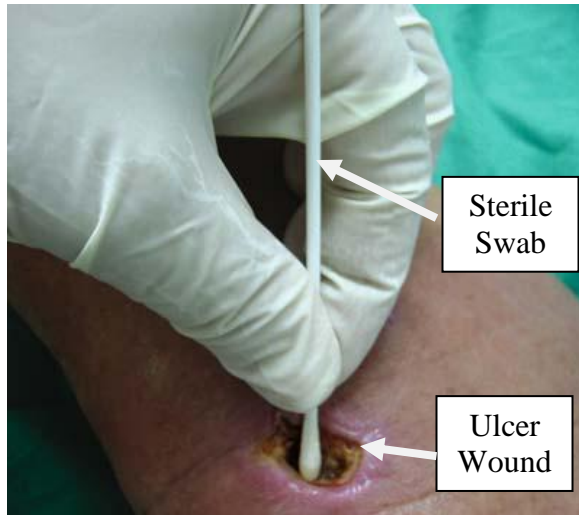


Figure 2.24: Technique for tracing the ulcer margin [36]

Another measuring tool named Kundin gauge has been developed for depth measurement. Besides that, the Kundin gauge also allows the measurement of length and width. Fig. 2.25 shows the Kundin gauge that was developed for three dimension (length, width and height) measurement.

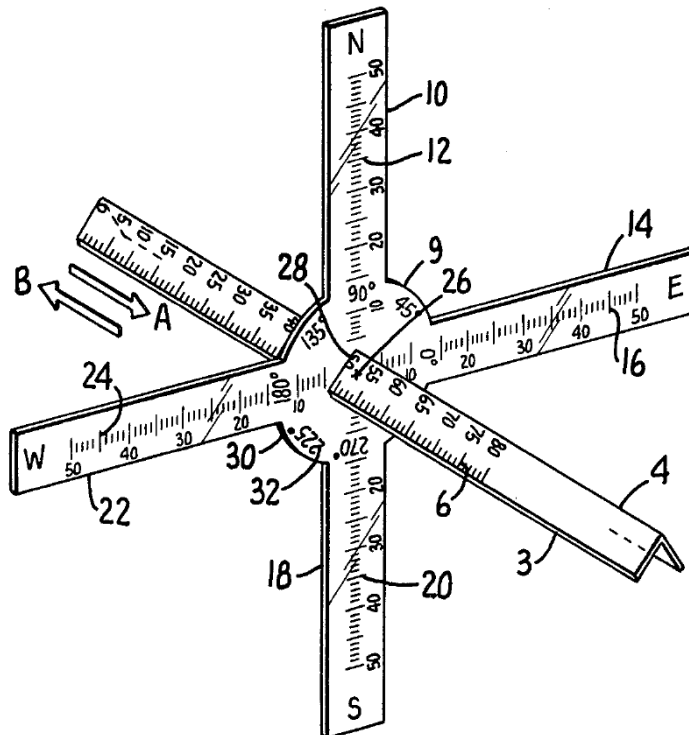


Figure 2.25: Kundin guage [40]

However, this method is not accurate enough for the accurate volume measurement and there are inherent errors. Wounds are rarely appear as regular solids, which may not have an uniform depth, width and length [37]. Measuring the three dimensions of the wound and multiplying each of them could result overestimating and underestimating the volume. These are due to irregular wounds and poor reproducibility of the boundary selection. Even though it gives overestimation and underestimation of the volume, but it can be served as a parameter for therapeutic effectiveness.

Instead of measuring the volume by multiplying the three dimension of wounds, there are two conventional methods to determine the volume of the ulcer cavity, which are the use of saline injection and mould making [41].

First technique is the saline injection method [42-43]. The ulcer is covered with transparent film and then filled with saline using a syringe. This is shown in Fig. 2.26. The volume dispensed from the syringe will show the volume of the ulcer wound [36]. However, the wound might absorb the saline and the shape of plastic covers might not be the same as the original healthy skin which will affect the accuracy of the exact ulcer volume.

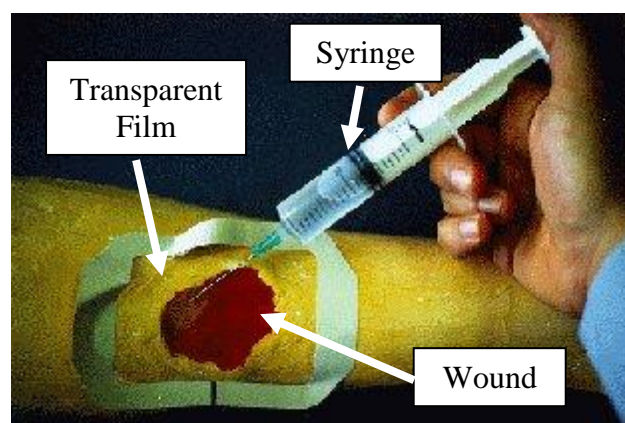


Figure 2.26: Technique for injecting saline [2]

Second technique of volume measurement is to fill the ulcer cavity with alginate mold or silicon based paste and weighing the amount of material used [43-44]. The entire material is placed into a beaker where the water dispensed from beaker indicates the

cavity volume. Other factors such as dehydration of the alginate material prior to weighing is less important and can be neglected [45]. This technique is invasive as it can bring discomfort and infection to the patients and is normally used for research purposes.

In general, assessment of the wound volume can be classified as invasive or non-invasive methods. Invasive methods include using saline or alginate paste to the wound cavity. Some difficulties arise when the invasive method is used: (a) invasive method can cause discomfort to patients and have a risk of wound infection. (b) overestimation and underestimation in volume tend to occur as the filling process is based on visualization. (c) it is not suitable for the large wounds, wounds which lay on limb with high curvature and shallow wounds. However, the volume computed by using the invasive method can serve as the reference volume for comparing the accuracy of the proposed system.

2.4 Wound Assessment Using Digital Imaging Technique

A lot of research on the wound assessment was done to develop wounds assessment tools that are low cost and easy to be operated by dermatologists or nurses. It can be classified into 2 categories, which are acquisition of 2D images and 3D images for measuring and monitoring the wound.

System based on 2D colour images typically reconstruct the characterization of tissue status from the segmentation, proposed in [46-47]. It can use to measure the percentage of granulation tissue and percentage of necrotic tissues. Depth is not considered in these researches since there is no information of depth in 2D images.

For the 3D measurements, some prototypes based on laser triangulation method [6, 48-49], structured light technique [50-51] or photogrammetry [39, 52] were tested to obtain the spatial measurement, but were not adapted to the clinical practice.

2.4.1 Structured Light

MAVIS (Measurement of Area and Volume Instrument System) is an instrument developed to measure the volume of skin wound, pressure sores and ulcer [53]. It is based on the principle of colour coded structured light. The image processing technique and hardware requirement can be found in [54].

Firstly, the operator has to define the boundary manually by tracing the edge of the images. Tracing also used for perimeter and area measurement of the wound. The second step is to reconstruct the healthy skin. Volume of wound is defined as the volume of region sandwiched between exposed surface and original healthy skin surface, which is imitated using cubic spline interpolation. Cubic spline interpolation has the tendency to create a minimum curvature that is similar to the behaviour of normal skin.

As shown in Fig. 2.27, MAVIS is a huge system that is mounted on a trolley and its weight is 110kg. Although MAVIS has better results compared to conventional measurement tools, it is not suitable for wound that are located in high curvature surfaces such as lower limbs. Besides that, it is incapable of measuring wounds that are undermined due to the optical principle. Generally, volume measurements with a large area/volume ratio are less precise than those with smaller ones.

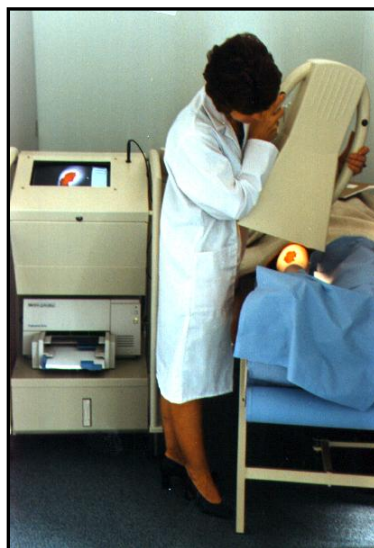


Figure 2.27: Trolley mounted MAVIS equipment [2]

2.4.2 Laser Triangulation

Derma is an integrated tool used to measure and monitor the evolution of skin lesions with a 3D system. It uses a laser triangulation 3D scanner to acquire geometry wound data and to capture a RGB image of wound. Derma supports all the geometric measures such as length (distance between critical points, perimeter, depth and different sub regions which is separated by colour), surface area and volumes. The selection of border is based on a semi automated manner. The border of wound is first defined by the user or dermatologist. Then, the system will improve the fit of a pre-defined border by considering the shape and colour gradient of a selected area. After that, the estimated healthy skin is reconstructed to cover the wound (which is called a lesion tap). The lesion tap is reconstructed by interpolating a thin strip passing the proximity of wound border as depicted in Fig. 2.28. Besides volume measurement for the wound, derma is also used to measure the percentage of granulation and necrotic tissue in wounds as shown in Fig. 2.29. Although Derma gives a promising result throughout the research, wounds that located in lower limb are not suitable for this approach since the leg is highly curvature in shape.

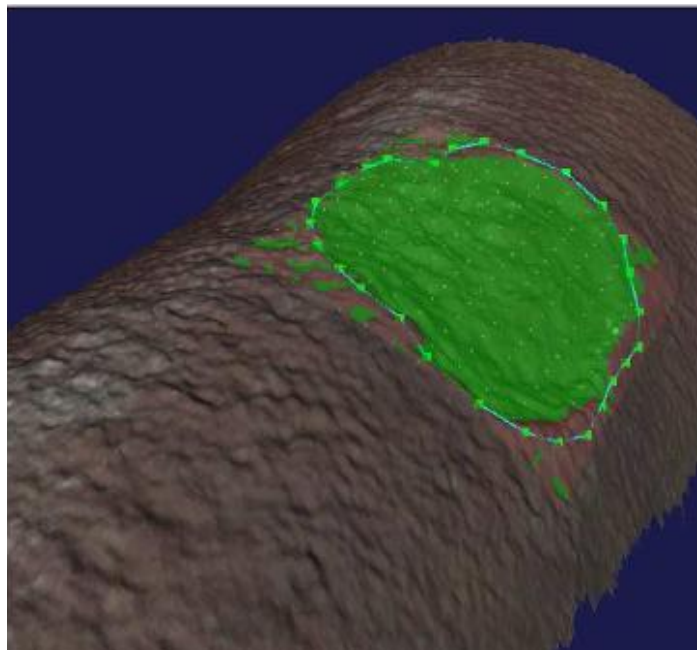


Figure 2.28: Wound covered with thin layer of healthy skin surface (green colour) for volume measurement [3]

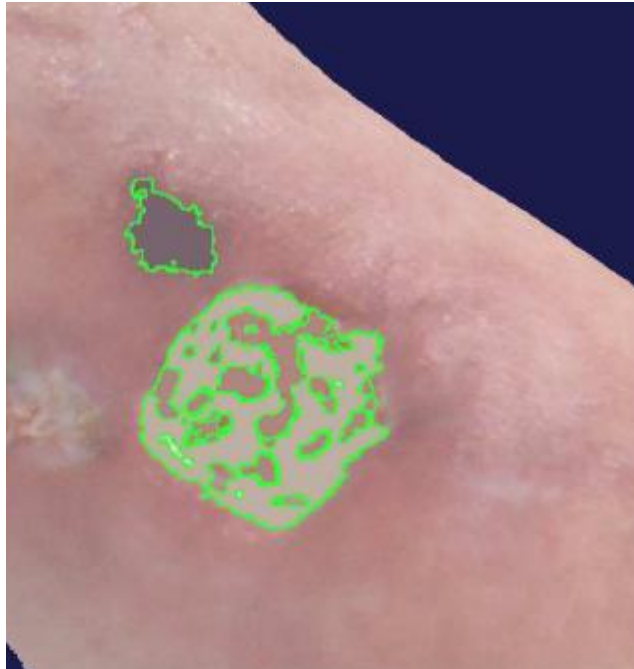


Figure 2.29: Tissue segmentation for area percentage measurement (necrotic, slough and granulation) [3]

2.4.3 Photogrammetric

Photogrammetric technology is typically based on the process of recording, measuring and interpreting photographic images (passive sensor) [55]. Some researches based on photogrammetric technology have been carried out to measure skin surfaces such as face, body and teeth [56-57].

MAVIS is now obsolete and replaced by the MAVIS II that uses only a reflex digital camera equipped with special dual lens optics to record two half images from slightly different viewpoints [2]. The operating principle of MAVIS II is based on stereophotogrammetry as shown in Fig. 2.30. Distance is directly measured by the displacement between corresponding points in stereo images. Although MAVIS II overcame the weaknesses that MAVIS was facing, such as size, costs, and time consuming measurements, the method of healthy skin reconstruction is not suitable for wounds with high curvature.

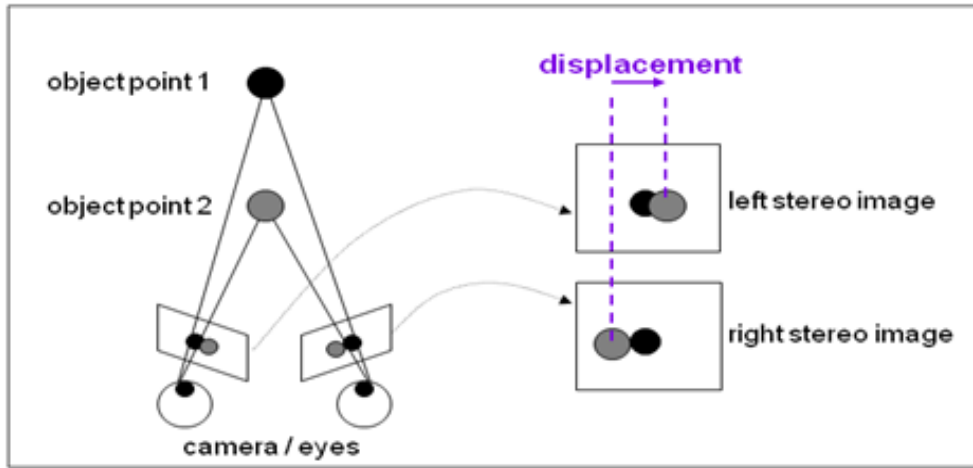


Figure 2.30: Stereo-photogrammetry operating principle [2]

Boersma [52] has developed a three camera vision system for wound measurements (shape and volume), especially for pressure ulcers. Three cameras are mounted on a triangular frame and a texture projection is in the centre as shown in Fig. 2.31. A commercial software package was designed for aerial photogrammetry to generate a digital surface model (DSM) automatically. Each three images are used to generate a precise DSM. The image taken should completely cover the wound together with some parts of healthy skin, since cavity volume is determined by using interpolation from surrounding healthy skin. This research shows the accuracy of created DSM.

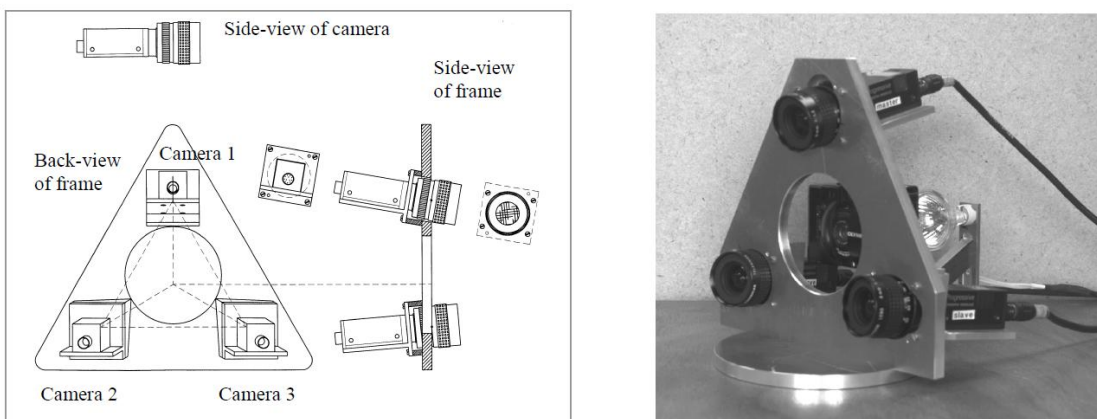


Figure 2.31: Camera configuration [52]

MEDPHOS (MEDical PHOtogrammetric System) [39, 58-59] was developed to provide three dimensional information, measurement and reconstruction of the wound

surface which are beneficial for the assessment of wound. MEDPHOS use three digital cameras and a pattern projector to capture the images of wound. Further investigation was done by using four digital synchronized cameras mounted on a rig and a pattern projector was fixed in centre of the rig as shown in Fig. 2.32. The working principle of MEDPHOS is based on the combination of active and passive 3D data acquisition technique. A dot target projection generated from a slide projector serves as an active camera with a known calibration parameter.

However, these researches are focused on the development of photogrammetry system whereas the accuracy of volume computation has not been done.

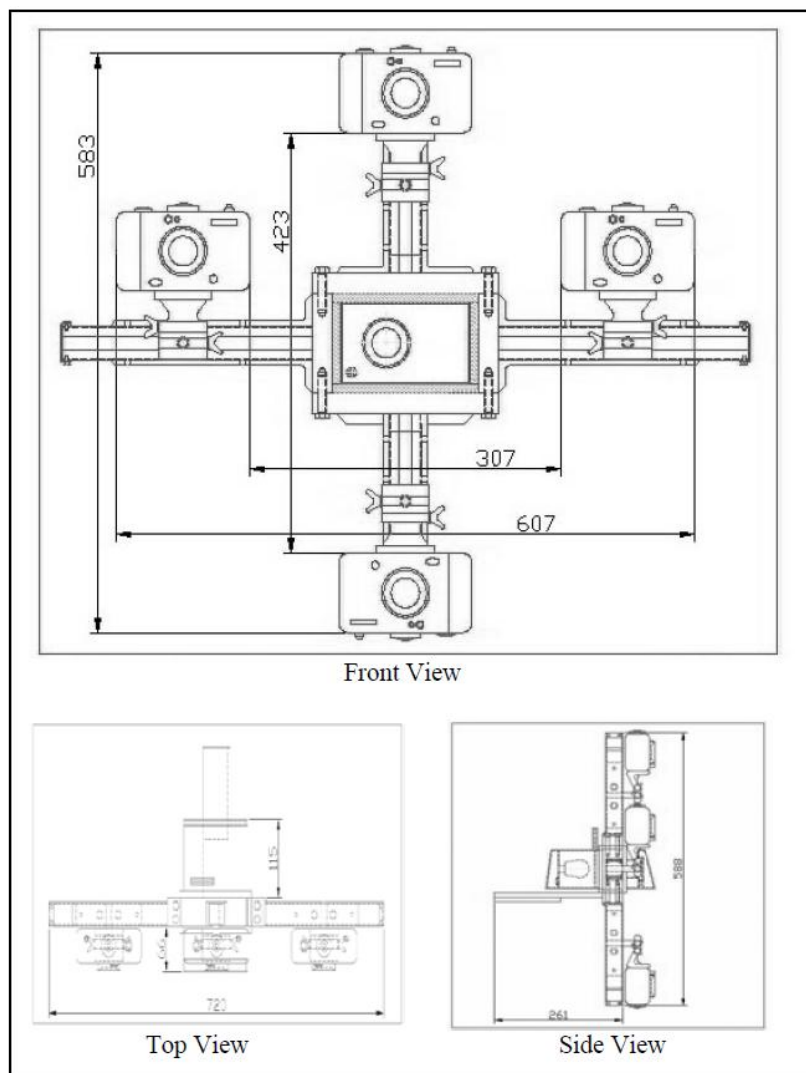


Figure 2.32: Camera photogrammetry system (MEDPHOS hardware) [58]

ESCALE (ESCarre Analyse Lisibilité Evaluation) is another system designed for the purpose of an objective and accurate 2D and 3D measurements of wound healing assessment [60]. There are two major parts in ESCALE: (a) 3D model reconstruction and volume measurement based on photogrammetry [61-63] (b) tissue classification [64-65]. The process flow of the ESCALE project is shown in Fig. 2.33. Although ESCALE provides 2D and 3D measurement of wound, some problems need to be solved before use in clinical practice. 3D reconstruction using uncalibrated views and reconstruction of healthy surface in ESCALE is the key point in order to develop an accurate wound measurement tool.

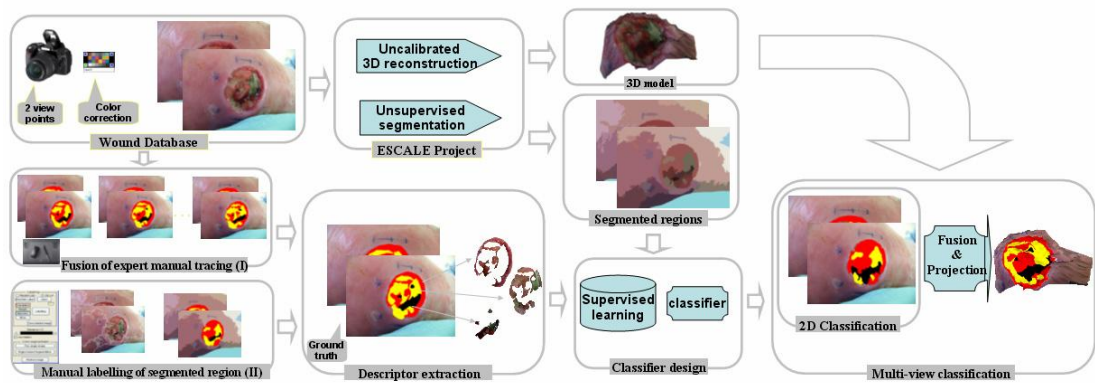


Figure 2.33: ESCALE wound assessment tool [65]

2.5 Surface Reconstruction and Volume Computation

A scanned wound was in the point cloud form which represents the surface of a particular wound. Since it is only the surface of wound, surface reconstruction must be performed prior to volume computation. Two methods had been developed for surface reconstruction of wound surface and volume computation, which are midpoint projection and convex hull approximation methods.

2.5.1 Midpoint Projection

In midpoint projection method, it is divided into two parts, which are surface reconstruction and volume computation. The application of this method is to reconstruct the estimated healthy surface of the ulcer wound and followed with the volume computation for the ulcer cavity. Hence, there are two factors that need to take into consideration prior to the method development: i) as the wound heals, red granulation tissue starts to grow from the base of the ulcer filling the wound cavity and reducing its volume. ii) the healing started from the base and the boundary shape is remaining the same.

Since the boundary shape remains the same while the wound is healing, the points located on the wound edges are used to determine and create the estimated healthy surface. The first step of this method is to determine the midpoint from the point cloud. Midpoint is determined from a numbers of points selected from the edges of wound or model which shown in Fig. 2.34.

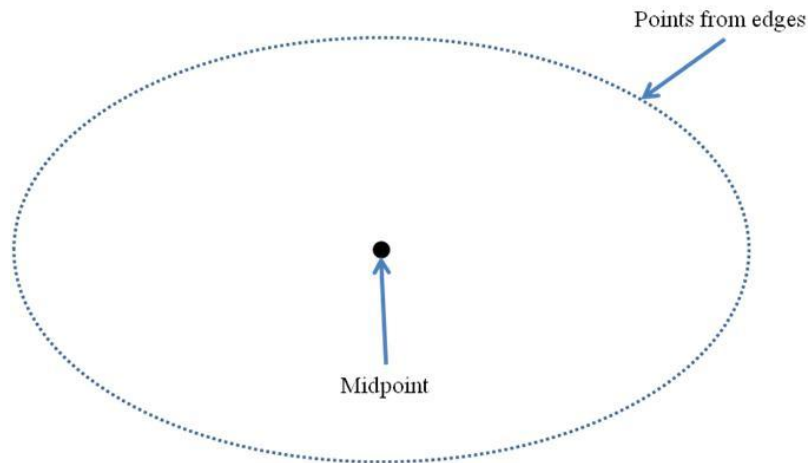


Figure 2.34: Midpoint generation by the points from the edges

The generated midpoint is used to connect with all the triangular faces to form numerous tetrahedral which shown in Fig. 2.35 Projecting the surface to a plane or reference point is useful for volume reconstruction [66]. Fig. 2.36 shows the tetrahedral and equation 2.12 was applied to calculate the volume of tetrahedron.

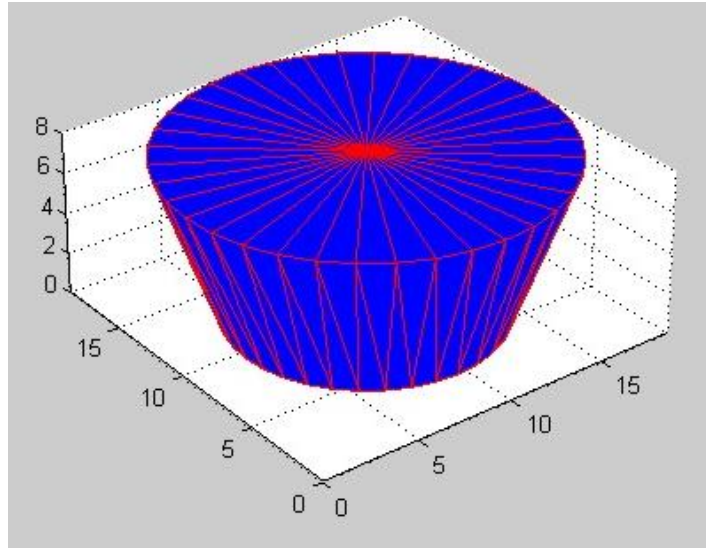


Figure 2.35: Tetrahedral form by connecting the triangular faces to the generated midpoint

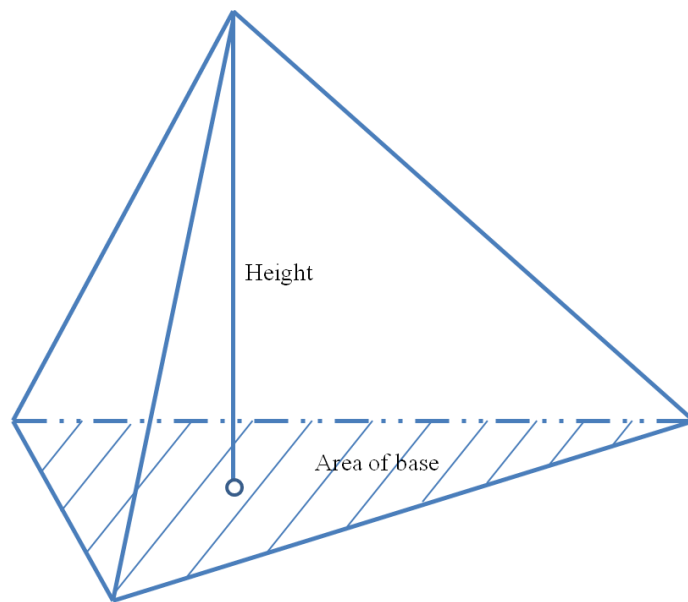


Figure 2.36: Midpoint generation by the points from the edges

$$\text{Volume, } V = \frac{1}{3} \times \text{Area of base} \times \text{Height} \quad (2.12)$$

The second step of this method is the volume computation. By summing up all the volume of all tetrahedral, the volume of wound/model cavity can be obtained. Midpoint has been selected to connect with all the triangular face instead of a point at

the boundary. If a point is randomly selected from the boundary, volume computation of that particular wound or model might not be reproducible. Hence, midpoint serves as a fix reference for volume computation and could produce more reproducible results. The process flow chart of surface reconstruction and volume computation using midpoint projection is shown in Fig. 2.37.

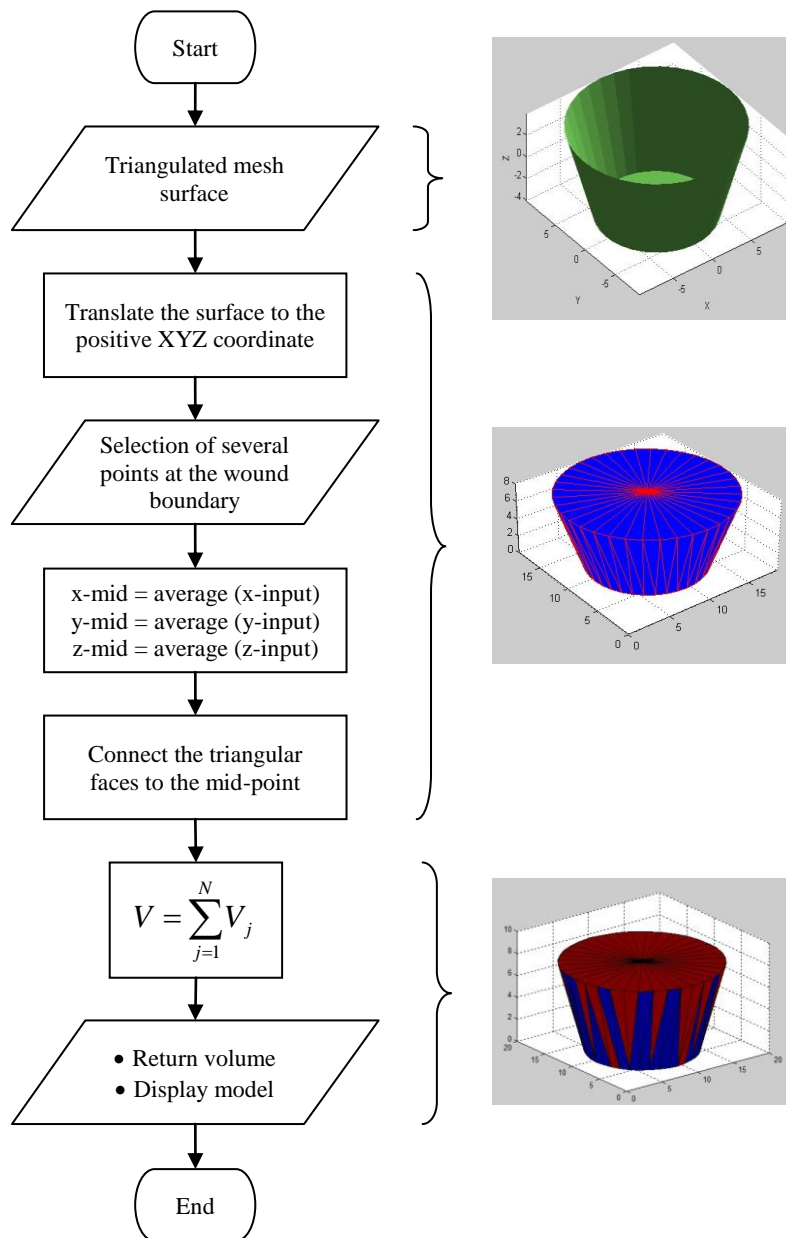


Figure 2.37: Process flow chart of surface reconstruction and volume computation using midpoint projection [66]

Midpoint projection has its own drawbacks. For unusual wound/model shape such as an L-shape, midpoint is expected to lie outside the borders as depicted in Fig. 2.38. If the midpoint is outside the border, overestimation of volume might occur. Besides that, this method is sensitive to the holes on the surface since the triangular mesh is used for volume computation. Hence, holes on the surface must be eliminated completely for accurate measurement.

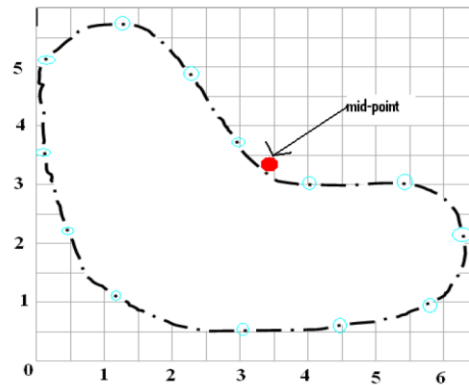


Figure 2.38: L shape border with midpoint lies outside the border [66]

2.5.2 Convex Hull Approximation

Convex hull approximation is another method to create a solid by constructing the surface. It is based on the Delaunay tetrahedralization technique. A tetrahedralization of V is a set of T of tetrahedra in 3D whose vertices collectively are v , whose interiors do not intersect each other and whose union is the convex hull of V [66]. In two dimensions, Delaunay triangulation will maximize the smallest angle, compared with all other triangulation of the same vertex set. A Delaunay triangulation is an ideal structure for searching points that are far from other vertices. This is because Delaunay triangle has no vertices in its circumcircle (and a Delaunay tetrahedralization has no vertices in its circumsphere) [67]. An edge, triangular face, or tetrahedron whose vertices are members of v is said to be Delaunay if there exists an empty sphere that passes through all its vertices [68] which shown in Fig. 2.39.

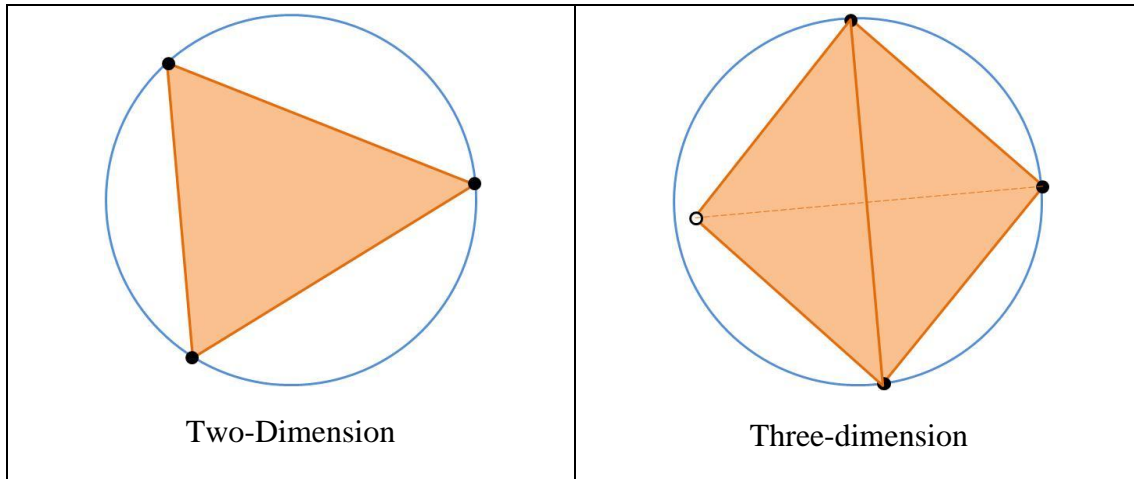


Figure 2.39: Working principle of Delaunay [68]

A convex hull is the smallest convex set that contains all the points inside its interior. The Quickhull algorithm for convex hulls [69] has been used to create the convex hull approximation that encloses all the vertices representing the surfaces in the smallest polyhedron.

Convex hull is constructed with three steps. Firstly, a tetrahedron is produced using four points selected from the system. It is the Delaunay 3-simplex which serves as a starting reference for the remaining Delaunay tetrahedral points.

The second step involves adding a subsequent point to the starting reference. Points located inside the current convex hull will be ignored whereas the points located outside the visible facets form a connected region on surface.

Finally, the last point will act as an apex for all visible faces in its horizon to connect with, adding several tetrahedra to the convex hull.

Convex hull represents the smallest bounding polyhedron created by connecting the furthest vertices around the surface. The resulting shape will not take account of all vertices in the original shape. Fig. 2.40 shows a volume estimation of 3D model enclosed with smallest convex shape.

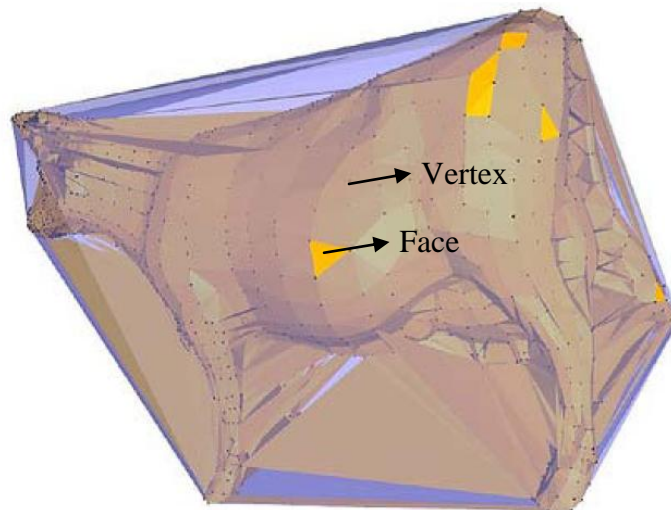


Figure 2.40: 3D model enclosed with smallest convex shape [66]

When dealing with 3D object, it is very common to decompose the complex object to a number of convex pieces [70]. Decomposition is aimed to partitioning the convex models to simpler components (approximate convex pieces) that similar benefit as convex component [71]. The original model will be divided into several divisions as predetermined by the user. When using convex hull approximation, decomposition of model into several pieces will give better approximation in terms of volume. Fig. 2.41 shows the decomposition of the dragon model which could provide better volume estimation. In order to achieve higher accuracy of the volume computation, surface division is needed prior to surface reconstruction.

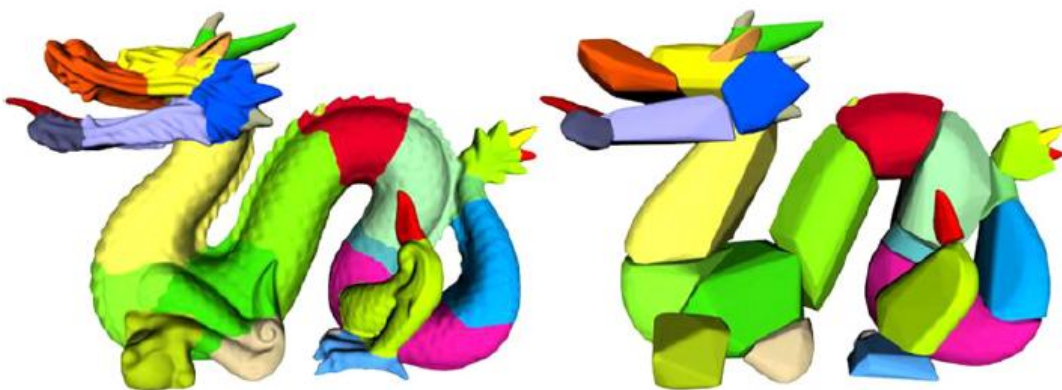


Figure 2.41: Example of convex hull approximation with surface division [71]

The process flow chart of surface reconstruction and volume computation using convex hull approximation is shown in Fig. 2.42.

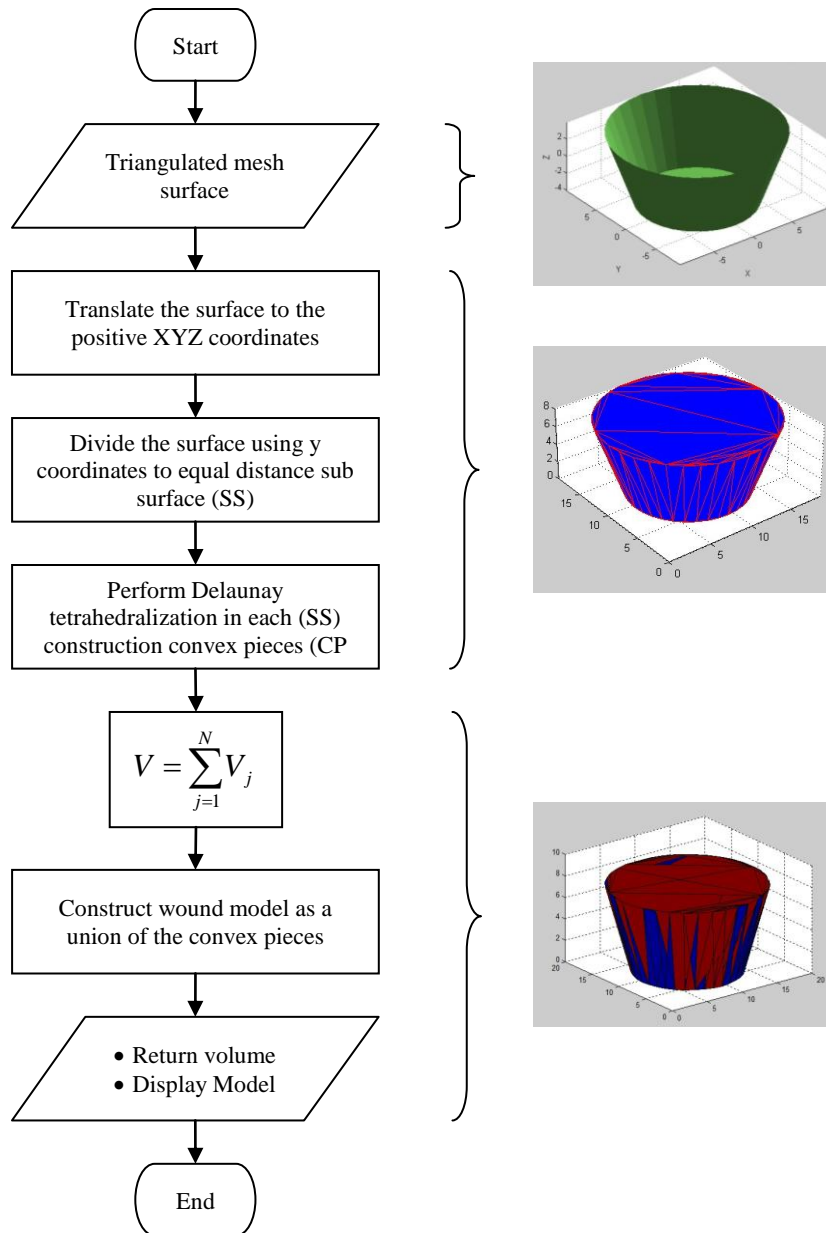


Figure 2.42: Process flow chart of surface reconstruction and volume computation using convex hull approximation [66]

2.6 Archimedes Principle in Volume Determination

Volume is the amount of three-dimensional space occupied by an object or geometric. Volume is usually quantified using the International System (SI) unit, which is cubic meter (m^3). However, it can be numerical quantified as cubic millimetre (mm^3), cubic centimetre (cm^3) and other relevant unit depending of the size of the object measured. The volume of simple shape object such as regular, circular and straight length shape were calculated easily using arithmetic formula. In the condition where the object is not regular and cannot be calculated using the arithmetic formula, volume measurement using Archimedes principle can be applied.

Archimedes' principle states that an object fully or partially immersed in a fluid is buoyed up by a force equal to the weight of the fluid that the object displaces [72-73]. There are two volume measuring techniques using the Archimedes principle, which are level and overflow methods. Fig. 2.43 show schematic diagram of level and overflow methods of measuring volume.

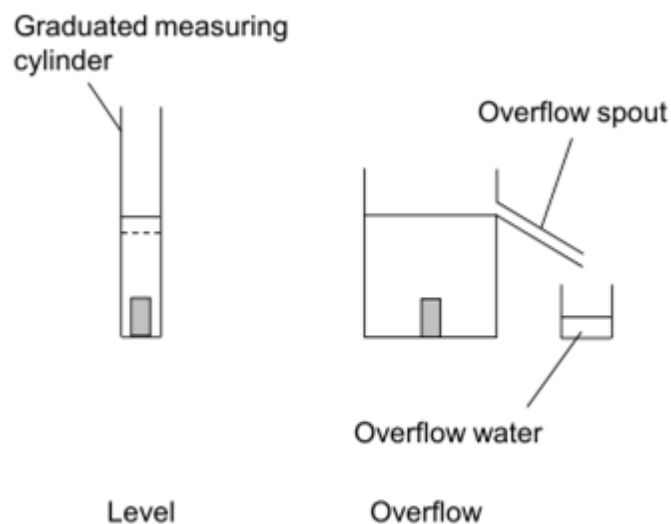


Figure 2.43: Schematic diagram of level and overflow methods of measuring volume [73]

2.6.1 Level Method

Volume measuring by level method is one of the common technique which using the Archimedes principle. The working principle for the level method is very straight forward and only involved measuring cylinder and the observation of the researcher. An object will be placed into the cylinder filled with water. The position of the meniscus was recorded before and after the placement of the object. The volume of an object is measured by the difference reading value before and after the placement of the object. This method is subjected to the human error where the meniscus water level to be taken and depending on the reading interval of the measuring cylinder.

2.6.2 Overflow Method

The second method of Archimedes principle is overflow method. This method involved a container with a downward pointing spout and a beaker and setup as per Fig. 2.43. The container was filled with water just above the bottom of spout. An object was dropped into the container and allowed the water overflow through the spout and drop down to the beaker for few minutes. The beaker was weighted before and after the overflow water.

Volume was calculated by dividing the weight of water by the water density:

$$\rho = \frac{m}{V} \quad (2.13)$$

Hence,

$$V = \frac{m}{\rho} \quad (2.14)$$

2.7 Common Error in 3D Wound Measurement

Every wound measurement method or technique has its strengths and limitations. However, there are 5 general problems that will directly affect their accuracy.

- Wound's boundary is often difficult to define. It usually depends on subjective judgement of the observer who performs the wound measurement. There are some of common question raised by the observer, such as "whether this region is belongs to wound or not".
- Slight movement, flexing of the muscle or change in the patient's position might significantly change the wound's appearance. The issue is emphasis on the repeatability of measurements rather than the accuracy of the measurement method or technique.
- Human body is curvature in nature. Wounds might extend around a limb causing problem for the measurement technique based on photography or optical method. In addition, those methods that ignore the surface curvature will produce inaccurate results.
- Wounds that are widely undermined may change their volume with patients' position. For instant, the volume of pressure sore at the heel is difficult to define since the original healthy surface is unclear.
- Wounds that occur in tissues with a thick layer of fat such as abdominal wounds will produce a cavity with significant volume even after healing completely. Hence, it is difficult to determine whether the wound has completely healed.

2.8 Prototyping of 3D Objects

It is very crucial to be able to generate free-from 3D objects in medical application using Rapid Prototyping (RP). Instead of doing experiment on the patient itself, prototype is more suitable to perform all the testing and experimental work. A RP machines receives 3D models as input and produce real-world object as output [74].

This technology allow us to promptly produce a physical object applying layer by layer technique by directly depositing from the STL (Standard Triangulation Language) CAD data format. Typically, the RP software will takes an input of triangulation mesh as described by an STL file. STL files format is simply containing

the list of triangular facets. It is important for the RP machine to convert the object shell defined by the surface mesh into a volumetric model prior to build the prototype.

Multi Jet modelling (MJM) build style is the technology used in solid printer to produce wax prototypes. MultiJet Modeling (MJM) is one of the techniques used in produce rapid prototype and the schematic diagram of MJM is shown in Fig. 2.44. It is one of the least expensive building styles in rapid prototyping technologies. Wax is the only material that can be use in this technique. Wax is heated and the droplets of materials are deposited with the multiple printing head. The process builds a part by printing thin layers of molten wax consecutively in the shape of the part's cross sections. Similar to most of the rapid prototyping, parts are built in z direction.

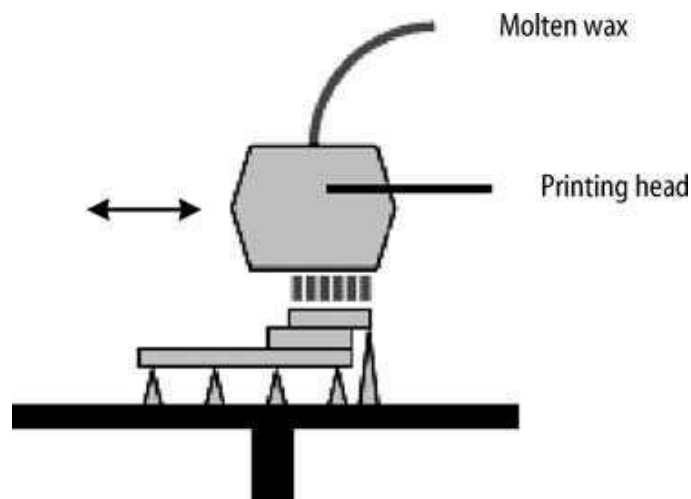


Figure 2.44: Schematic diagram of MultiJet Modeling process [1]

However, not all the STL file will promise in building the prototype successfully. It is very depending on the mesh characteristic of STL files. Fig. 2.45 shows five examples of mesh characteristic which is commonly seen.

In order to guarantee the prototype being successfully created, the STL model must prevent the constraints listed below:

- Non-manifold Surfaces
 - Situation where a mesh self-intersects (Fig. 2.45b).
 - Situation where a mesh edge is shared by more than two triangles (Fig. 2.45c).

- Open surfaces
 - Situation where a mesh edge only has one connected triangle (Fig. 2.45d).
 - Situation where standalone surface patches exist which should be a single contiguous surface (Fig. 2.45e).
- Non-orientable
 - The surface normal and hence the determination of the object inside and outside is ambiguous.

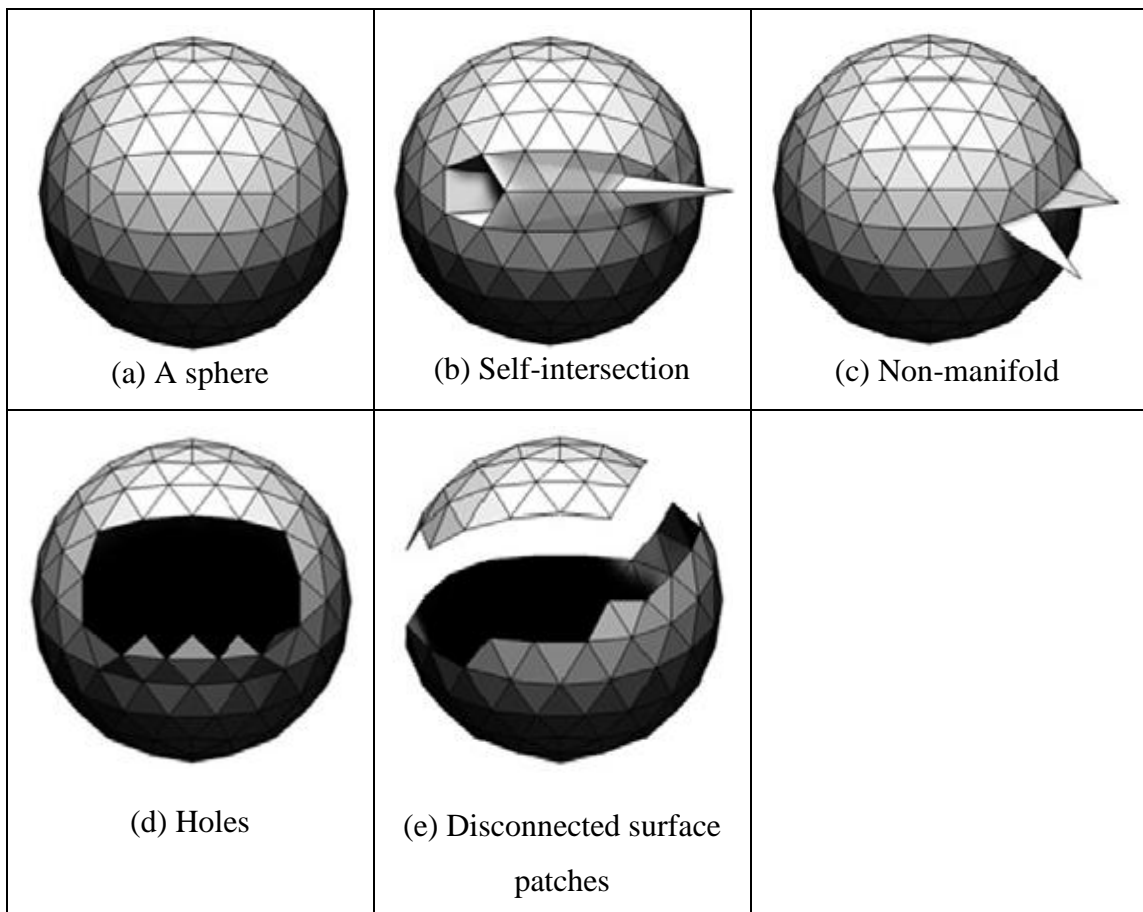


Figure 2.45: Fine mesh characteristic (a) and mesh characteristic which cause failure in generating accurate prototype objects (b-e)

2.9 Coefficient of Determination

The coefficient of determination (R^2), commonly called as R squared is the statistical measure of how well the regression line approximates the ideal line [75-77]. The main purpose of having R squared is either applying for the prediction of future outcomes or the testing of hypotheses with the basis of other related information.

$$R^2 = \frac{SSR}{SST} = \frac{SST - SSE}{SST} = 1 - \frac{SSE}{SST} = 1 - \frac{\sum(y_i - \hat{y}_i)^2}{\sum(y_i - \bar{y}_i)^2} \quad (2.15)$$

Definition:

R^2 = Coefficient of Determination

SSR = Regression sum of squares

SST = Total sum of squares

SSE = Sum of squared Errors

R^2 is a number between 0 and 1, which is $0 \leq R^2 \leq 1$. The R^2 value of 1.0 show the regression line perfectly fits the ideal data which demonstrate the stronger linear relationship between x and y. In contrast, R^2 value of 0.0 indicates the line has no explanatory value and so the linear relationship is weak. A reliable or trustable result on the relationship between x and y normally having the R squared value between 0.99 to near 1.0.

2.10 Summary

RE is commonly used in automotive industrial and cultural heritage reconstruction to obtain generate a computerize representation of an existing object from the object surface. RP is another emerging technology that enables us to quickly fabricate the physical 3D object using a layered manufacturing technique. Both RE and RP are now making inroads into medical field.

Chronic wounds arise from the wound that does not heal within the predicted time frame. Not only pain compromises the patient, but also time consuming outpatient

treatment, transportation to the physician and also financial burden. The appropriate treatment and dressing will significantly reduce the healing time. The effectiveness in measuring changes of wound volume is the key factor to shorten the healing period.

The assessment is mainly relying on visual inspection of dermatologist which is very qualitative and subjective. Conventional measuring methods such as alginate paste and saline injection might bring infection and discomfort to the patients. Three-dimension skin surface imaging technique is used to replace conventional method to produce more objective and quantitative measurement. Three-dimension skin surface imaging components are including data acquisition and also volume computation.

Among the 3D data acquisition method, laser triangulation and structured light technique are most often being used. Laser triangulation using the similar triangles equation to measure and located the object position whereas structured light using the intensity produced from the fringe pattern to find the objects location.

Two methods are used to reconstruct the cavity surface and compute cavity volume, known as midpoint projection and convex hull approximation. Midpoint projections connect all the vertices to the generated midpoint to form tetrahedral whereas convex hull approximations create the smallest bounding polyhedron by connecting the furthest vertices around the surface. By summing up all the tetrahedral from both methods, the total cavity volume can be obtained.

In the fitting of linear regression equations, the R^2 is one of the common statistical tool to assess the goodness-of-fit of the equation.

CHAPTER 3

METHODOLOGY

This chapter discusses the methodology for volume measurement. Conventional measuring method using mould material and 3D skin surface imaging method are two different approaches to measure the cavity volume of ulcer. RE is used to rebuild the geometrical CAD of ulcer which involved the process of data acquisition, data processing and model regeneration. RP is used to generate the prototype of ulcer wound for the experimental work to avoid direct contact to the patients. The methodology is divided into two stages, which is the validation of various wound attribute models with known volume followed by volume measurement of the ulcer wound. Two methods are used to compute the volume cavity.

3.1 Validation of Various Wound Attribute Models with Known Volume and Volume Measurement of Ulcer Wound Model

Fig. 3.1 shows the overall process for the research work that was done. This process is divided into two stages, which is the wound attribute validation stage followed by real ulcer wound volume measurement. In the validation stage, it is mainly to identify the relationship of wound attributes towards the data acquisition techniques and volume computation methods. Whereas in real ulcer wound volume measurement stage, the ulcer measurement was done by using the best method selected from the validation stage.

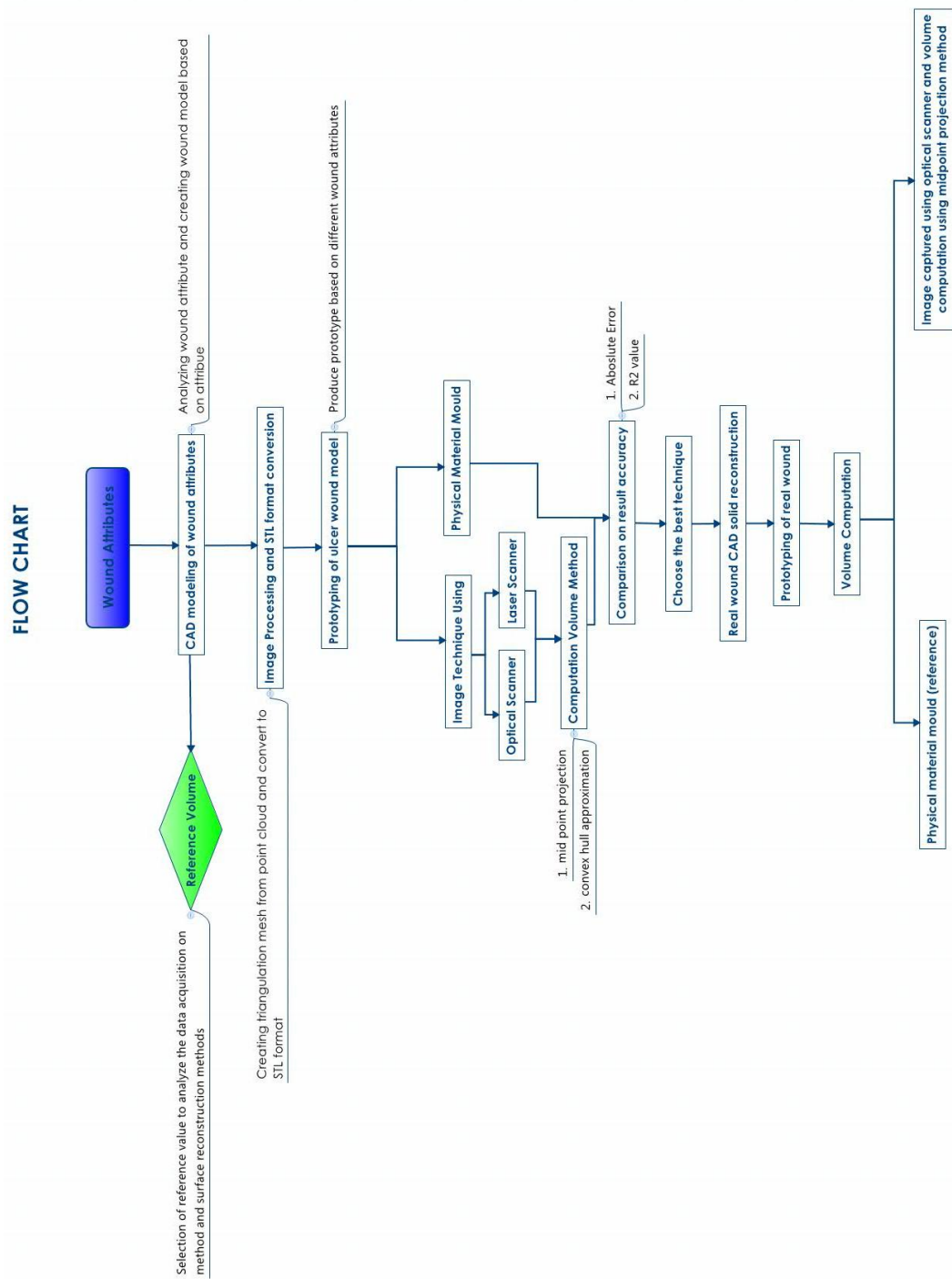


Figure 3.1: Ulcer Wound Attribute and Real Ulcer Wound Volume Determination

3.1.1 CAD Modeling of Ulcer Attribute

Ulcers can appear in various shapes with different sizes such as round, ellipse or even an almost rectangular shape. Each type of ulcer has a different diagnosis and is classified based on the location and the wound shape. According to [78], we can describe the ulcer wound with several wound attributes which are shown in Fig. 3.2. In addition, each attributes can be further described with the descriptor shown in Table 3.1.

Wound attributes can be classified into four classes, which are wound boundary, wound edges, wound base, and wound depth. In each attribute, the descriptor is introduced to further assist in the wound assessment. Wound can be defined as regular and irregular in shape where it can be judged based on the boundary of the wound. Regular boundary is referred to the wound boundary which is visually symmetrical whereas irregular boundary is defined as the wound boundary which is not visually symmetrical. It is impossible to have a perfectly symmetrical wound boundary, hence, wounds that have a visually symmetrical shape will be judged as having a regular boundary and vice versa. Three descriptors are used to explain the edges of the wound, which are sloped (an inclination of slant), punched out (chopped edge) and undermined (overhanging margin). For the wound base, an elevated base represents an upwards curvature base, depressed base represents a downwards curvature base and a homogeneous base represents the flat surface of the wound bed.

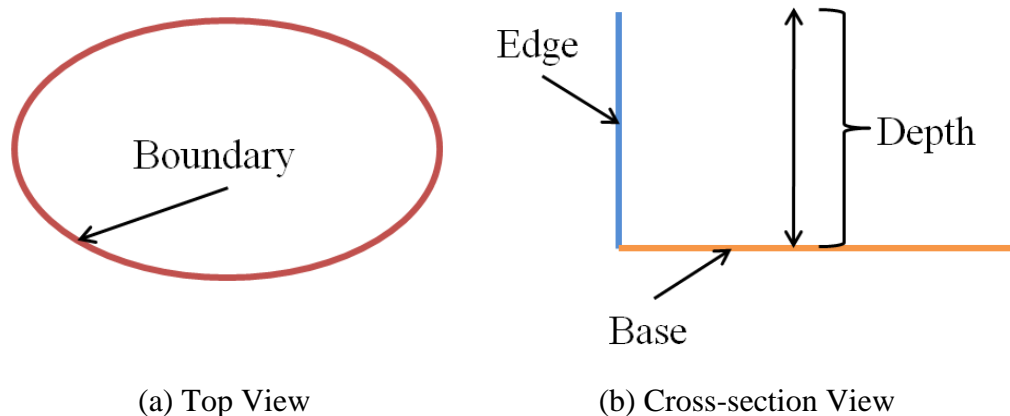
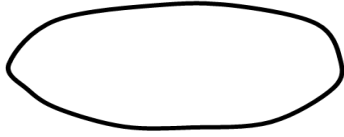







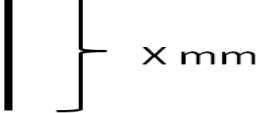


Figure 3.2: Schematic diagram of ulcer attributes

Table 3.1: Common wound attributes, descriptor and their schematic diagram

| Attributes | Descriptor | Schematic |
|------------|-------------|--|
| Boundary | Regular |  |
| | Irregular |  |
| Edge | Sloped |  |
| | Punched Out |  |
| | Undermined |  |
| Base | Elevated |  |
| | Homogenous |  |
| | Depressed |  |
| Depth | Unit (mm) |  |

With a combination of these attributes and descriptors, several CAD models were created for validation purposes. Due to the optical principle of equipments used, it is incapable of measuring wounds that are undermined. Hence, an undermined edge is not considered throughout this research. The models were developed using CAD modelling software.

At the initial stage, a rectangular prism with specific length, width and height was created. The model's volume, calculated from the CAD modelling software is recorded. Then, seventeen models based on these attributes were created, and their volumes are recorded respectively. Based on the clinical practice and advice from dermatologist, wounds tend to be in regular shape, sloped edge and homogeneous base. Hence, the seventeen models are focusing on various combinations of the wound attributes such as regular shape, sloped edge, homogeneous and elevated base which were shown in Table 3.2.

Fig. 3.3 shows a model created based on wound's attributes with regular boundary, sloped edge, 3 mm depth and 2 mm elevated base. The cavity volume is obtained from the difference between solid rectangular prism and model with wound attributes.

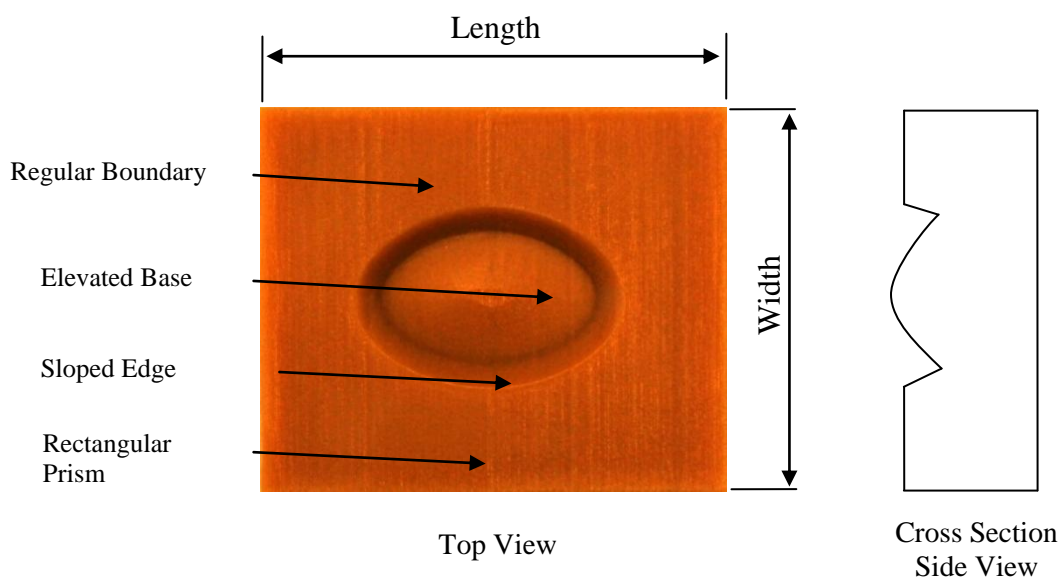

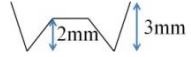



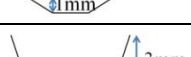
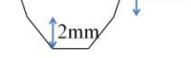








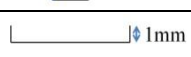
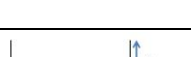


Figure 3.3: Model with regular boundary, sloped edge, 3 mm depth and 2 mm elevated base

Table 3.2: Seventeen models based with different wound attributes

| Model | Boundary Shape | Edge | Depth | Base | Base's Height | Cross-sectional View |
|--------|----------------|-------------|-------|-------------|---------------|---|
| RSD1H | Regular | Sloped | 1 mm | Homogeneous | 0 mm |  |
| RSD3E2 | Regular | Sloped | 3 mm | Elevated | 2 mm |  |
| RSD3E1 | Regular | Sloped | 3 mm | Elevated | 1 mm |  |
| RSD3H | Regular | Sloped | 3 mm | Homogeneous | 0 mm |  |
| RSD3D1 | Regular | Sloped | 3 mm | Depressed | 1 mm |  |
| RSD3D2 | Regular | Sloped | 3 mm | Depressed | 2 mm |  |
| RSD5E2 | Regular | Sloped | 5 mm | Elevated | 2 mm |  |
| RSD5E1 | Regular | Sloped | 5 mm | Elevated | 1 mm |  |
| RSD5H | Regular | Sloped | 5 mm | Homogeneous | 0 mm |  |
| RSD5D1 | Regular | Sloped | 5 mm | Depressed | 1 mm |  |
| RSD5D2 | Regular | Sloped | 5 mm | Depressed | 2 mm |  |
| RPO1H | Regular | Punched Out | 1 mm | Homogeneous | 0 mm |  |
| RPO3H | Regular | Punched Out | 3 mm | Homogeneous | 0 mm |  |
| RPO5H | Regular | Punched Out | 5 mm | Homogeneous | 0 mm |  |
| IRSD1H | Irregular | Sloped | 1 mm | Homogeneous | 0 mm |  |
| IRSD3H | Irregular | Sloped | 3 mm | Homogeneous | 0 mm |  |
| IRSD5H | Irregular | Sloped | 5 mm | Homogeneous | 0 mm |  |

3.1.2 Prototyping of the 17 Wound Attribute Models

CAD models based on the wound attributes were created from the CAD modelling software. STL format is the only input to produce prototype, hence, it is necessary to convert the CAD model to STL format. The converted STL format CAD file is ready for prototyping using solid object printer.

By using solid object printer software, the STL format file was imported and the arrangements of models are shown in Fig. 3.4. The platform size is 250 cm x 185 cm and the imported models should not be larger than the platform size. The support material and prototype material are both using Thermal Jet 88 Build Material (Wax).

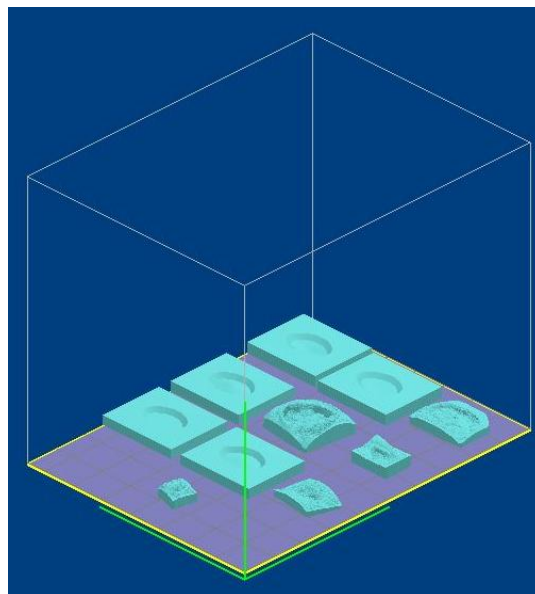


Figure 3.4: Arrangement of 3D model in solid object printer.

There is one post-processing work for the MultiJet modelling, which is removal of support material. The support material is built below the parts and the gap between materials. The entire support structures are in the form of very fine column of build material that extends from the platform up to any overhanging surface. It can be rubbed off or removed manually using finger or sand paper. For the best result, the parts can be placed into a freezer for an hour to make the support become brittle and hence much easier to remove. Fig. 3.5 shows the prototypes produced by the solid object printer.

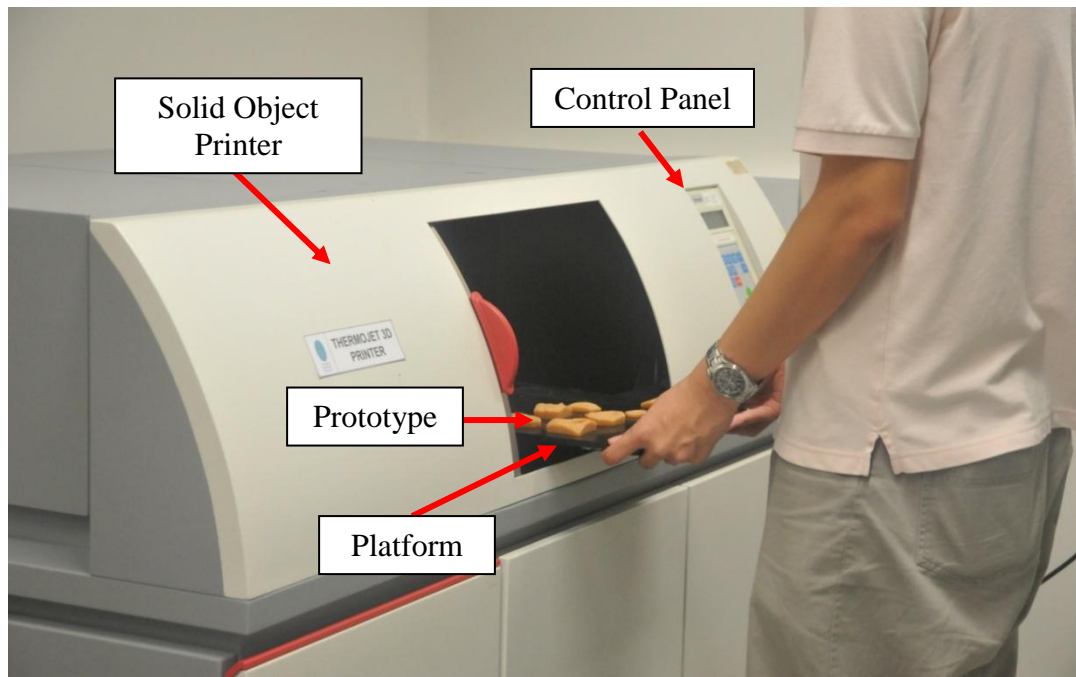


Figure 3.5: Prototype produced by solid object printer

3.1.3 Volume Computation and Data Analyzing

In the first stage of the validation of various wound attribute models with known volume, cavity volume calculated by the CAD software were served as a reference volume for comparison with three different volume measurement approaches.

The first method is using the conventional method for volume measurement i.e. saline injection and mould material. Wax mould material was chosen for this study as saline injection requires water which having high adhesive surface tension properties that resulted inflate surface area and inaccurate measurement. In addition, water with its adhesive property is not suitable for high curvature wound especially in the lower extremes part as water tends to leak out from the wound and affect the accuracy of the measurement.

Second and third methods are using reverse engineering tools to obtain geometrical information of prototype. Laser triangulation and structured light data acquisition techniques are two of the most common techniques in reverse engineering to obtain

CAD of an object. These two techniques were selected to capture 3D skin surface images. Midpoint projection and convex hull approximation are two methods to reconstruct the estimated surface and followed with the volume computation.

3.1.3.1 Conventional Method

Mould material (plasticine) is a flexible material that can be shaped into any shape. Hence, it was selected as the medium for the conventional approach rather than saline. In this section, a description of how the measurement results using mould material are explained. Before the measurements are performed, the electronic balance is set-up and it must be calibrated in order to obtain consistent and accurate measurements. The adjuster of the electronic balance is being turned until the bubble rests in the centre of the circle on the level as shown in Fig. 3.6. Once the leveling of the electronic balance is done, the volume measurement can be started. After that, the zero/tare button is pressed to reset the reading to zero to avoid an error in readings.



Figure 3.6: Securing the exact level of the balance

Once the calibration of the electronic balance is done, the volume measurement can be started. Table 3.3 illustrates the volume measurement process using mould material.

Several assumptions were made prior to the measurement:

- 1 ml of water approximately equal to 1 g
- 1 ml of water equal to 1 mm³

Table 3.3: Volume measurement process using mould material


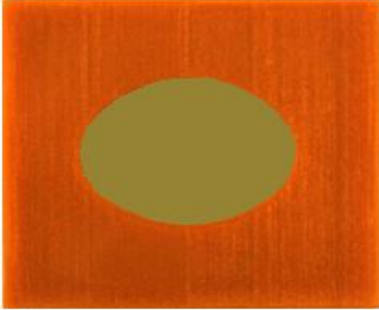
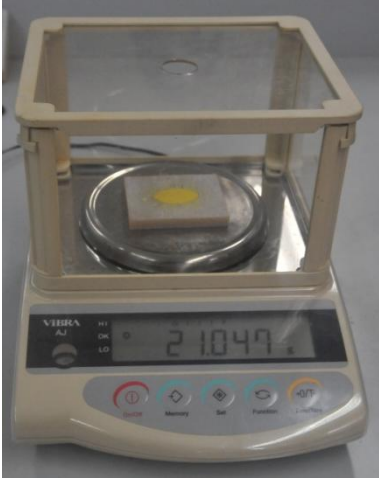
| | |
|--|---|
|  <p>Figure 3.7: The reading of empty model</p> | <p>The net weight of each model, are being measured.</p> |
|  <p>Figure 3.8: Model filled with mould material</p> | <p>After measuring the net weight of models and measuring cylinder, the models' cavities are filled with mould material.</p> |
|  <p>Figure 3.9: The reading of model which filled with mould material</p> | <p>Models filled with mould material, are being weighted and recorded. The amount of mould material is calculated by subtracting with net weight of measuring cylinder.</p> |



Figure 3.10: The mould material placed into the measuring cylinder which filled with 2ml distilled water

The amount of mould material being used is then placed into the measuring cylinder which filled with 2ml distilled water. The final reading of the volume is indicating the volume displaced

3.1.3.2 Reverse Engineering Method

Laser triangulation technique is the most common technique used to digitize and scan an object surface. It utilizes distance measurement based on similar triangles and trigonometric functions. The advantages of laser scanner is having an image which is exactly aligned with the 3D geometry and simplifying the post processing work for scanned data [79].

Capturing 3D images of leg ulcer were done using the non-contact 3D laser scanner. The procedure and risk for the 3D image capturing is same as taking a photograph. Fig. 3.11 shows the working principle of the laser scanner and it is based on the laser triangulation technique.

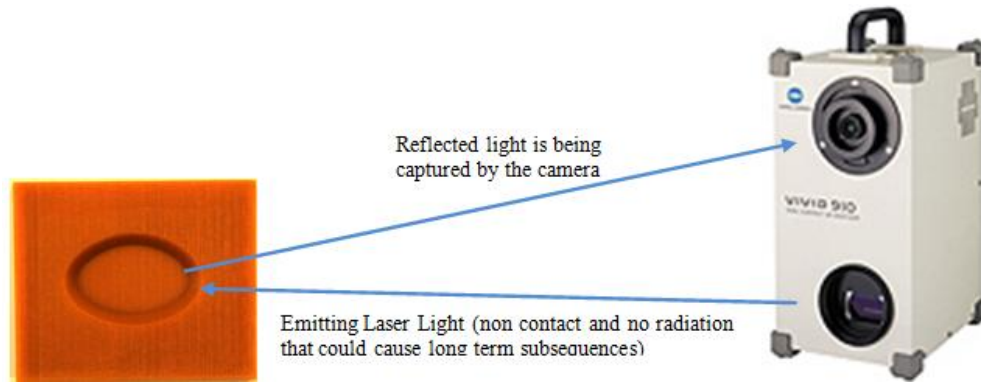


Figure 3.11: Working principle of noncontact 3D laser scanner

According to the user manual, the recommended ambient light condition is 500 lx or lesser. The ambient light condition was checked before the surface scanning process in order to obtain more accurate raw data for the wound surface. Illuminance meter was selected for measurements of a wide range of illuminance, shown in Fig. 3.12.



Figure 3.12: Illuminance meter

Fig. 3.13 shows the setup of laser scanning device. The distance from the lens of laser scanner to the prototype was always kept at 0.7 m based on the user manual. The scanned images will be very blur and the thus creating a very rough surface when the object is located further than 1.2 m. In contrast, the scanned images cannot be seen when it was too near to the scanner and thus no object will be captured.

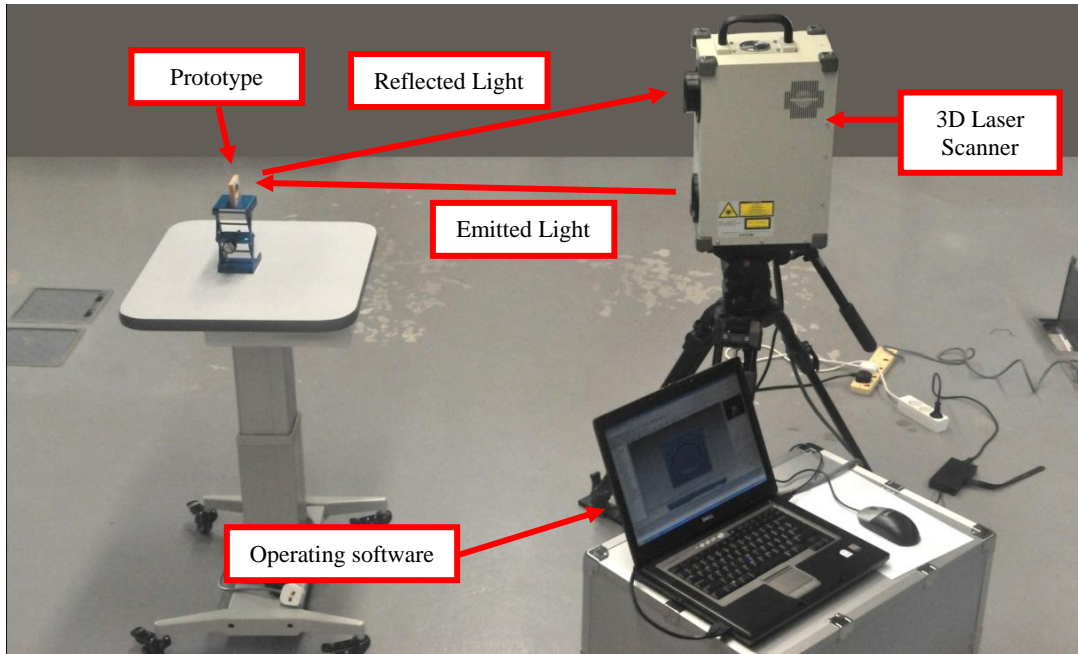


Figure 3.13: Setup for noncontact 3D laser scanner

The preliminary setup and illuminance checking were done prior to the surface scan to avoid the bad images being captured during data acquisition. By operating the laser scanner, the surface scan of the prototype is obtained.

Optical scanner is another scanner that was used to capture the surface information. The setup of optical scanner and schematic diagram is shown in Fig. 3.14 and 3.15. The working principle (Fig. 3.16) is based on structured light data acquisition technique with phase shifting method. Patterns generated from the projector are projected onto object surface and the reflective patterns are captured with a camera.

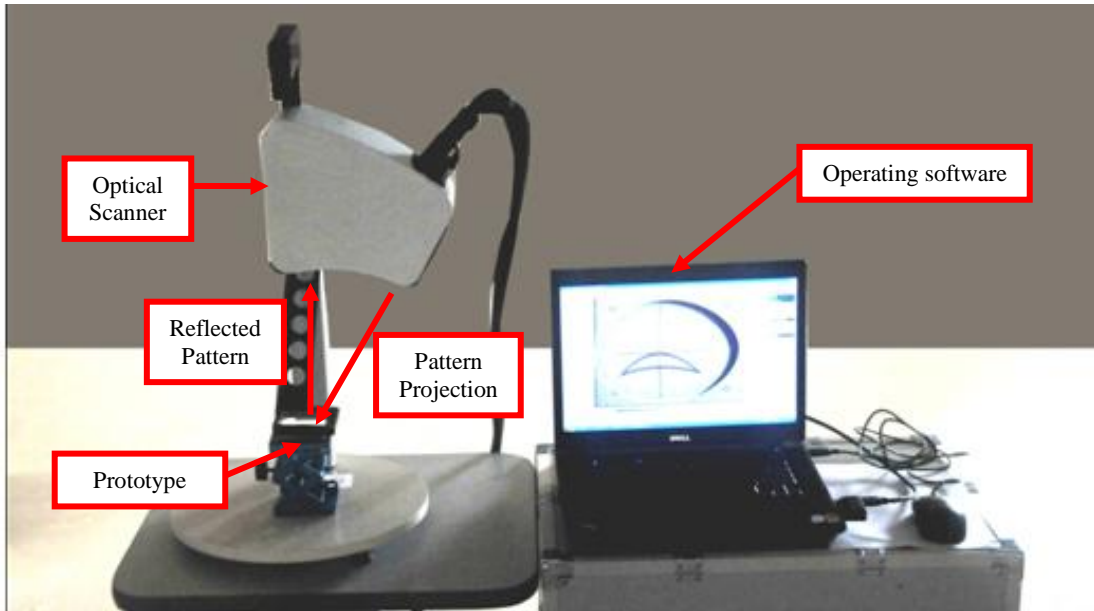


Figure 3.14: Setup of optical scanner

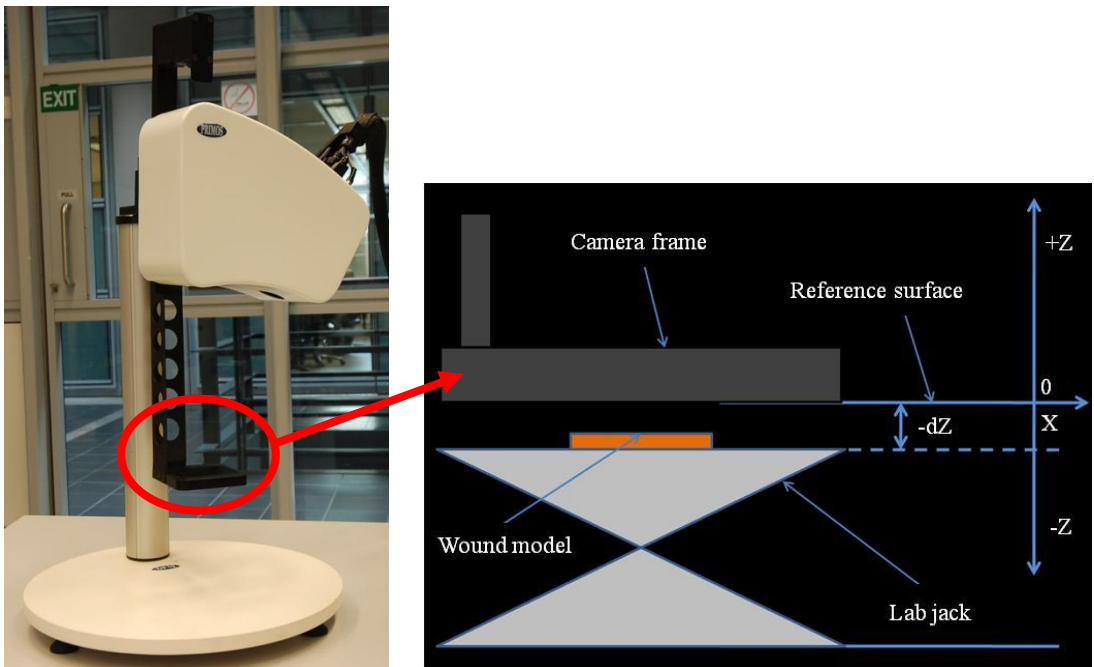


Figure 3.15: Schematic of optical scanner

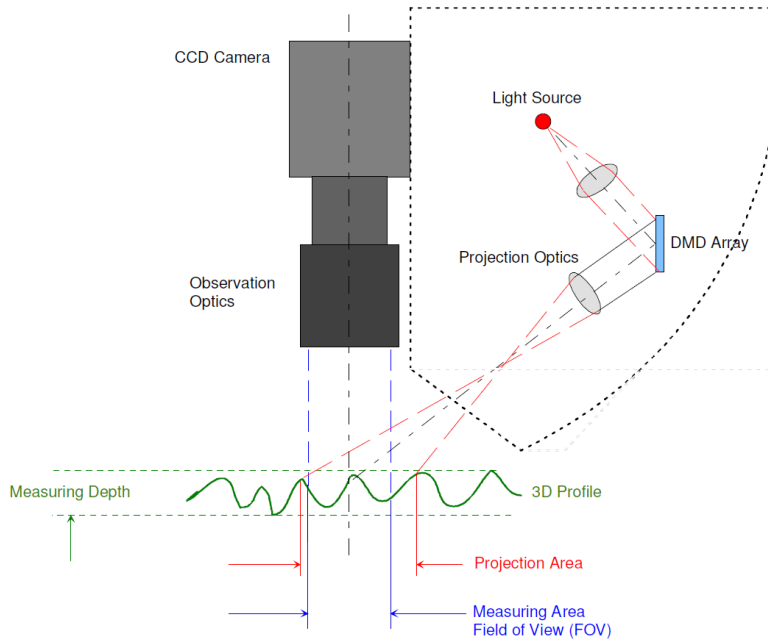


Figure 3.16: Working principle of optical scanner

Fig. 3.17 shows the deviations of the patterns which represents the changes in object's height. Prior to the surface scan, the object is required to be in the well focused position. Fig. 3.18 shows the correct position where the projected crosshair and a blended in crosshair appeared on the screen in order for the target object being focused.

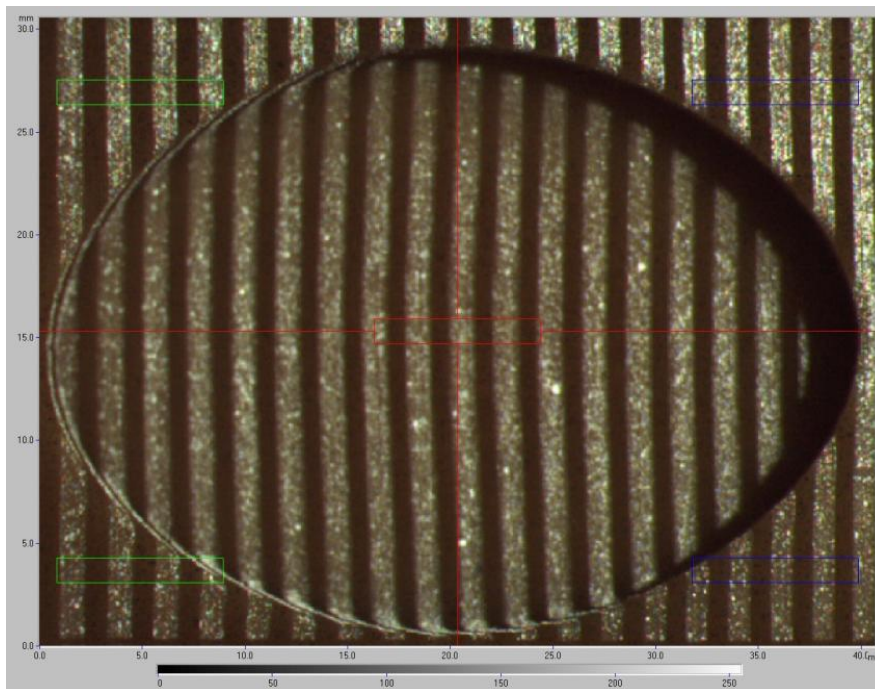


Figure 3.17: Fringe pattern on targeted object

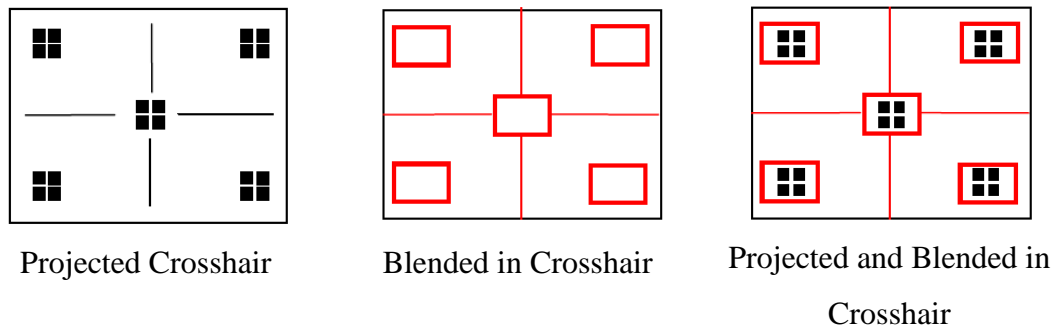


Figure 3.18: The correct position for the object being focused

The position of the projected crosshair is required to be within the blended in crosshair, indicating the object is being focused. Fig. 3.19 shows the example of the item to be measured and the position of crosshair in focus. The recommended distance of the camera frame to the deepest base of the object, dZ is 8 mm or less. The distance larger than 8 mm is considered out of focus. Throughout this research, optical scanner used as alternative equipment for the data acquisition and comparative studies between laser triangulation with structured light technique.

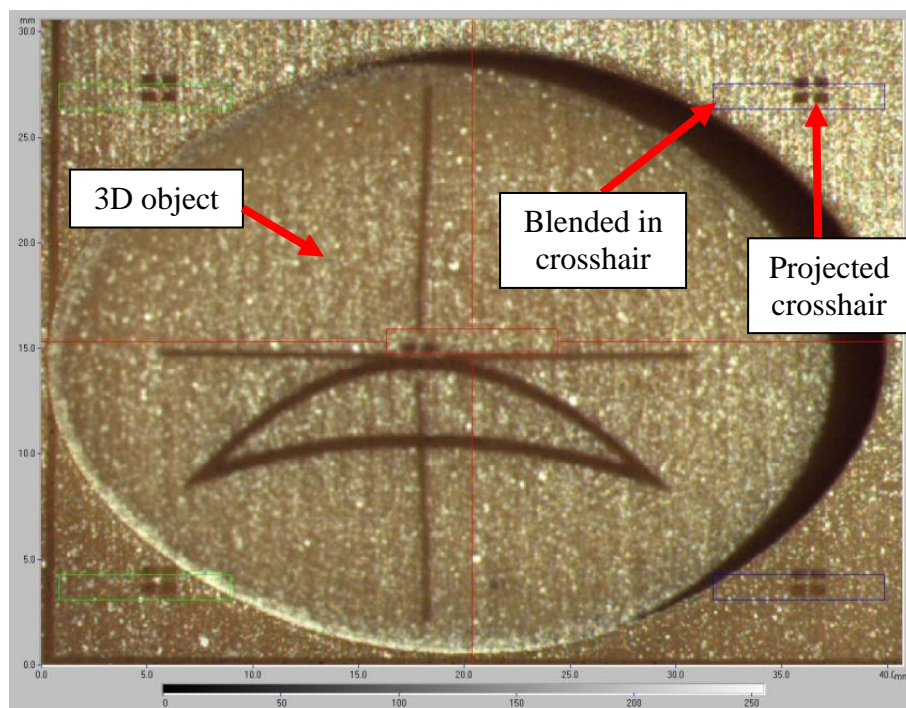
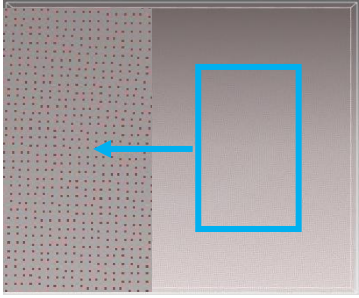
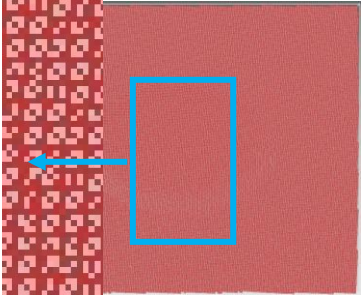
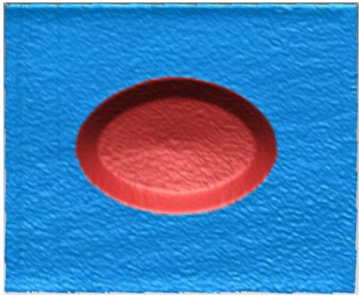
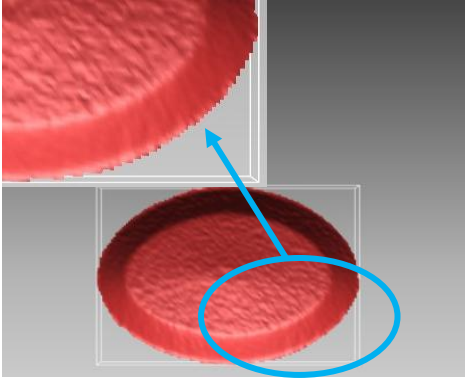
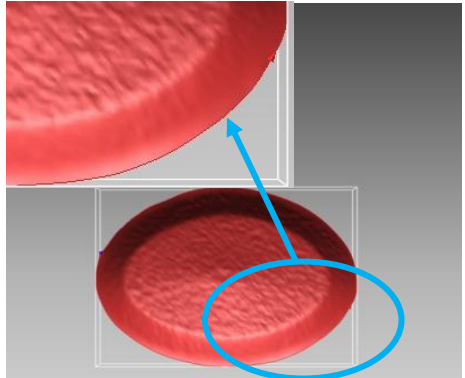


Figure 3.19: Operating system and image focusing to perform surface scan

The surface information was digitized using these two techniques and it is in the form of points. The entire points cloud will undergo the process of data processing which including sampling, aligning, merging multiple points, hole filling and smoothing. Table 3.3 shows the process of point processing prior to the volume computation.

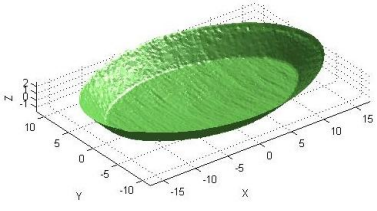
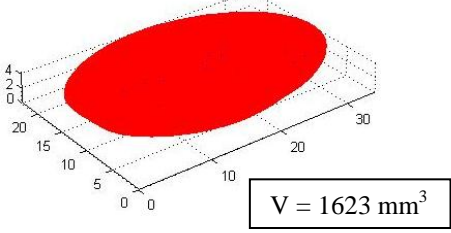
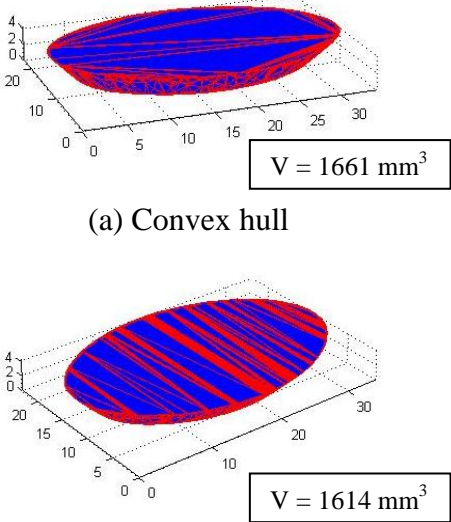
Table 3.4: Steps of data processing

| | |
|--|--|
|  <p>Figure 3.20: Points cloud</p> | <p>Cloud of points is generated by digitizing or scanning of an object.</p> |
|  <p>Figure 3.21: Triangulation mesh</p> | <p>The process of points connected in triangles/quadrilaterals (in two dimensions) or tetrahedra/hexahedral bricks (in three dimensions) which form the triangulation mesh called meshing.</p> |
|  <p>Figure 3.22: Boundary selection</p> | <p>The model cavity and flat surface should be distinguished and the cavity is cropped out carefully for cavity volume measurement purpose.</p> |

| | |
|---|--|
|  <p data-bbox="300 622 766 654">Figure 3.23: Zigzag boundary shape</p> | <p data-bbox="813 259 1385 618">Due to the characteristic of CAD file being in a triangulation mesh form, the cropped models show irregular boundary and zigzag shape which is shown in Fig. 3.23, However, it might introduce some overestimation in volume and it needs to be removed.</p> |
|  <p data-bbox="300 1131 766 1162">Figure 3.24: Fit boundary to curves</p> | <p data-bbox="813 799 1385 1104">Fit boundary to curve function is used to rearrange or clean the boundary meshes by curves. This operation can be used for repairing the boundary edges of a model that may have been introduced during the scanning process.</p> |

Before computing the volume, a solid model must be reconstructed from a surface scan. Two methods were used to reconstruct the solid model from the cropped cavity volume, which are midpoint projection and convex hull approximation. Each method reconstructs the surface to form a solid in a different way. The working principle of midpoint projection was discussed in section 2.5.1 whereas convex hull approximation was discussed in section 2.5.2. The suitability of each method toward the wound attributes will be figured out. Table 3.4 shows the surface reconstruction using midpoint projection and convex hull approximation methods.

Table 3.5: Surface reconstruction prior to volume computation

| | |
|--|--|
|  <p>Figure 3.25: Prototype model RSD3D1</p> | <p>The reconstructed surface for the cropped model cavity is generated with two selected methods (midpoint projection and convex hull approximation). Fig. 3.25 shows the isometric view of the model.</p> |
|  <p>Figure 3.26: Surface reconstruction using midpoint projection</p> | <p>Midpoint projection method reconstructs the surface by connecting all the points in the model to the calculated midpoint to form tetrahedral. The volume of the model cavity is calculated by summing up total volume of tetrahedral generated.</p> |
|  <p>(a) Convex hull</p> <p>(b) Convex hull with surface division 10x</p> <p>Figure 3.27: Surface reconstruction using convex hull approximation</p> | <p>Surface reconstruction using convex hull is created by connecting the farthest vertices around the surface and the resulting shape will not take account of all vertices in the original shape. The original model is divided into several divisions as predetermined form user to gives better approximation in terms of volume. The volume of the model cavity is calculated by summing up total volume of tetrahedral generated.</p> |

3.1.4 Volume measurement of Ulcer Wound Model

The results obtained from the validation of various wound attributes are very important to ensure the entire process and system produces consistent and desirable result over a period of time. The results also serve as a guideline to analyze ulcer wound model whereas the best method validated from the validation stage are used to establish the accuracy of leg ulcer wound volume determination. Figure 3.28 represents the flow of the real case study analysis.

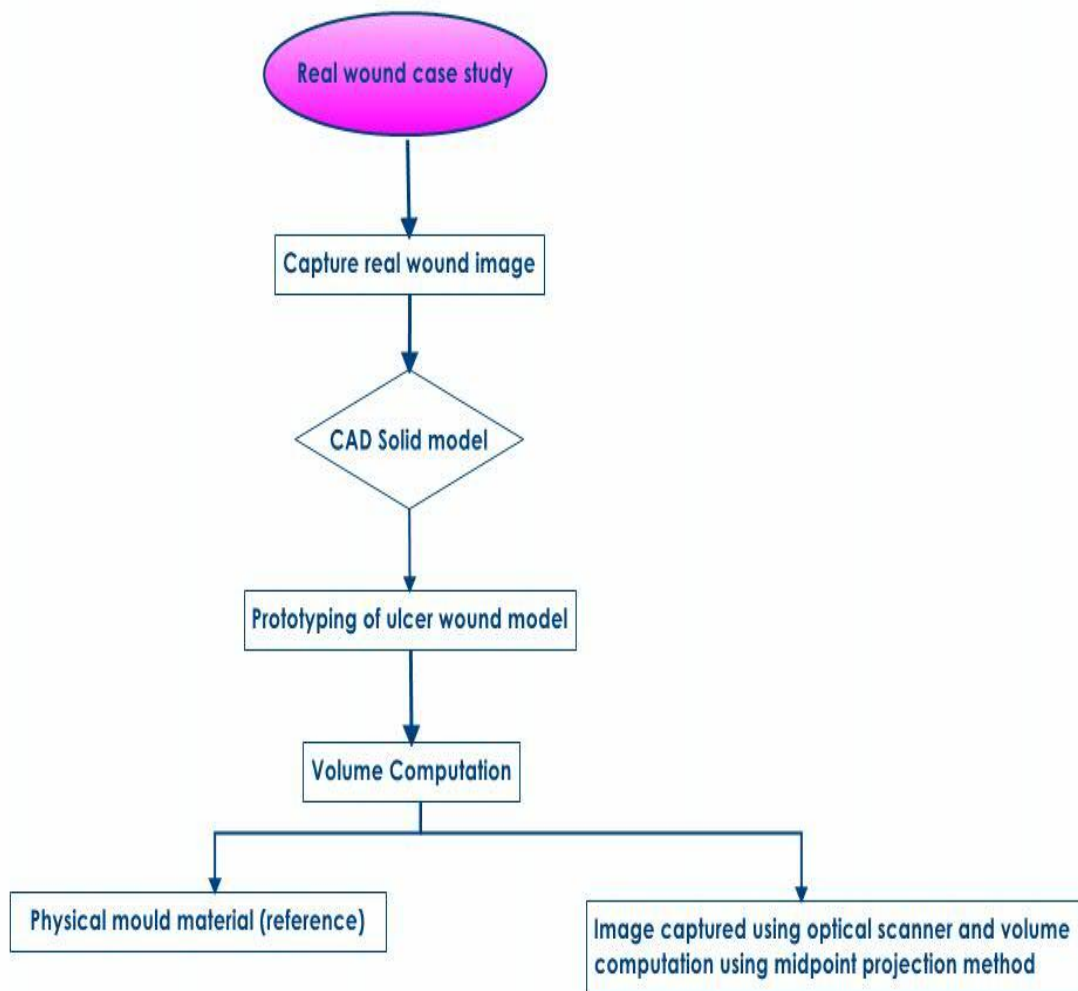


Figure 3.28: Real Wound Case Study Flow

3.1.5 Leg Ulcer Wound and Data Acquisition of Leg ulcer

Leg ulcers generally classified into 4 categories, which are venous, arterial, combined venous with arterial and neuropathy ulcer. The target population of this research was adult patients attending the Dermatology Clinic, Department of Dermatology Hospital Kuala Lumpur and the Outpatient Department Hospital Kuala Lumpur with diagnosis of chronic leg ulcer of any cause. Among all the patients with chronic ulcers, only patients age 18 years old and older, who were able to give consent will be selected for the research. Sample of consent form was attached in Appendix B. The targeted wounds dimension was smaller than 5 cm x 6 cm.

Data collection was carried out using a non-contact 3D scanner and a DSLR camera to provide 3D surface scans and 2D coloured images of ulcers. 2D coloured images were required for a record regarding the ulcer colour and appearance. 3D surface scans were needed to investigate the accuracy of the proposed approach in measuring ulcer cavity volume (in mm³) with different scanning techniques.

There was no clinical intervention. This study was involved digital photography and 3D images of leg ulcers. There were no expected risks, discomfort and radiation that could cause long term consequences associated with the study. The procedure and risk for taking the 3D images were similar to normal daily photography.

Twenty three patients with consent were involved in this research to provide twenty six 3D scanned images of leg ulcer. Laser scanner was used to perform surface scan of leg ulcers. The equipment was set-up in a particular room in HKL as shown in Fig. 3.29. It is the same equipment which using in the laboratory for the validation stage.

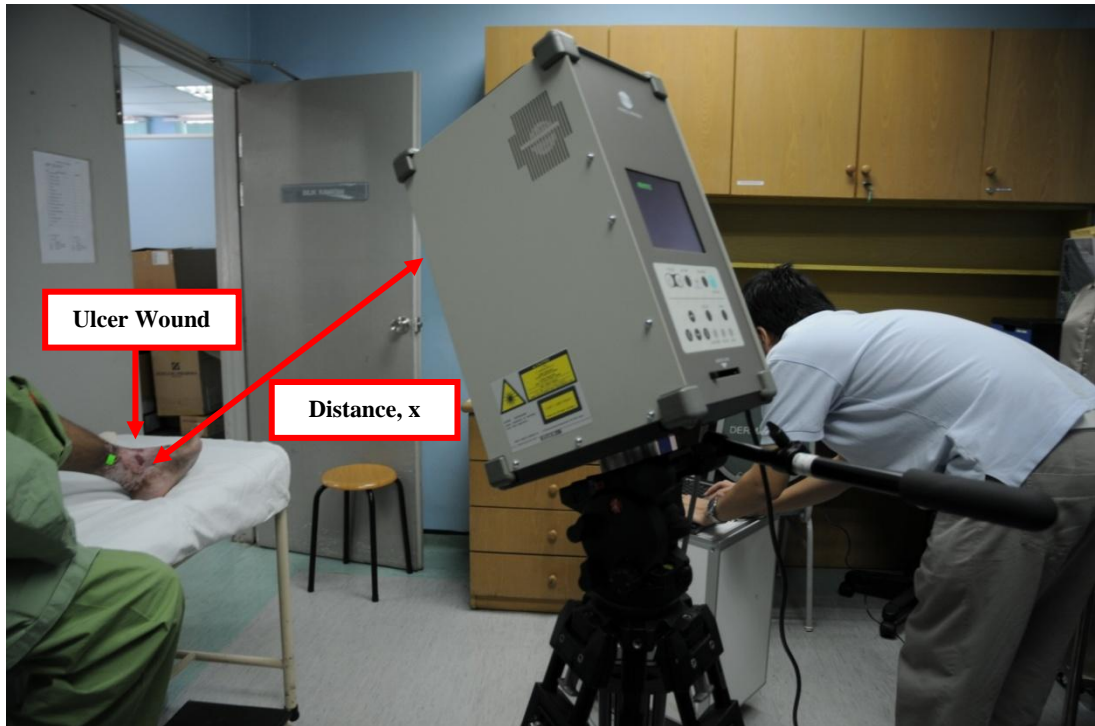


Figure 3.29: Equipment set-up in HKL

Patients were advised to lie down on the bed in their most comfortable position before the photography and scanning on leg ulcer. After the patient had found the most comfortable position to lie down, the photograph and 3D surface of the ulcer was taken using non-contact 3D laser scanner. Collection of data was performed according to the methodology stated. The images collected in Hospital Kuala Lumpur were stored in a particular laptop which is only accessible by the doctors and the researchers involved.

3.1.6 Image Processing and STL Format Conversion

As mentioned above, the scanned data was in the points of cloud. Processing has to be done prior to application of the CAD model. Image processing works includes triangulation meshing, noise removal (deleting spikes, and small clusters) and aligning.

Natural scanned surfaces have no thickness. It is necessary for the surface scan to form a solid model prior to producing a prototype. In 3D scanning software, extrusion operation was used to convert open shells that do not bound volume into a closed solid model. This operation allowed the surface scan of leg ulcer to extrude to the specific plane (reference plane) to form a solid model as depicted in Fig. 3.30. After that, 3D solid models were saved in STL format file as it was the only input for rapid prototyping.

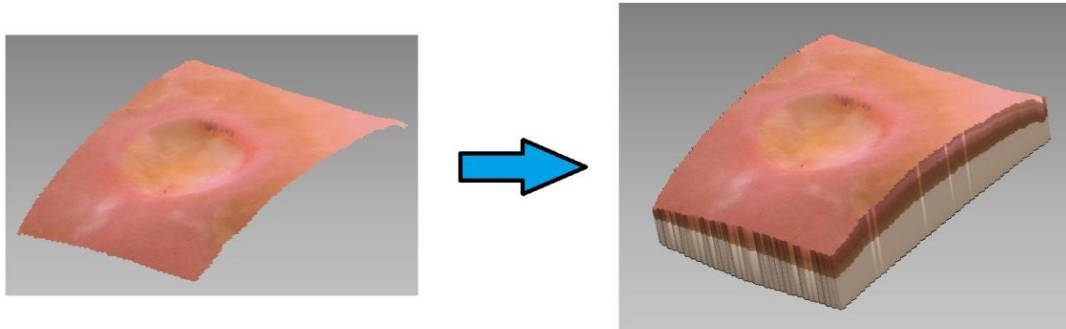


Figure 3.30: Extrusion operation to form a leg ulcer solid model

3.1.7 Prototyping of Ulcer Wound Model

For research purposes, alginate mould and saline injection are often used for leg ulcer volume measurement. However, these techniques are invasive and might bring infection and discomfort to the patient. In this research, the methodology was to avoid any direct contact between the instrument (and material used) and the patient. In total, 26 wound prototypes were produced by the solid object printer which was used to achieve the objectives of this research. The procedures to build an ulcer wound prototype were listed in section 3.1.2.

3.1.8 Volume Computation and Data Analyzing

Unlike to the validation stage in section 3.1.3, only two approaches were used for volume measurement, which were the Archimedes method by using plasticine and the reverse engineering method by using structured light technique. In previous stages,

cavity's volume was generated when designing for models with different attributes using CAD modelling software. The generated volume serves as the reference volume. In volume measurement of ulcer wound model, volume was computed using mould material and served as the reference volume to verify the accuracy of structured light technique.

3.2 Summary

This chapter explains in details the steps and consideration taken in the methodology of volume measurement of ulcer wound. At the beginning, four wound attributes were being identified to assist the assessment of leg ulcer, which were the boundary shape, edge, base and depth. Three dimension models were being modelled by combination of four wound attributes. The volumes computed from CAD modelling software were served as reference value for the accuracy comparison. In total, seventeen wound attributes models with known volume prototype were built for the validation stages. The prototypes was scanned and digitized to obtain the surface information and hence creating the triangulation mesh to regenerate CAD model of the prototype. Two different data acquisition method was used to acquire the surface information, which are the laser triangulation and structured light technique. Pre-determine the model boundary processing was needed and prepared for volume computation. Surface reconstruction of the cropped area was performed using midpoint projection and convex hull method to create the solid model for the cavity. Midpoint projection method creates the midpoint from the border edges. Tetrahedral were formed by connecting all the points to the generated midpoints and the total volume was measured by summing up the volume of each tetrahedron. In contrast, surface division prior to convex hull approximation divide the model into several partitions as determined by the user. By connecting the furthest vertices around the surface, the smallest bounding polyhedron was formed and total volume is measured by total up the tetrahedral volume. The methods listed above were using the 3D skin surface imaging technique. Conventional measuring method which fills the model cavity with mould material and weighing the amount of material used was also used in this

research for comparison purpose. The entire material was placed into a beaker where the water dispensed from beaker indicates the cavity volume.

The second stage of the volume measurement was performed on wound ulcer model. Ulcer surface scanned were obtained from HKL and twenty three patients with consent were involved to provide twenty six ulcer wound surface scan. From the ulcers surface scan, the CAD format was then converted to the STL format to produce prototypes of ulcer wounds. Volume computation of ulcer wound models were conventional method and the best method selected from validation stage. Volume computation by conventional method was served as the reference volume. The method selected from the validation stage is use to determine the accuracy towards the ulcer wound volume measurement.

CHAPTER 4

RESULTS AND DISCUSSION

Volume computation analysis results are discussed in this chapter. In the first section, the validation results which were obtained from the application of the volume computation on different attributes model with a known volume model were discussed. The validation results are used to establish the effect or the accuracy of the data acquisition technique and volume computation method on the volume of wound attributes. Second part of this section discussed on the effect of volume measurement techniques and computation methods on the volume of real ulcer wound model. In this study, the absolute error of each model volume was used to analyze and investigate the accuracy of each method.

4.1 Volume Computation of Various Wound Attribute Models with Known

Volume

The validation process is performed on the designed models that imitate the wound attributes. As mention Section 3.1.1, seventeen various wound attribute models were built based on the advice from dermatologist. The volume for those models are known and stated in the CAD modelling software during the design process. This section shows the validation results of volume computation.

There are several factors that will directly affect the volume computation accuracy. Wound attribute is the first factor that could affect the volume computation accuracy. Hence, four main wound attributes had been classified.

Another aspect that can improve the volume assessment is the data acquisition technique. Each technique has its strength and limitation in acquiring 3D data. Hence, two data acquisition techniques, which were structured light (optical scanner) and laser triangulation (laser scanner) were used to acquire the 3D scanned surfaces. Third factor that could affect the volume computation accuracy is the volume computation method. Midpoint projection (refer to Section 2.5.1) and convex hull approximation (refer to Section 2.5.2) are two methods that used to compute the volume cavity of the model. The strength, limitation and suitability of each method towards the wound attributes are discussed to improve the volume assessment of ulcer wound.

4.1.1 Comparison of Laser Triangulation And Structured Light Data Acquisition Technique Using Midpoint Projection Method

In this section, midpoint projection method is used for surface reconstruction followed with volume computation. The equations that were used to determine the performance of each proposed technique and also their accuracies are shown in equation 4.1 and 4.2.

$$\text{Absolute error} = |y_i - \hat{y}_i| \quad (4.1)$$

$$R^2 = \frac{SSR}{SST} = \frac{SST - SSE}{SST} = 1 - \frac{SSE}{SST} = 1 - \frac{\sum(y_i - \hat{y}_i)^2}{\sum(y_i - \bar{y}_i)^2} \quad (4.2)$$

The R^2 is highlighted in Section 2.9. It is the statistical measure of how well the regression line approximates the ideal line. An R^2 value of 1.0 show the regression line perfectly fits the ideal data. From the equation, y_i represents the volume measured for each model. \hat{y} is the reference volume (obtained from the 3D modeling software) for each model and \bar{y} representing mean value for the measured volume.

Volume measurement for each technique is repeated three times and the average of the measured value is obtained. Table 4.1 shows the results of volume computation

using the midpoint projection method. The absolute error of each data acquisition technique is also stated in this table. Fig. 4.1 shows the absolute error of volume computed using midpoint projection method for both sets of scanned surfaces.

Table 4.1: Volume computation using midpoint projection

| Model | Reference Value, \hat{y} (mm ³) | Optical Scanner | | Laser Scanner | |
|--------|---|---|----------------|---|----------------|
| | | Measure Value, y_i (mm ³) | Absolute Error | Measure Value, y_i (mm ³) | Absolute Error |
| IRSD1H | 363 | 371 | 8 | 391 | 28 |
| RSD5E1 | 2673 | 2683 | 10 | 2706 | 33 |
| RPO1H | 361 | 371 | 10 | 384 | 23 |
| RSD1H | 397 | 408 | 11 | 423 | 26 |
| RSD3E1 | 1284 | 1306 | 22 | 1308 | 24 |
| RPO3H | 1082 | 1108 | 26 | 1113 | 31 |
| IRSD3H | 1317 | 1348 | 31 | 1351 | 34 |
| RSD3H | 1428 | 1462 | 34 | 1468 | 40 |
| RSD5H | 2816 | 2856 | 40 | 2892 | 76 |
| IRSD5H | 2618 | 2666 | 48 | 2726 | 108 |
| RSD3D1 | 1571 | 1623 | 52 | 1624 | 53 |
| RSD3D2 | 1713 | 1765 | 52 | 1770 | 57 |
| RSD5E2 | 2530 | 2591 | 61 | 2617 | 87 |
| RSD5D1 | 2960 | 3034 | 74 | 3041 | 81 |
| RSD5D2 | 3102 | 3191 | 89 | 3200 | 98 |
| RSD3E2 | 1141 | 1237 | 96 | 1269 | 128 |
| RPO5H | 1803 | 1951 | 148 | 1921 | 118 |

Indicator:

R = Regular Boundary
IR = Irregular Boundary

SD# = Sloped Edge
PO# = Punched Out Edge
= Height

E# = Elevated Base
H = Homogeneous Base
D# = Depressed base

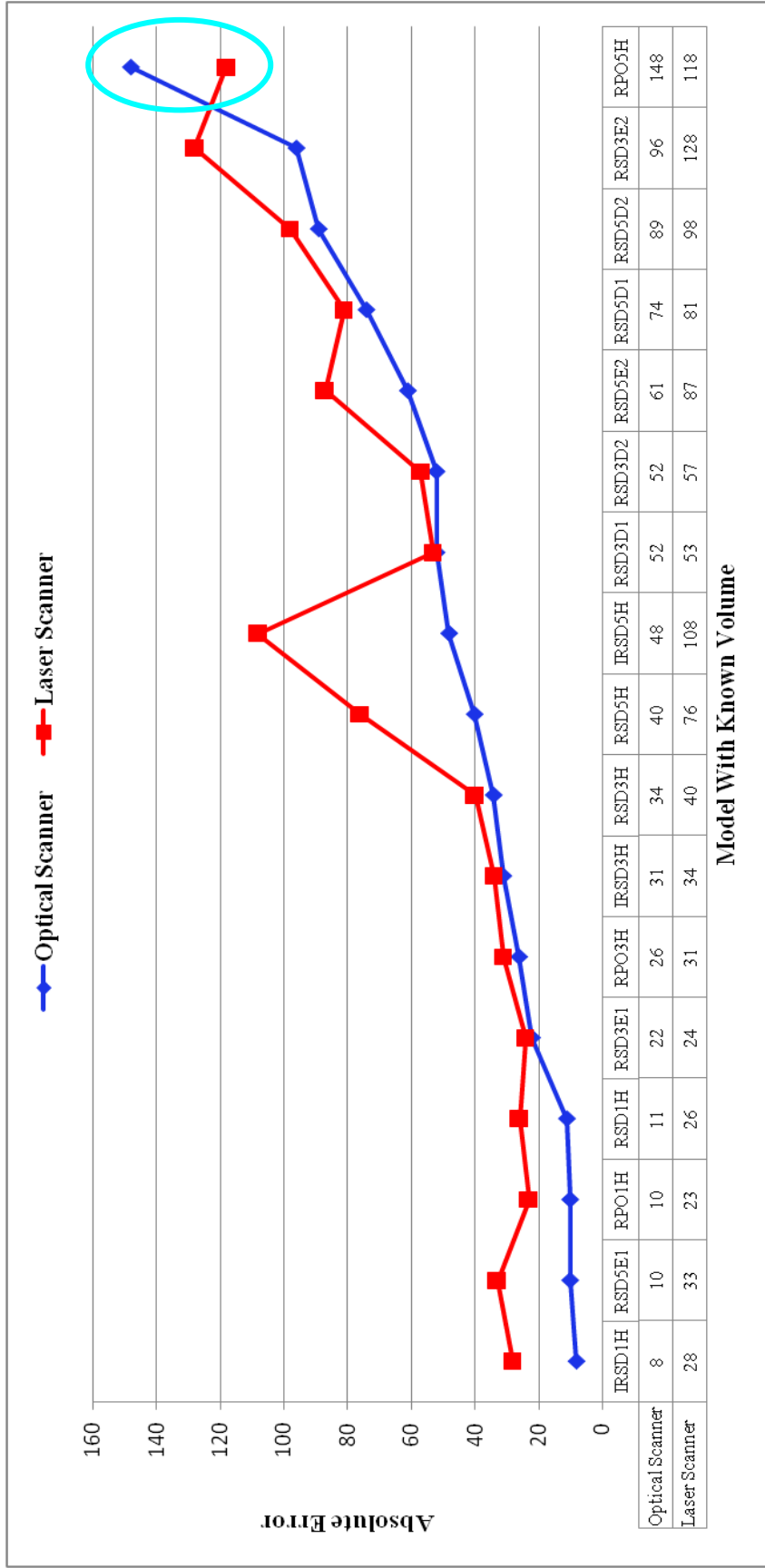


Figure 4.1: Absolute error of volume computed using midpoint projection

Fig. 4.1 shows the midpoint projection results obtained by using optical and laser scanner respectively. Most of the model except RPO5H gives less absolute error when optical scanner used. Optical and laser scanner shows R^2 value at 0.9957 and 0.9940 respectively. RPO5H model (regular shape, punched out edge with 5mm depth and homogeneous base) has the significant absolute error for both image taken by optical scanner and laser scanner. This is because a shadow appeared when projection angle over the boundary occurring over a large area which leads to miscalculation of volume. Hence, this model is an outlier data which is neglected. Fig. 4.2 shows how the partial area of the model is blocked by its shadow

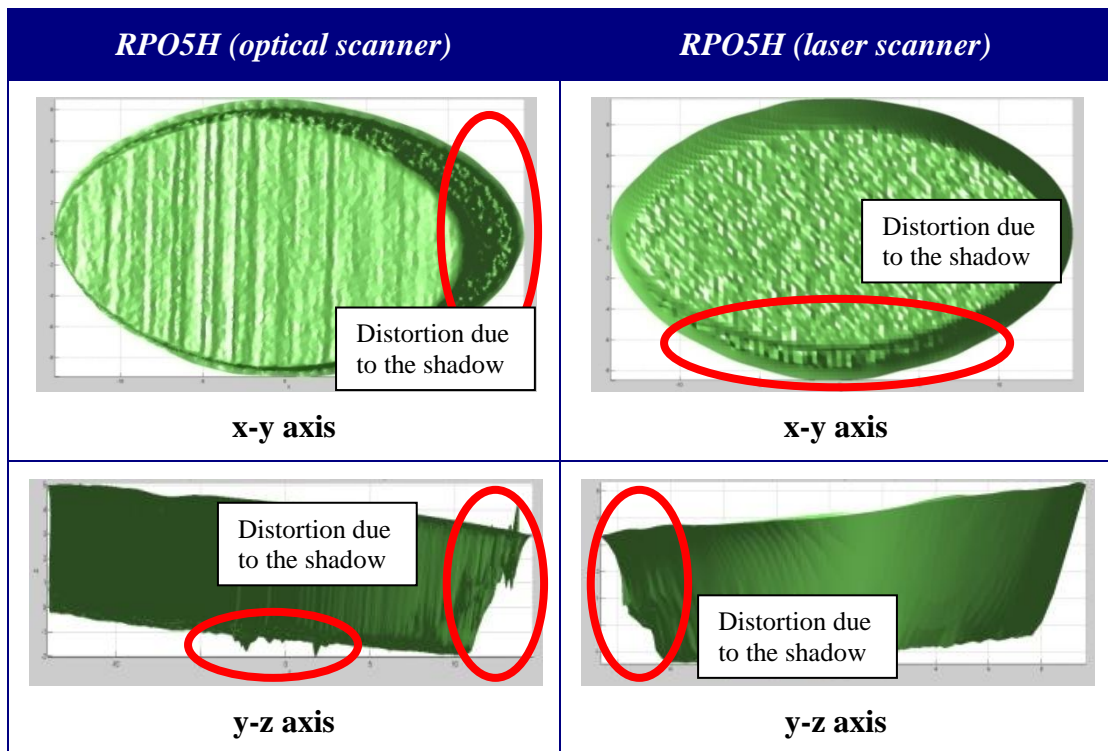


Figure 4.2: Visual inspection on RPO5H model

4.1.2 Comparison of Laser Triangulation And Structured Light Data Acquisition Technique Using Convex Hull Approximation Method

Convex hull approximation method is used in this section for surface reconstruction and volume computation. Surface division is applied to overcome the overestimation

in volume. Volume measurement for each technique is repeated three times and the average of the measure value is recorded. Table 4.2 shows example of 5 models with up to 20 surface divisions which acquired using optical scanner. By increasing the surface division, it shows the decrease in volume. However, there is a challenge in selecting the suitable surface division for each model. Based on the statistical analysis, the process is terminated when it reach to the saturation point. In our studies, saturation point refers to the stage where the volume of the surface division decreased steadily or remains unchanged. Generally, each model has started to reach the saturation point at 10 surface divisions. Different in model's shape, edge, base and total depth will affect the saturation point. By using the statistical analysis, the overall saturation point can be obtained by taking the mean value from 10 to 20 surface divisions.

Table 4.3 gives the result of each model's volume computed using convex hull approximation with surface division. Equation 4.2 is used to calculate the R^2 . Optical shows the highest value of R^2 which at 0.9876 whereas laser scanner shows the R^2 value at 0.9702.

Fig. 4.3 represents a comparison of the response from convex hull approximation method by using laser scanner and optical scanner. It is clearly seen that the absolute error from optical scanner always smaller than laser scanner. However, there are some exceptions which highlighted in Fig. 4.3. Three models show unexpected result in the graph, which were RSD3E1, RSD3E2 and RSD5E2. These three models have the same attributes of regular shape and sloped edge except for the total depth and base height. The difference between these three models with other models is elevated base while other models having depressed and homogenous base. This is the drawback of using convex hull approximation and it can be explained using Fig. 4.4 and Fig. 4.5.

Table 4.2: Example of 20 surface division for 5 models

| Model | Surface Division | | | | | | | | | | | | | | | | | | | |
|--------|------------------|------|------|------|------|------|------|------|------|------|------|------|------|------|------|------|------|------|------|------|
| | 1 | 2 | 3 | 4 | 5 | 6 | 7 | 8 | 9 | 10 | 11 | 12 | 13 | 14 | 15 | 16 | 17 | 18 | 19 | 20 |
| RSD1H | 440 | 422 | 409 | 405 | 402 | 401 | 399 | 397 | 399 | 396 | 396 | 395 | 394 | 393 | 392 | 392 | 392 | 390 | 390 | 389 |
| RSD1H | 442 | 426 | 410 | 408 | 405 | 402 | 401 | 402 | 398 | 398 | 397 | 397 | 396 | 395 | 393 | 394 | 394 | 392 | 392 | 391 |
| RSD1H | 441 | 424 | 410 | 407 | 403 | 401 | 400 | 401 | 397 | 397 | 396 | 396 | 394 | 393 | 392 | 393 | 392 | 390 | 390 | 389 |
| RSD3E2 | 1519 | 1496 | 1478 | 1469 | 1466 | 1468 | 1464 | 1461 | 1456 | 1455 | 1455 | 1453 | 1452 | 1450 | 1448 | 1449 | 1448 | 1445 | 1445 | 1445 |
| RSD3E2 | 1520 | 1497 | 1480 | 1470 | 1469 | 1470 | 1465 | 1462 | 1459 | 1457 | 1456 | 1455 | 1454 | 1452 | 1451 | 1450 | 1450 | 1448 | 1447 | 1445 |
| RSD3E2 | 1521 | 1497 | 1481 | 1471 | 1470 | 1471 | 1466 | 1464 | 1460 | 1459 | 1458 | 1456 | 1456 | 1453 | 1452 | 1452 | 1452 | 1449 | 1449 | 1448 |
| RSD3E1 | 1493 | 1442 | 1421 | 1408 | 1416 | 1403 | 1399 | 1396 | 1395 | 1393 | 1390 | 1390 | 1388 | 1385 | 1385 | 1382 | 1381 | 1380 | 1378 | 1378 |
| RSD3E1 | 1494 | 1443 | 1421 | 1408 | 1415 | 1403 | 1398 | 1396 | 1395 | 1393 | 1390 | 1389 | 1388 | 1385 | 1384 | 1383 | 1381 | 1380 | 1378 | 1379 |
| RSD3E1 | 1494 | 1443 | 1422 | 1409 | 1416 | 1404 | 1399 | 1397 | 1398 | 1394 | 1392 | 1391 | 1390 | 1386 | 1386 | 1385 | 1383 | 1383 | 1380 | 1381 |
| RSD3H | 1552 | 1492 | 1476 | 1474 | 1466 | 1459 | 1459 | 1451 | 1449 | 1448 | 1446 | 1443 | 1440 | 1440 | 1440 | 1436 | 1434 | 1432 | 1431 | 1431 |
| RSD3H | 1550 | 1491 | 1474 | 1473 | 1463 | 1458 | 1456 | 1452 | 1449 | 1446 | 1446 | 1443 | 1441 | 1439 | 1440 | 1436 | 1435 | 1434 | 1432 | 1430 |
| RSD3H | 1551 | 1492 | 1472 | 1471 | 1464 | 1456 | 1454 | 1449 | 1447 | 1445 | 1443 | 1440 | 1438 | 1436 | 1437 | 1433 | 1431 | 1431 | 1427 | 1428 |
| RSD3D1 | 1659 | 1642 | 1625 | 1620 | 1618 | 1615 | 1613 | 1612 | 1610 | 1609 | 1609 | 1606 | 1605 | 1603 | 1602 | 1603 | 1601 | 1598 | 1600 | 1594 |
| RSD3D1 | 1660 | 1644 | 1629 | 1622 | 1619 | 1618 | 1615 | 1614 | 1614 | 1611 | 1610 | 1609 | 1609 | 1605 | 1604 | 1605 | 1604 | 1603 | 1602 | 1598 |
| RSD3D1 | 1661 | 1646 | 1630 | 1625 | 1621 | 1620 | 1616 | 1617 | 1614 | 1614 | 1612 | 1611 | 1610 | 1607 | 1606 | 1608 | 1605 | 1603 | 1602 | 1601 |

Table 4.3: Volume computation using convex hull approximation

| Model | Reference Value, \hat{y} (mm ³) | Optical Scanner | | Laser Scanner | |
|--------|---|---|----------------|---|----------------|
| | | Measure Value, y_i (mm ³) | Absolute Error | Measure Value, y_i (mm ³) | Absolute Error |
| IRSD1H | 363 | 370 | 7 | 322 | 41 |
| RSD5E1 | 2673 | 2742 | 69 | 2574 | 99 |
| RPO1H | 361 | 370 | 9 | 319 | 42 |
| RSD1H | 397 | 393 | 4 | 358 | 39 |
| RSD3E1 | 1284 | 1385 | 101 | 1251 | 33 |
| RPO3H | 1082 | 1084 | 2 | 956 | 126 |
| IRSD3H | 1317 | 1298 | 19 | 1262 | 55 |
| RSD3H | 1428 | 1437 | 9 | 1400 | 28 |
| RSD5H | 2816 | 2818 | 2 | 2600 | 216 |
| IRSD5H | 2618 | 2594 | 24 | 2594 | 24 |
| RSD3D1 | 1571 | 1605 | 34 | 1504 | 67 |
| RSD3D2 | 1713 | 1687 | 26 | 1511 | 202 |
| RSD5E2 | 2530 | 2766 | 236 | 2696 | 166 |
| RSD5D1 | 2960 | 2956 | 4 | 2759 | 201 |
| RSD5D2 | 3102 | 3144 | 42 | 2817 | 285 |
| RSD3E2 | 1141 | 1451 | 310 | 1353 | 212 |
| RPO5H | 1803 | 1826 | 23 | 1578 | 225 |

Indicator:

R = Regular Boundary
IR = Irregular Boundary

SD# = Sloped Edge
PO# = Punched Out Edge
= Height

E# = Elevated Base
H = Homogeneous Base
D# = Depressed base

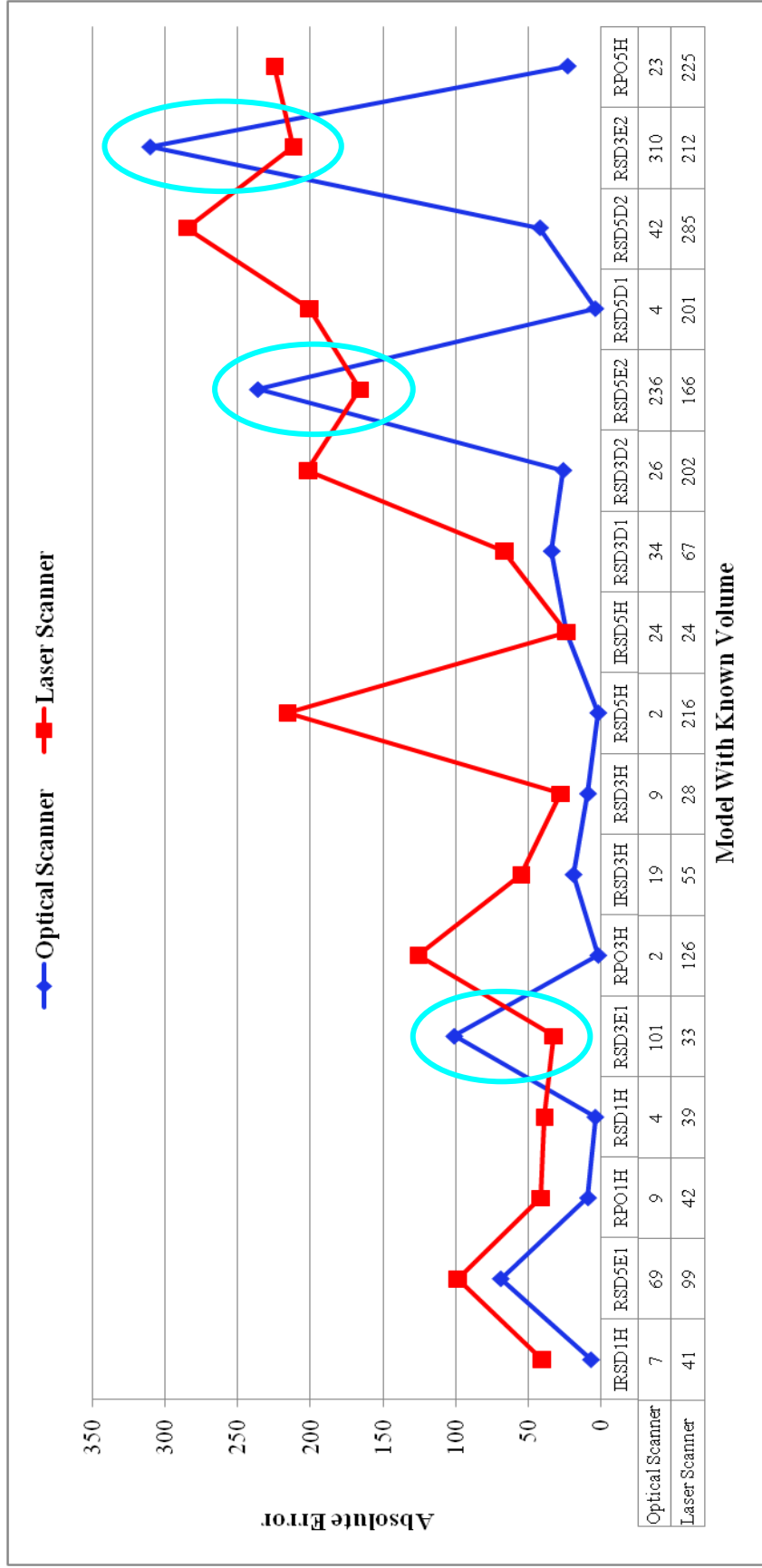


Figure 4.3: Absolute error of volume computed using convex hull method

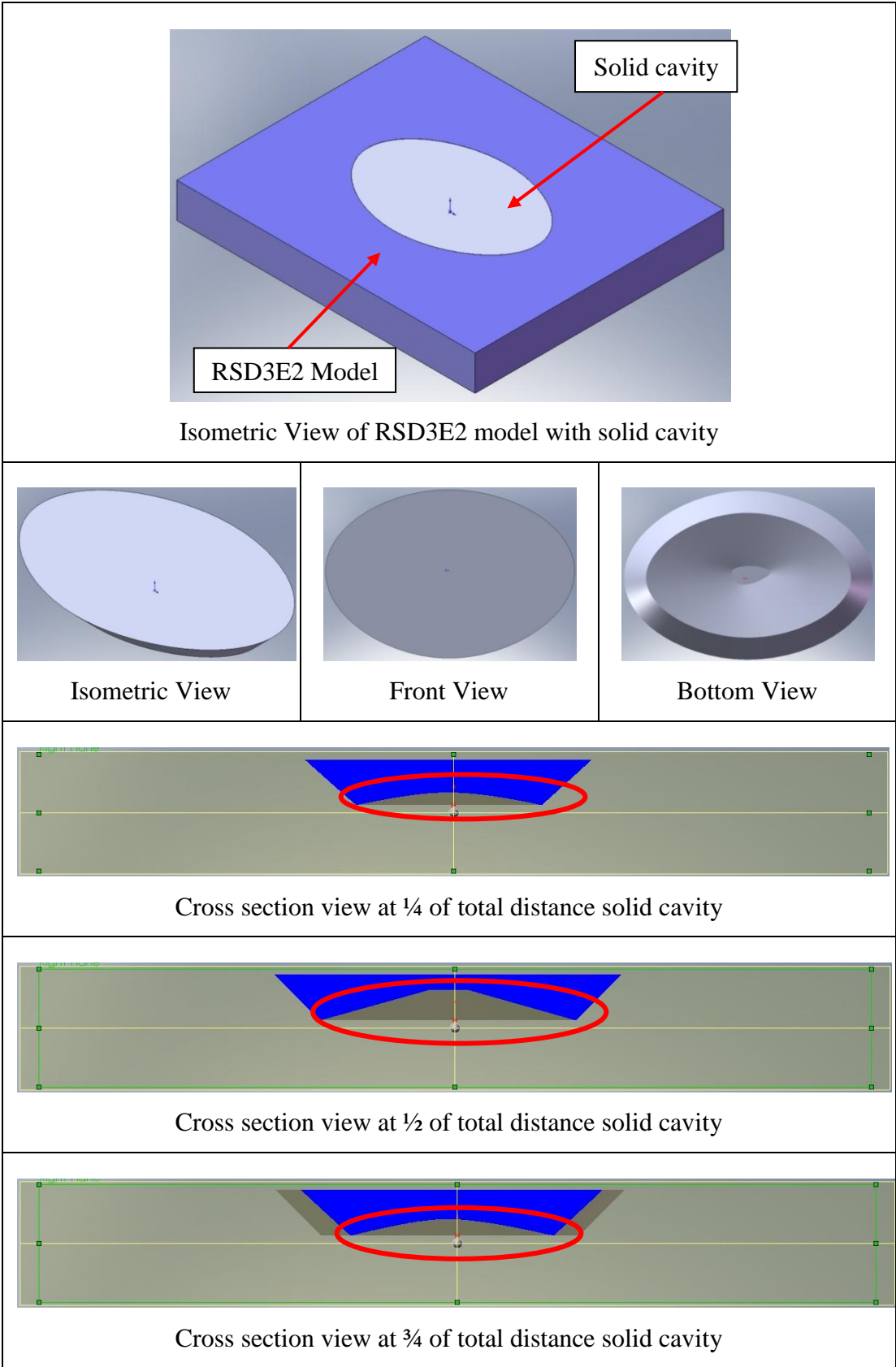


Figure 4.4: Multiple view of the estimated RSD3E2 solid cavity

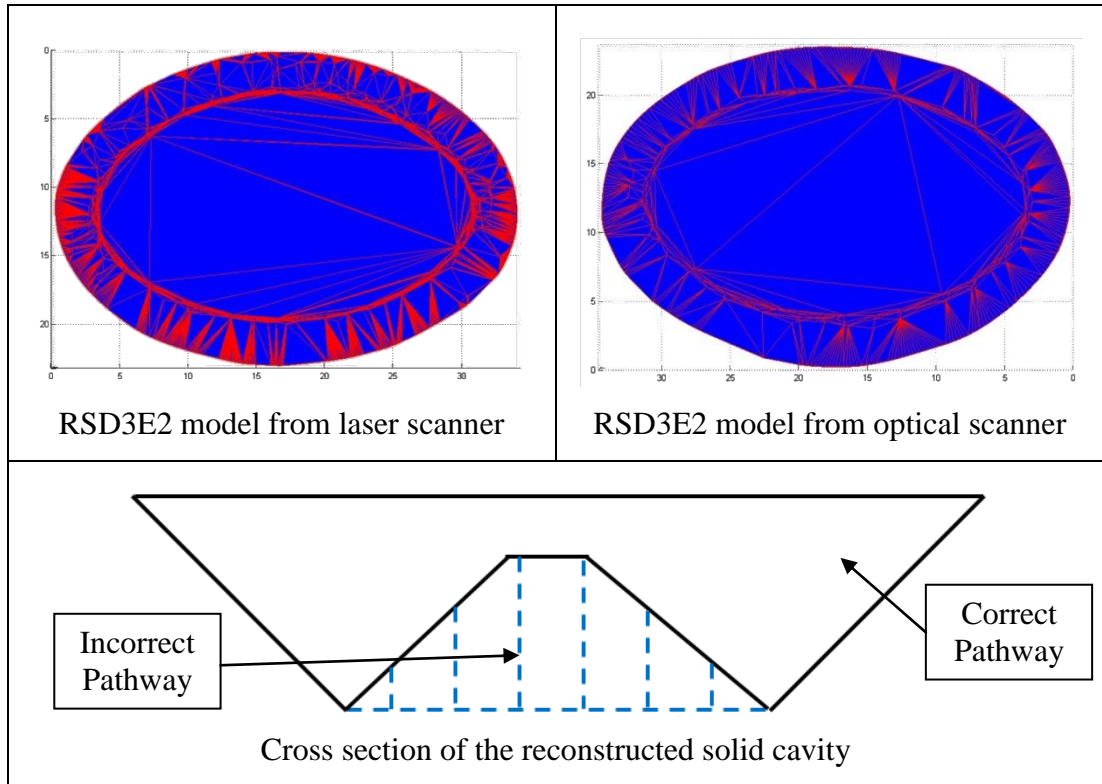


Figure 4.5: Reconstructed RSD3E2 solid cavity using convex hull approximation

Fig. 4.4 shows the multiple view of estimated solid cavity for model RSD3E2 whereas Fig. 4.5 represents the reconstructed solid cavity by using convex hull approximation. The base of the solid cavity is not flat and it shows curved in to the model. When the surface reconstruction by using convex hull approximation is applied to the models with elevated base, the result of wrapping is always overestimated and follows an incorrect pathway as depicted in Fig. 4.5.

Fig. 4.6 shows an example of irregular boundary shape (IRSD1H) which applies surface division prior to convex hull. Convex hull always gives overestimation in volume whereas surface division prior to convex hull approximation gives better representation of the estimated volume which results in a more accurate volume computation and reduces errors.

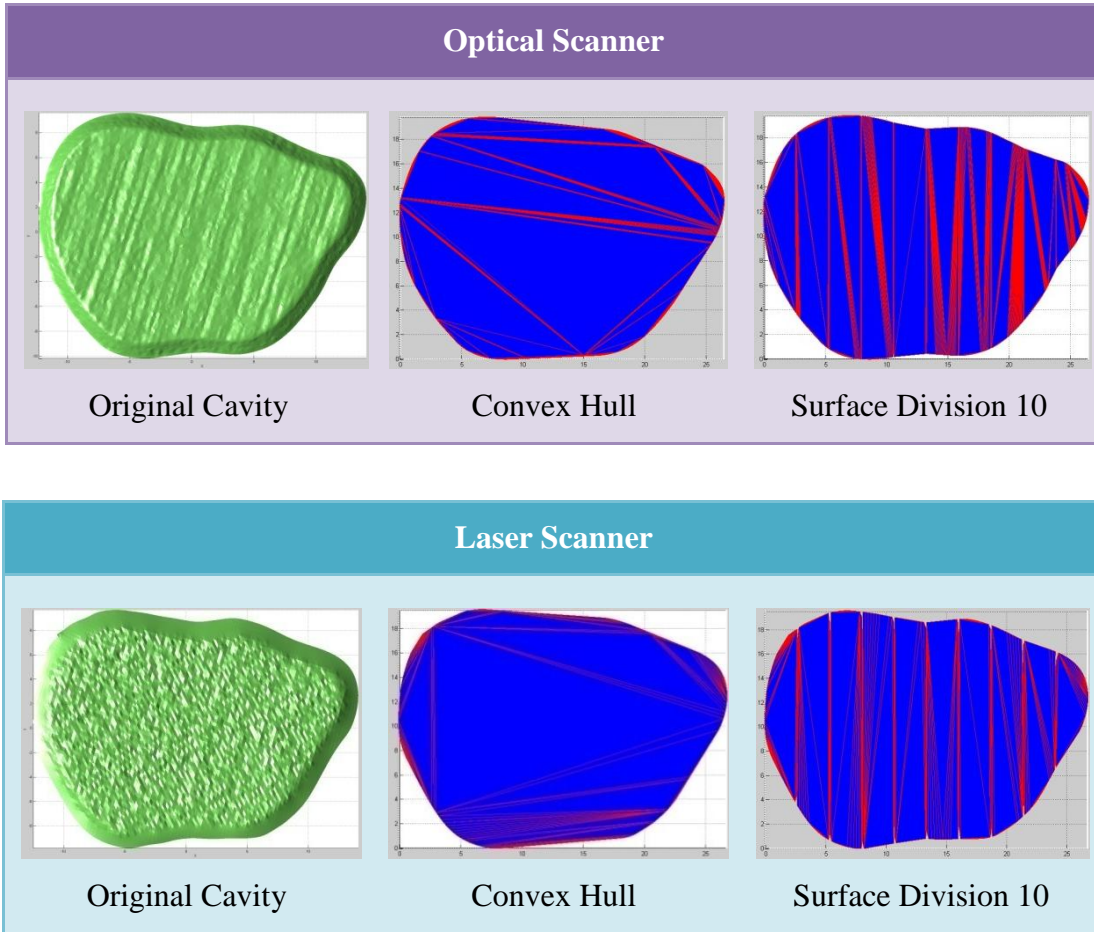


Figure 4.6: Model IRSD1H with surface division prior to convex hull

4.1.3 Comparison of Midpoint Projection, Convex Hull Approximation Method And Conventional Volume Computation Method

In this section, the results obtained are used for the comparison of midpoint projection and convex hull approximation method for each scanning techniques. The results obtained from the optical scanner and laser scanner are listed in Table 4.4 and 4.5

Table 4.4: Volume measurement using midpoint projection method

| Model | Reference Value, \hat{y} (mm ³) | Optical Scanner | | Laser Scanner | | Mould Material | |
|--------|---|---|----------------|--------------------------------------|----------------|--------------------------------------|----------------|
| | | Measure Value, y_i (mm ³) | Absolute Error | Mean Value, y_i (mm ³) | Absolute Error | Mean Value, y_i (mm ³) | Absolute Error |
| IRSD1H | 363 | 371 | 8 | 391 | 28 | 350 | 13 |
| RSD5E1 | 2673 | 2683 | 10 | 2706 | 33 | 2600 | 73 |
| RPO1H | 361 | 371 | 10 | 384 | 23 | 350 | 11 |
| RSD1H | 397 | 408 | 11 | 423 | 26 | 400 | 3 |
| RSD3E1 | 1284 | 1306 | 22 | 1308 | 24 | 1300 | 16 |
| RPO3H | 1082 | 1108 | 26 | 1113 | 31 | 1100 | 18 |
| IRSD3H | 1317 | 1348 | 31 | 1351 | 34 | 1300 | 17 |
| RSD3H | 1428 | 1462 | 34 | 1468 | 40 | 1400 | 28 |
| RSD5H | 2816 | 2856 | 40 | 2892 | 76 | 2800 | 16 |
| IRSD5H | 2618 | 2666 | 48 | 2726 | 108 | 2600 | 18 |
| RSD3D1 | 1571 | 1623 | 52 | 1624 | 53 | 1600 | 29 |
| RSD3D2 | 1713 | 1765 | 52 | 1770 | 57 | 1700 | 13 |
| RSD5E2 | 2530 | 2591 | 61 | 2617 | 87 | 2500 | 30 |
| RSD5D1 | 2960 | 3034 | 74 | 3041 | 81 | 3000 | 40 |
| RSD5D2 | 3102 | 3191 | 89 | 3200 | 98 | 3150 | 48 |
| RSD3E2 | 1141 | 1237 | 96 | 1269 | 128 | 1200 | 59 |
| RPO5H | 1803 | 1951 | 148 | 1921 | 118 | 1850 | 47 |

Indicator:

R = Regular Boundary
IR = Irregular Boundary

SD# = Sloped Edge
PO# = Punched Out Edge
= Height

E# = Elevated Base
H = Homogeneous Base
D# = Depressed base

Table 4.5: Volume measurement using convex hull approximation method

| Model | Reference Value, \hat{y} (mm ³) | Optical Scanner | | Laser Scanner | | Mould Material | |
|--------|---|---|----------------|---|----------------|---|----------------|
| | | Measure Value, y_i (mm ³) | Absolute Error | Measure Value, y_i (mm ³) | Absolute Error | Measure Value, y_i (mm ³) | Absolute Error |
| IRSD1H | 363 | 370 | 7 | 322 | 41 | 350 | 13 |
| RSD5E1 | 2673 | 2742 | 69 | 2574 | 99 | 2600 | 73 |
| RPO1H | 361 | 370 | 9 | 319 | 42 | 350 | 11 |
| RSD1H | 397 | 393 | 4 | 358 | 39 | 400 | 3 |
| RSD3E1 | 1284 | 1385 | 101 | 1251 | 33 | 1300 | 16 |
| RPO3H | 1082 | 1084 | 2 | 956 | 126 | 1100 | 18 |
| IRSD3H | 1317 | 1298 | 19 | 1262 | 55 | 1300 | 17 |
| RSD3H | 1428 | 1437 | 9 | 1400 | 28 | 1400 | 28 |
| RSD5H | 2816 | 2818 | 2 | 2600 | 216 | 2800 | 16 |
| IRSD5H | 2618 | 2594 | 24 | 2594 | 24 | 2600 | 18 |
| RSD3D1 | 1571 | 1605 | 34 | 1504 | 67 | 1600 | 29 |
| RSD3D2 | 1713 | 1687 | 26 | 1511 | 202 | 1700 | 13 |
| RSD5E2 | 2530 | 2766 | 236 | 2696 | 166 | 2500 | 30 |
| RSD5D1 | 2960 | 2956 | 4 | 2759 | 201 | 3000 | 40 |
| RSD5D2 | 3102 | 3144 | 42 | 2817 | 285 | 3150 | 48 |
| RSD3E2 | 1141 | 1451 | 310 | 1353 | 212 | 1200 | 59 |
| RPO5H | 1803 | 1826 | 23 | 1578 | 225 | 1850 | 47 |

Indicator:

R = Regular Boundary
IR = Irregular Boundary

SD# = Sloped Edge
PO# = Punched Out Edge
= Height

E# = Elevated Base
H = Homogeneous Base
D# = Depressed base

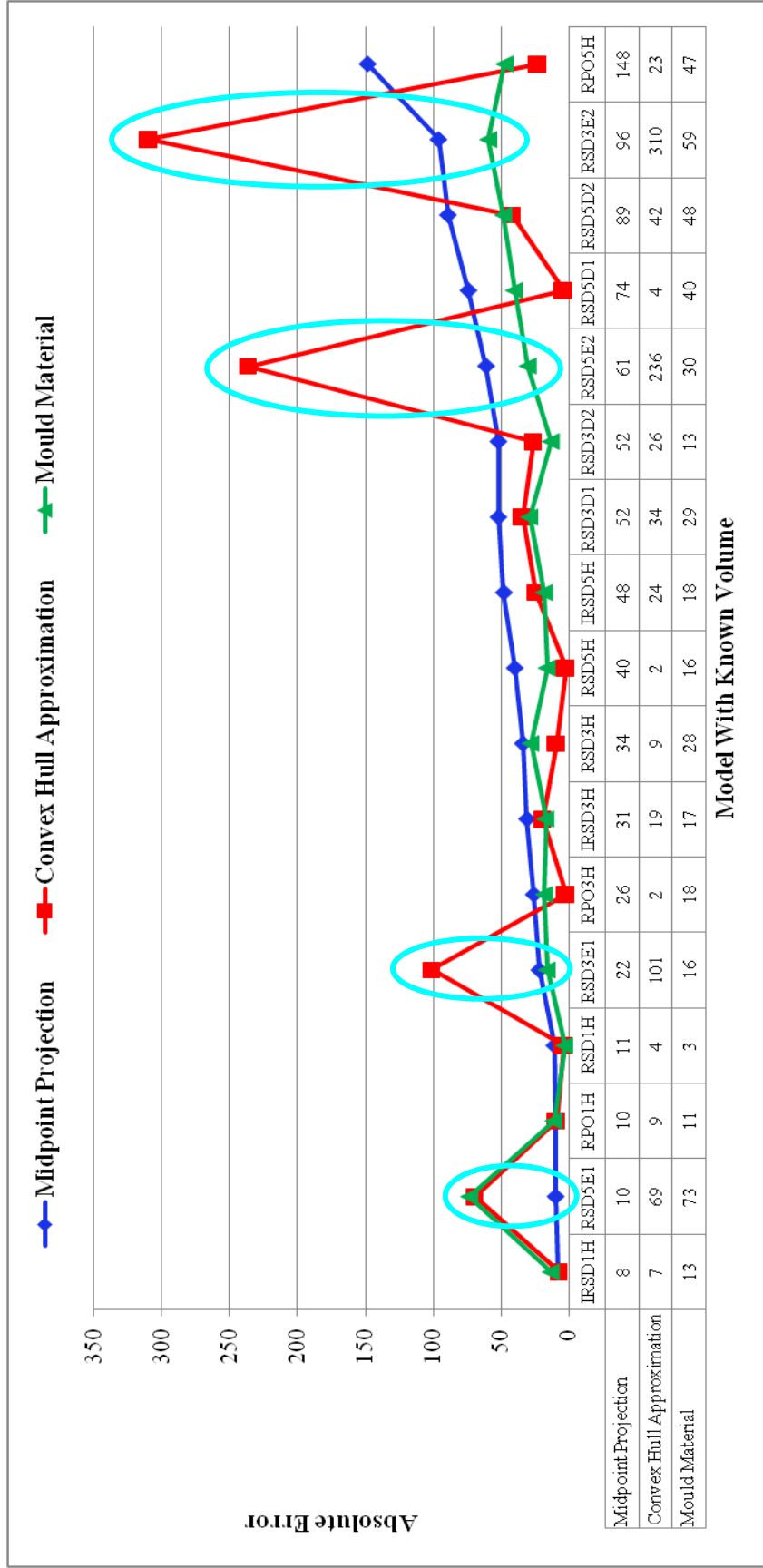


Figure 4.7: Optical scanner with midpoint projection and convex hull approximation method

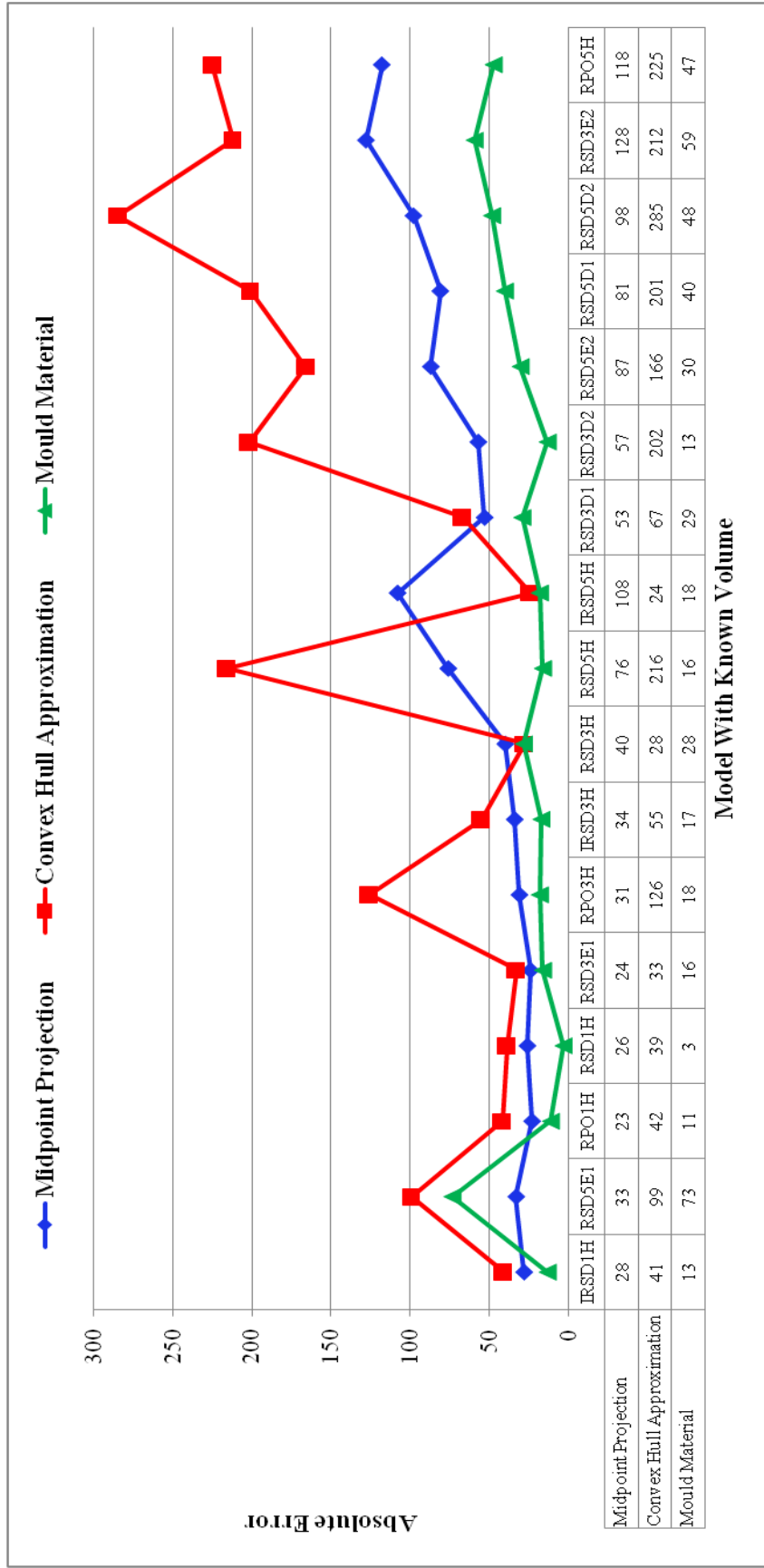


Figure 4.8: Laser scanner with midpoint projection and convex hull approximation method

The results obtained by various methods are analyzed based on the absolute error of the sample and R^2 value. Fig. 4.7 represents the absolute error occurred at three different methods i.e. midpoint projection method and Convex Hull Approximation method when optical scanner used and also the volume computation using mould material. Based on the absolute error shown in Fig. 4.7, mould material show a very high consistent result to almost all the models. Besides that, convex hull approximation provides better results if compared to the midpoint projection. For example, model IRSD1H, RPO1H, RSD1H, RPO3H, IRSD3H, RSD3H, RSD5H, IRSD5H, RSD3D1, RSD3D2, RSD5D1, RSD5D2 and RPO5H obtained less absolute error by using convex hull approximation method. However, the model of RSD5E1, RSD3E1, RSD5E2 and RSD3E2 which elevated base gave higher absolute error. It could be suggested that the convex hull approximation method can be used for the general wound shape and cannot be applied for elevated base wound. The reason is explained in section 4.1.2. The wrapping follows the incorrect path where overestimation in volume occurs. The phenomenon happens due to the limitation of the method, and hence, it can occur to any data acquisition method. Volume computation using mould material gives the best fitting toward reference volumes with the R^2 value of 0.9986 and followed by the optical scanner and laser scanner. For optical scanner, midpoint projection and convex hull approximation present R^2 value at 0.9957 and 0.9876 respectively.

Fig. 4.8 illustrates the absolute errors of the volume obtained from laser scanner and mould material. Midpoint projection and convex hull approximation are the two computation methods to obtain the volume of wound model that using laser scanner. Apparently, volume measurement using mould material still gives the highest accuracy and consistency on the volume with the value of R^2 of 0.9986. For laser scanner, midpoint projection and convex hull approximation shows R^2 value at 0.9940 and 0.9702 respectively. In convex hull approximation, surface division is needed in order to give better illustration of the wound shape.

Generally, the surface division will cause some gaps in between each division and the level of error introduced is dependent on the point clouds of the model. The greater

the points in the model, the gap introduced is smaller. Fig. 4.9 shows the gap introduced from surface division which causes major loss in terms of volume.

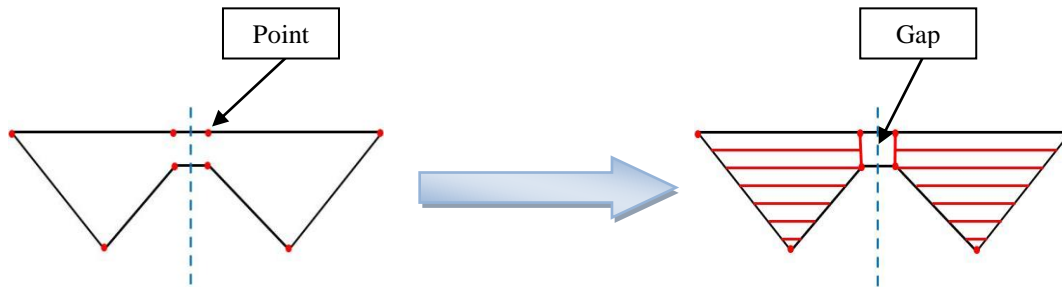


Figure 4.9: Gaps introduced from surface division

Based on the results obtained with the known volume, it is strongly believed that the volume obtained by mould material can be used as reference volume for the unknown volume (real wound) as it provides consistent and accuracy results. Both midpoint projection and convex hull show convincing result with high value of R^2 . Due to the higher R^2 value of the midpoint projection and limitation of convex hull approximation on the gap introduced from the surface division, midpoint projection was selected to analyzed thoroughly in the next section.

4.2 Volume Computation of Ulcer Wound Model

The volume computation processes begin with the models of a known volume followed with the ulcer wound model. Twenty three patients with consent are involved in this research to provide twenty six ulcer wound models. The volume computation using mould material gives higher value of R^2 and showing lower absolute error for most of the models. However, it is invasive and not suitable to be used on wounds. Hence, it serves as a reference volume to further analyzing the best method selected from validation stage.

Table 4.6: Volume computation using midpoint projection.

| Model | Reference Value (mm ³) | Optical Scanner | |
|----------|------------------------------------|----------------------------------|----------------|
| | | Measure Value (mm ³) | Absolute Error |
| Ulcer 01 | 250 | 250 | 0 |
| Ulcer 02 | 200 | 201 | 1 |
| Ulcer 03 | 300 | 301 | 1 |
| Ulcer 04 | 500 | 502 | 2 |
| Ulcer 05 | 250 | 246 | 4 |
| Ulcer 06 | 300 | 295 | 5 |
| Ulcer 07 | 100 | 93 | 7 |
| Ulcer 08 | 100 | 93 | 7 |
| Ulcer 09 | 1000 | 1007 | 7 |
| Ulcer 10 | 250 | 258 | 8 |
| Ulcer 11 | 150 | 141 | 9 |
| Ulcer 12 | 650 | 663 | 13 |
| Ulcer 13 | 150 | 163 | 13 |
| Ulcer 14 | 100 | 86 | 14 |
| Ulcer 15 | 100 | 116 | 16 |
| Ulcer 16 | 1000 | 1021 | 21 |
| Ulcer 17 | 50 | 29 | 21 |
| Ulcer 18 | 150 | 128 | 22 |
| Ulcer 19 | 200 | 224 | 24 |
| Ulcer 20 | 100 | 75 | 25 |
| Ulcer 21 | 850 | 876 | 26 |
| Ulcer 22 | 1400 | 1428 | 28 |
| Ulcer 23 | 500 | 529 | 29 |
| Ulcer 24 | 2200 | 2163 | 37 |
| Ulcer 25 | 450 | 493 | 107 |
| Ulcer 26 | 1400 | 1719 | 319 |

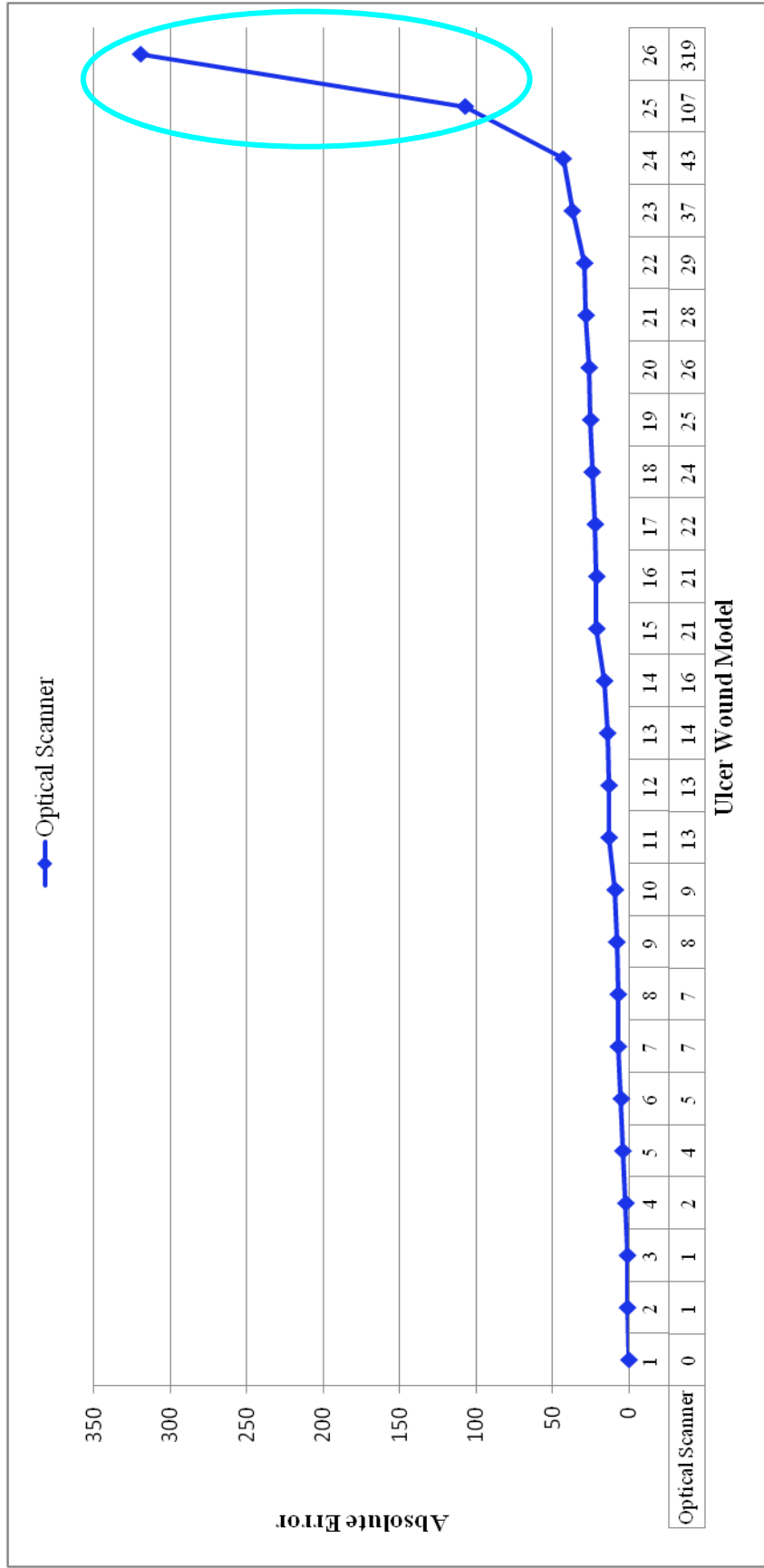


Figure 4.10: Absolute error for models using midpoint projection

Table 4.6 shows the result obtained by using midpoint projection computation method for the wound images taken by optical scanner. Fig. 4.10 shows the absolute error generated by midpoint projection for optical scanner. The absolute error of the volume is obtained where the reference volume is given by the result of mould material. The optical scanner shows the R^2 value at 0.9841. It shows that volume computation result obtained from optical scanner gives the best fitting toward reference volumes compared to the laser scanner.

The absolute errors for the models obtained from optical scanner using midpoint projection method are always linear except for ulcer wound model 25 and 26.

In model 26, the ulcer shows the over granulation in the ulcer wound bed which shown in Fig. 4.11. Over granulation occurs when the healing of the granulation tissue continues to grow, and fills the area until it is proud of the wound. Since the midpoint is generated using the points located in the boundary, there will be extra volume introduced above the reconstructed surface.

For ulcer 25, the 3D scanned surface shows some deviation that affect the accuracy of the volume computation. The deviation error occurred due to the scanning limitation of the optical scanner to rapid changes in the height of wound bed as shown in Fig. 4.12.

However, most of the 3D wound models obtained from optical scanner have better accuracy in volume computation using convex hull approximation.

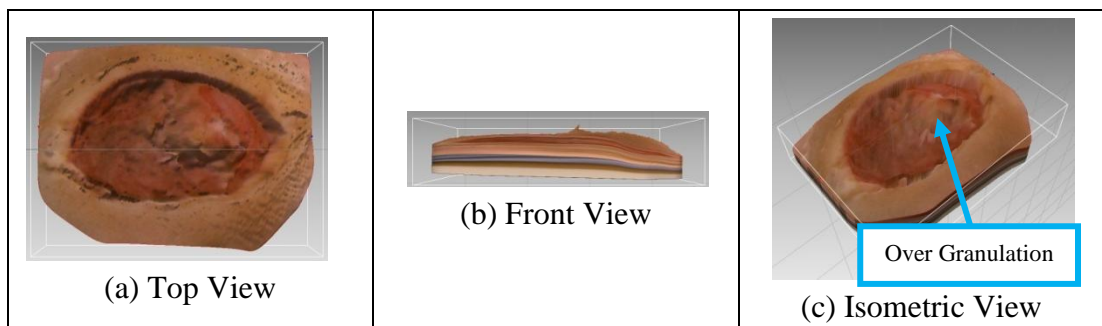


Figure 4.11: Multiple view of ulcer wound model 26

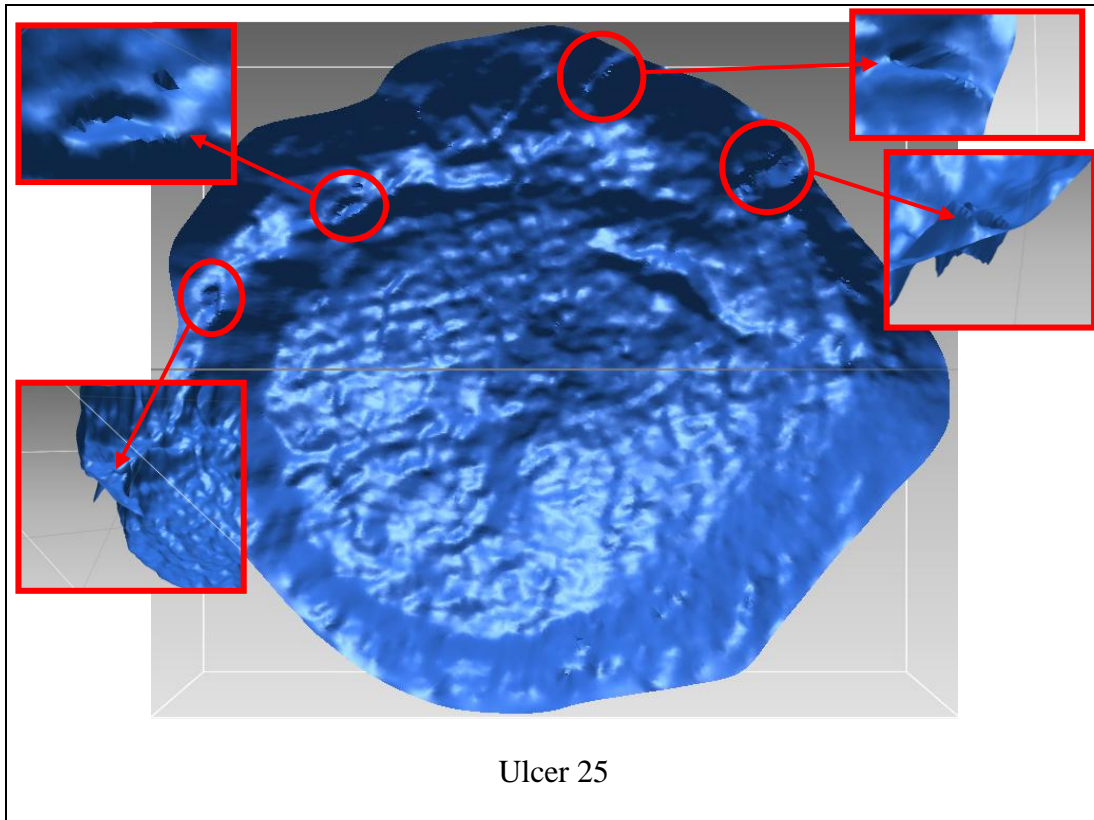


Figure 4.12: Deviation of the 3D surface scanned of wound model

4.3 Summary

This chapter includes all the results from the volume measurement with the various wound attribute models and ulcer wound model. Measurement were perform with the prototype model without involve any contact to the ulcer wound which could cause infection and discomfort to the patients.

In the first stage, volume measurements were performed on the various wound attribute models with known volume. Seventeen models were involved in giving the R^2 for each volume computation technique. Conventional cavity volume measurement which weighing the amount of mould material being used to filled up the cavity shows the highest R^2 value at 0.9986 with. Optical scanner has shown better accuracy in R^2 value compared to laser scanner. Volume computation using convex hull

approximation has slightly better accuracy for every case except for the model with elevated base. However, due to the limitation on the convex hull that could not fit for the entire wound attribute and the gap introduced from the surface division, midpoint projection was selected to analyzed thoroughly in second stage.

The second stage shows the result for volume measurements on ulcer wound model. Twenty six ulcer wound prototype in total were used in this stage. Conventional cavity volume measurements are very accurate and hence served as reference volume. In most of the model, optical scanner using midpoint projection give a linear result except for the circumstances such as rapid changes in height and over granulation.

CHAPTER 5

CONCLUSIONS AND RECOMMENDATIONS

5.1 Conclusions

Reverse engineering method in leg ulcer assessment gives a promising future in providing a more accurate, reliable and quantitative measurement especially in volume measurement. Experiment had been conducted to verify the accuracy of laser triangulation and structured light data acquisition techniques in capturing 3D information of ulcer wounds, to assess the suitability and reliability of the method for surface reconstruction and volume computation of ulcer cavity and also to investigate the performance of conventional method (mould material) in volume cavity measurement. The following conclusions can be drawn from this research.

- The study reveals that both structured light (optical scanner) and laser triangulation (laser scanner) data acquisition technique can be used to retrieve the 3D geometrical CAD of the ulcer wound. In generating CAD model for both data acquisition techniques, when the boundary edge and the elevated base increases to certain level, shadow appears affects the accuracy. It was established and verified that structured-light-based 3D technique produces better accuracy compared with laser triangulation data acquisition technique.
- It was shown that both midpoint projection and convex hull approximation methods works on most of the wound attributes. Midpoint projection volume computation is suitable for all the wound type whereas convex hull is suitable for all types of wound except wound with elevated base. It was assessed and demonstrated that midpoint projection method produce better result in volume measurement and suitable for all wound attributes introduced.

- Volume computation using conventional method (mould material) shows the highest accuracy among all the measuring methods. However, this method is invasive as it can bring discomfort and infection to the patients and only suitable for the research purpose.
- This research establishes that ulcer wound can be modelled with various wound attributes (boundary, edge, base and depth). It has also been shown that each attribute has an effect on data acquisition and volume computation accuracy.
- The outputs of this research highlight the strengths and limitations of each data acquisition technique and choice of method. They can be used to develop a biomedical measuring system which is potential to replace the conventional clinical evaluation.

5.2 Recommendations

Some parts in this system were done manually by a trained person. In the future, some improvements can be carried out:

1. Automatic segmentation of the ulcer boundary.
 - This system is expected to be user friendly and easily to operate. 3D surface scan of the ulcer wound will be operated manually by an operator. After the 3D surface scan was obtained, the system will automatically select the boundary of the ulcer for cropping.
2. Automatic volume computation method selection for different ulcer wound attributes.
 - Midpoint projection and convex hull approximation have their own strengths and limitations. In the current system, the selection of the volume computation method towards wound shape is done manually.
 - In the future, the cropped area will analyzed immediately to select the most appropriate volume computation method associate to the ulcer shape and size.

- Eventually, the system will help in measuring ulcer wound cavity volume and store in the system. The record of the patient can be reviewed by the dermatologists and immediately healing progress of the ulcer wound can be known. Hence, dermatologist can also track back the previous record and according the monitoring system to decide the most appropriate dressing and treatment.

REFERENCES

- [1] V. Raja and K. J. Fernandes, *Reverse Engineering: An Industrial Perspective*: Springer Publishing Company, Incorporated, 2007.
- [2] (2009, September 23). *MAVIS II: 3D Wound Instrument Measurement*. Available:
<http://www.comp.glam.ac.uk/pages/staff/pplassma/MedImaging/PROJECTS/WOUNDS/MAVIS-II/INDEX.HTML>
- [3] M. Callieri, P. Cignoni, P. Pingi, R. Scopigno, M. Coluccia, G. Gaggio, and M. Romanelli, "Derma: monitoring the evolution of skin lesions with a 3D system," presented at the Proceedings of the Vision, Modeling, and Visualization Conference 2003 Munich, Germany, 2003.
- [4] D. A. Perednia, "What Dermatologists Should Know About Digital Imaging," *J Am Acad Dermatol*, vol. 25, pp. 89-108, 1991.
- [5] M. G. Woodbury, P. E. Houghton, K. E. Campbell, and D. H. Keast, "Development, Validity, Reliability, and Responsiveness of a New Leg Ulcer Measurement Tool," *Advances in Skin & Wound Care*, vol. 17, pp. 187-196, 2004.
- [6] N. Kecelj-Leskovec, M. Jezeršek, J. Možina, M. D. Pavlović, and T. Lunder, "Measurement of venous leg ulcers with a laser-based three-dimensional method: Comparison to computer planimetry with photography," *Wound Repair and Regeneration*, vol. 15, pp. 767-771, 2007.
- [7] T. Wild, M. Prinz, N. Fortner, W. Krois, K. Sahora, S. Stremitzer, and T. Hoelzenbein, "Digital measurement and analysis of wounds based on colour segmentation," *European Surgery*, vol. 40, pp. 5-10, 2008.
- [8] V. H. Chan, C. Bradley, and G. W. Vickers, "A multi-sensor approach to automating co-ordinate measuring machine-based reverse engineering," *Computers in Industry*, vol. 44, pp. 105-115, 2001.
- [9] T. Várady, R. R. Martin, and J. Cox, "Reverse engineering of geometric models--an introduction," *Computer-Aided Design*, vol. 29, pp. 255-268, 1997.
- [10] K. H. Lee and H. Woo, "Direct integration of reverse engineering and rapid prototyping," *Computers & Industrial Engineering*, vol. 38, pp. 21-38, 2000.
- [11] Y. Ke, S. Fan, W. Zhu, A. Li, F. Liu, and X. Shi, "Feature-based reverse modeling strategies," *Computer-Aided Design*, vol. 38, pp. 485-506, 2006.

- [12] L. Xinmin, L. Zhongqin, H. tian, and Z. Ziping, "A study of a reverse engineering system based on vision sensor for free-form surfaces," *Computers & Industrial Engineering*, vol. 40, pp. 215-227, 2001.
- [13] H.-T. Yau, "Reverse engineering of engine intake ports by digitization and surface approximation," *International Journal of Machine Tools and Manufacture*, vol. 37, pp. 855-871, 1997.
- [14] H.-M. Rho, Y. Jun, S. Park, and H.-R. Choi, "A rapid reverse engineering system for reproducing 3D human busts," *CIRP Annals - Manufacturing Technology*, vol. 51, pp. 139-143, 2002.
- [15] J. G. D. M. Franca, M. A. Gazziro, A. N. Ide, and J. H. Saito, "A 3D scanning system based on laser triangulation and variable field of view," in *Image Processing, 2005. ICIP 2005. IEEE International Conference on*, pp. I-425-8, 2005.
- [16] A. Peiravi and B. Taabbodi, "A Reliable 3D Laser Triangulation-based Scanner with a New Simple but Accurate Procedure for Finding Scanner Parameters," *Journal of American Science*, vol. 6, pp. 80-85, 2010.
- [17] J. F. Collado, "New Methods for Triangulation-based Shape Acquisition using Laser Scanners," Doctoral, Departament d'Electrònica Informàtica i Automàtica, Universitat de Girona, 2004.
- [18] J. Park and G. N. DeSouza, "3-D Modeling of Real-World Objects Using Range and Intensity Images," in *Machine Learning and Robot Perception*. vol. 7, B. Apolloni, A. Ghosh, F. Alpaslan, L. C. Jain, and S. Patnaik, Eds., ed: Springer Berlin / Heidelberg, pp. 203-264, 2005.
- [19] G. Frankowski, R. Hainich, S. Emerging Digital Micromirror Device Based, and Applications, III, "DLP/DSP-based optical 3D sensors for the mass market in industrial metrology and life sciences," *Proc SPIE Int Soc Opt Eng Proceedings of SPIE - The International Society for Optical Engineering*, vol. 7932, 2011.
- [20] G. Frankowski, R. Hainich, S. Emerging Digital Micromirror Device Based, and Applications, "DLP-Based 3D metrology by structured light or projected fringe technology for life sciences and industrial metrology," *Proc SPIE Int Soc Opt Eng Proceedings of SPIE - The International Society for Optical Engineering*, vol. 7210, 2009.
- [21] S. S. Gorthi and P. Rastogi, "Fringe projection techniques: Whither we are?," *Opt Lasers Eng Optics and Lasers in Engineering*, vol. 48, pp. 133-140, 2010.
- [22] S. Jaspers, H. Hopermann, G. Sauermann, U. Hoppe, R. Lunderstädt, and J. Ennen, "Rapid in vivo measurement of the topography of human skin by

- active image triangulation using a digital micromirror device," *Skin Research and Technology*, vol. 5, pp. 195-207, 1999.
- [23] R. Ishiyama, S. Sakamoto, J. Tajima, T. Okatani, and K. Deguchi, "Absolute phase measurements using geometric constraints between multiple cameras and projectors," *Appl. Opt.*, vol. 46, pp. 3528-3538, 2007.
- [24] H. Tak-Wai and G. K. H. Pang, "3-D Measurement of Solder Paste Using Two-Step Phase Shift Profilometry," *Electronics Packaging Manufacturing, IEEE Transactions on*, vol. 31, pp. 306-315, 2008.
- [25] L. Di Stefano and F. Boland, "A new phase extraction algorithm for phase profilometry," *Machine Vision and Applications*, vol. 10, pp. 188-200, 1997.
- [26] H. Yingsong, X. Jiangtao, L. Enbang, J. Chicharo, and Y. Zongkai, "Shift estimation method based fringe pattern profilometry and performance comparison," in *Signal Processing and Its Applications, 2005. Proceedings of the Eighth International Symposium on*, pp. 863-866, 2005.
- [27] H. J. Tiziani, N. Kerwien, and G. Pedrini, "9.1 Interferometry," in *9 Interferometry*. vol. 1A2, H. Weber, G. Herziger, and R. Poprawe, Eds., ed.
- [28] S. L. Robbins, V. Kumar, and R. S. Cotran, *Robbins and Cotran pathologic basis of disease*. Philadelphia, PA: Saunders/Elsevier, 2010.
- [29] C. National Digestive Diseases Information. (2010, *H. pylori and peptic ulcers*. Available: <http://purl.access.gpo.gov/GPO/LPS124293>
- [30] C. Scully and D. H. Felix, "Oral medicine--update for the dental practitioner. Aphthous and other common ulcers," *British Dental Journal*, vol. 199, pp. 259-64, 2005.
- [31] T. W. Schafer, "Peptic Ulcer Disease."
- [32] A. Foster and A. Sommer, "Corneal ulceration, measles, and childhood blindness in Tanzania," *The British journal of ophthalmology*, vol. 71, pp. 331-43, 1987.
- [33] N. J. London and R. Donnelly, "ABC of arterial and venous disease. Ulcerated lower limb," *BMJ (Clinical research ed.)*, vol. 320, pp. 1589-91, 2000.
- [34] F. Werdin, M. Tennenhaus, H. E. Schaller, and H. O. Rennekampff, "Evidence-based management strategies for treatment of chronic wounds," *Eplasty*, vol. 9, p. e19, 2009.
- [35] K. Wolff, T. B. Fitzpatrick, and R. A. Johnson, *Fitzpatrick's color atlas and synopsis of clinical dermatology*. New York [u.a.: McGraw-Hill, 2009.

- [36] A. Shai, H. I. Maibach, and C. Ebooks, "Ulcer Measurement and Patient Assessment," in *Wound Healing and Ulcers of the Skin : Diagnosis and Therapy - the Practical Approach*, ed Dordrecht: Springer-Verlag Berlin and Heidelberg GmbH & Co. KG, pp. 89-102, 2005.
- [37] R. J. Goldman and R. Salcido, "More than one way to measure a wound: an overview of tools and techniques," *Advances in Skin & Wound Care*, vol. 15, 2002.
- [38] C. Dealey, *The care of wounds : a guide for nurses*. Oxford: Blackwell, 2005.
- [39] A. Malian, A. Azizi, F. A. van den Heuvel, and M. Zolfaghari, "Development of a Robust Photogrammetric Metrology System for Monitoring the Healing of Bedsores," *The Photogrammetric Record*, vol. 20, pp. 241-273, 2005.
- [40] J. I. Kundin, "Apparatus and method for measuring deformed areas of skin surface," United States Patent 4483075, 1984-11-20 1984.
- [41] D. Langemo, J. Anderson, D. Hanson, S. Hunter, and P. Thompson, "Measuring Wound Length, Width, and Area: Which Technique?," *Advances in Skin & Wound Care*, vol. 21, pp. 42-45 10.1097/01.ASW.0000284967.69863.2f, 2008.
- [42] A. Shai, H. I. Maibach, and SpringerLink, *Wound healing and ulcers of the skin diagnosis and therapy : the practical approach*. Berlin; New York: Springer, 2005.
- [43] S. Baranoski and E. A. Ayello, *Wound care essentials : practice principles*. Philadelphia, Pa.; London: Lippincott Williams & Wilkins, 2007.
- [44] M. De La Brassinne, L. Thirion, and L. I. Horvat, "A novel method of comparing the healing properties of two hydrogels in chronic leg ulcers," *Journal of the European Academy of Dermatology and Venereology*, vol. 20, pp. 131-135, 2006.
- [45] J. S. Covington, J. W. Griffin, R. K. Mendius, R. E. Tooms, and J. K. Clifft, "Measurement of Pressure Ulcer Volume Using Dental Impression Materials: Suggestion from the Field," *Physical Therapy*, vol. 69, pp. 690-694, August, 1989.
- [46] M. Herbin, F. X. Bon, A. Venot, F. Jeanlouis, M. L. Dubertret, L. Dubertret, and G. Strauch, "Assessment of healing kinetics through true color image processing," *Medical Imaging, IEEE Transactions on*, vol. 12, pp. 39-43, 1993.
- [47] J. R. Mekkes and W. Westerhof, "Image processing in the study of wound healing," *Clinics in Dermatology*, vol. 13, pp. 401-407, 1995.

- [48] R. B. Smith, B. Rogers, G. P. Tolstykh, N. E. Walsh, M. G. Davis, L. Bunegin, and R. L. Williams, "Three-Dimensional laser imaging system for measuring wound geometry," *Lasers in Surgery and Medicine*, vol. 23, pp. 87-93, 1998.
- [49] F. Chen, G. M. Brown, and M. Song, "Overview of three-dimensional shape measurement using optical methods," *Optical Engineering*, vol. 39, pp. 10-22, 2000.
- [50] C. Ozturk, S. Dubin, M. E. Schafer, S. Wen-Yao, and C. Min-Chih, "A new structured light method for 3-D wound measurement," in *Bioengineering Conference, 1996., Proceedings of the 1996 IEEE Twenty-Second Annual Northeast*, pp. 70-71, 1996.
- [51] T. A. Krouskop, R. Baker, and M. S. Wilson, "A noncontact wound measurement system," *Journal of Rehabilitation Research and Development*, vol. 39, pp. 337-346, 2002.
- [52] S. M. Boersma, "Photogrammetric wound measurement with a three-camera vision system," *International archives of photogrammetry and remote sensing = Archives internationales de photogrammétrie et de télédétection /*, vol. 33, pp. 84-91, 2000.
- [53] P. Plassmann and T. D. Jones, "MAVIS: a non-invasive instrument to measure area and volume of wounds," *Medical engineering & physics*, vol. 20, pp. 332-338, 1998.
- [54] B. F. Jones and P. Plassmann, "An instrument to measure the dimensions of skin wounds," *Biomedical Engineering, IEEE Transactions on*, vol. 42, pp. 464-470, 1995.
- [55] P. Drap, M. Sgrenzaroli, M. Canciani, G. Cannata, and J. Seinturier, "Laser scanning and close range photogrammetry: Towards a single measuring tool dedicated to architecture and archaeology," presented at the CIPA XIXth international symposium, Turkey, 2003.
- [56] H. L. Mitchell and I. Newton, "Medical photogrammetric measurement: overview and prospects," *ISPRS Journal of Photogrammetry and Remote Sensing*, vol. 56, pp. 286-294, 2002.
- [57] M. Romanelli, G. Gaggio, M. Coluccia, F. Rizzello, and A. Piaggese, "Technological Advances in Wound Bed Measurements," *Wounds : a compendium of clinical research and practice.*, vol. 14, pp. 58-66, 2002.
- [58] A. Malian, A. Azizi, and F. A. Van Den Heuvel, "Medphos: A New Photogrammetric System for Medical Measurement," *International archives of photogrammetry remote sensing and spatial information sciences*, vol. 35, pp. 311-316, 2004.

- [59] A. Malian, F. A. van den Heuvel, and A. Azizi, "A robust photogrammetric system for wound measurement," *International archives of photogrammetry remote sensing and spatial information sciences*, vol. 34, pp. 264-269, 2002.
- [60] H. Wannous, Y. Lucas, S. Treuillet, and B. Albouy, "A complete 3D wound assessment tool for accurate tissue classification and measurement," in *Image Processing, 2008. ICIAP 2008. 15th IEEE International Conference on*, pp. 2928-2931, 2008.
- [61] B. Albouy, E. Koenig, S. Treuillet, and Y. Lucas, "Accurate 3D Structure Measurements from Two Uncalibrated Views," in *Advanced Concepts for Intelligent Vision Systems*. vol. 4179, J. Blanc-Talon, W. Philips, D. Popescu, and P. Scheunders, Eds., ed: Springer Berlin / Heidelberg, pp. 1111-1121, 2006.
- [62] B. Albouy, S. Treuillet, Y. Lucas, and J. C. Pichaud, "Volume Estimation from Uncalibrated Views Applied to Wound Measurement," in *Image Analysis and Processing – ICIAP 2005*. vol. 3617, F. Roli and S. Vitulano, Eds., ed: Springer Berlin / Heidelberg, pp. 945-952, 2005.
- [63] B. Albouy, Y. Lucas, and S. Treuillet, "3D Modeling from Uncalibrated Color Images for a Complete Wound Assessment Tool," in *Engineering in Medicine and Biology Society, 2007. EMBS 2007. 29th Annual International Conference of the IEEE*, pp. 3323-3326, 2007.
- [64] H. Wannous, S. Treuillet, and Y. Lucas, "Supervised Tissue Classification from Color Images for a Complete Wound Assessment Tool," in *Engineering in Medicine and Biology Society, 2007. EMBS 2007. 29th Annual International Conference of the IEEE*, pp. 6031-6034, 2007.
- [65] H. Wannous, S. Treuillet, Y. Lucas, and B. Albouy, "Mapping Classification Results on 3D model: a Solution for Measuring the Real Areas Covered by Skin Wound Tissues," in *Information and Communication Technologies: From Theory to Applications, 2008. ICTTA 2008. 3rd International Conference on*, pp. 1-6, 2008.
- [66] N. M. Elteгани, "Assessment of ulcer wounds using 3D skin surface imaging," Master Thesis, Electrical and Electronics Engineering, Universiti Teknologi PETRONAS, 2009.
- [67] J. R. Shewchuk, "Tetrahedral mesh generation by Delaunay refinement," presented at the Proceedings of the fourteenth annual symposium on Computational geometry, Minneapolis, Minnesota, United States, 1998.
- [68] J. R. Shewchuk, "Delaunay refinement mesh generation," School of Computer Science, Carnegie Mellon University, Pittsburgh, Pa., 1997.

- [69] C. B. Barber, D. P. Dobkin, and H. Huhdanpaa, "The quickhull algorithm for convex hulls," *ACM Trans. Math. Softw.*, vol. 22, pp. 469-483, 1996.
- [70] P. Hachenberger, "Exact Minkowski sums of polyhedra and exact and efficient decomposition of polyhedra in convex pieces," presented at the Proceedings of the 15th annual European conference on Algorithms, Eilat, Israel, 2007.
- [71] J.-M. Lien and N. M. Amato, "Approximate convex decomposition of polyhedra and its applications," *Computer Aided Geometric Design*, vol. 25, pp. 503-522, 2008.
- [72] D. Halliday, R. Resnick, and J. Walker, *Fundamentals of physics [5th ed.]*. New York, NY: Wiley, 1997.
- [73] S. W. Hughes, "Archimedes Revisited: A Faster, Better, Cheaper Method of Accurately Measuring the Volume of Small Objects," *Physics Education*, vol. 40, pp. 468-474, 2005.
- [74] A. Willis, J. Speicher, and D. B. Cooper, "Rapid prototyping 3D objects from scanned measurement data," *Image and Vision Computing*, vol. 25, pp. 1174-1184, 2007.
- [75] A. G. Asuero, A. Sayago, and A. G. González, "The Correlation Coefficient: An Overview," *Critical Reviews in Analytical Chemistry*, vol. 36, pp. 41-59, 2006/01/01 2006.
- [76] J. A. Cornell, "Factors that Influence the Value of the Coefficient of Determination in Simple Linear and Nonlinear Regression Models," *Phytopathology Phytopathology*, vol. 77, 1987.
- [77] J.-R. L. M. B. o. G. o. t. F. R. S. Kurz-Kim, *A note on the coefficient of determination in models with infinite variance variables*. [Washington, D.C.: Board of Governors of the Federal Reserve System, 2007.
- [78] A. Hani, N. Elteгани, S. Hussein, A. Jamil, and P. Gill, "Assessment of Ulcer Wounds Size Using 3D Skin Surface Imaging," in *Visual Informatics: Bridging Research and Practice*. vol. 5857, H. Badioze Zaman, P. Robinson, M. Petrou, P. Olivier, H. Schröder, and T. Shih, Eds., ed: Springer Berlin / Heidelberg, pp. 243-253, 2009.
- [79] C. Rocchini, P. Cignoni, C. Montani, and R. Scopigno, "Acquiring, stitching and blending diffuse appearance attributes on 3D models," *The Visual Computer*, vol. 18, pp. 186-204, 2002.

PUBLICATIONS

- [1] K. K. Chong, A. M. Abdul-Rani, M. H. Ahmad Fadzil, Y. B. Yap and A. Jamil, "Analytical Studies on Volume Determination of Leg Ulcer using Laser Triangulation and Structured Light Data Acquisition Technique," in 18th Iranian Conference on BioMedical Engineering, Tehran, Iran, December 14-16, 2011.
- [2] K. K. Chong, A. M. Abdul-Rani, A. F. M. Hani, F. B. B. Yap and A. Jamil, "Volume Assessment of Various Wound Attributes Models using 3D Skin Surface Imaging," in International Conference in Green and Ubiquitous Technology, December 14-16, 2012.
- [3] A. M. A. Rani, A. F. M. Hani, E.-T. Nejoor, E. Chong, and A. Sagar, "Quantitative Assessment of Ulcer Wound Volume," in *Surface Imaging for Biomedical Applications*, ed: CRC Press, pp. 219-272, 2014.

APPENDIX A

LEG ULCER MEASUREMENT TOOL (LUMT)

Figure 1. LUMT FORM AND INSTRUCTIONS
LEG ULCER MEASUREMENT TOOL (LUMT)[®]

| ITEM / DOMAIN | RESPONSE CATEGORIES | SCORE | | | | | |
|--|---|-------------------|-----------|-----------|-----------|-----------|-----------|
| | | Date (mm/dd/yyyy) | | | | | |
| | | — / — / — | — / — / — | — / — / — | — / — / — | — / — / — | — / — / — |
| (A) CLINICIAN RATED DOMAINS | | | | | | | |
| A1. Exudate type | 0 None 1 Serosanguineous 2 Serous 3 Seropurulent 4 Purulent | | | | | | |
| A2. Exudate amount | 0 None 1 Scant 2 Small 3 Moderate 4 Copious | | | | | | |
| A3. Size (from edge of advancing border of epithelium) | (Length x Width) 0 Healed 1 <2.5 cm ² 2 2.5-5.0 cm ² 3 5.1-10.0 cm ² 4 10.1 cm ² or more | | | | | | |
| A4. Depth | Tissue Layers 0 Healed 1 Partial thickness skin loss 2 Full thickness 3 Tendon/joint capsule visible 4 Probes to bone | | | | | | |
| A5. Undermining | Greatest at ___ o'clock 0 0 cm 1 >0 - 0.4 cm 2 >0.4 - 0.9 cm 3 >0.9 - 1.4 cm 4 >1.5 cm | | | | | | |
| A6. Necrotic tissue type | 0 None 1 <i>Loose</i> white to yellow slough 2 <i>Attached</i> white to yellow slough or fibrin 3 <i>Soft</i> grey to black eschar 4 <i>Hard</i> dry black eschar | | | | | | |
| A7. Necrotic tissue amount | 0 None visible 1 1 to 25% of wound bed covered 2 26 to 50% of wound bed covered 3 51 to 75% of wound bed covered 4 76 to 100% of wound bed covered | | | | | | |
| A8. Granulation tissue type | 0 Healed 1 Bright beefy red 2 Dusky pink 3 Pale 4 Absent | | | | | | |
| A9. Granulation tissue amount | 0 Healed 1 76 to 100% of wound bed covered 2 51 to 75% of wound bed covered 3 26 to 50% of wound bed covered 4 1 to 25% of wound bed covered | | | | | | |
| A10. Edges | 0 Healed 1 ≥50% advancing border of epithelium or indistinct borders 2 <50% advancing border of epithelium 3 Attached, no advancing border of epithelium 4 Unattached or undermined | | | | | | |

| ITEM / DOMAIN | RESPONSE CATEGORIES | SCORE | | | | | |
|--|--|-------------------|----------|----------|----------|----------|----------|
| | | Date (mm/dd/yyyy) | | | | | |
| | | __/__/__ | __/__/__ | __/__/__ | __/__/__ | __/__/__ | __/__/__ |
| A11. Perilucer skin viability | Number of factors affected | | | | | | |
| - callus | 0 None | | | | | | |
| - dermatitis (pale) | 1 One only | | | | | | |
| - maceration | 2 Two or three | | | | | | |
| - induration | 3 Four or five | | | | | | |
| - erythema (bright red) | 4 Six or more factors | | | | | | |
| - purple blanchable | | | | | | | |
| - purple non-blanchable | | | | | | | |
| - skin dehydration | | | | | | | |
| A12. Leg edema type | 0 None | | | | | | |
| | 1 Non-pitting or firmness | | | | | | |
| | 2 Pitting | | | | | | |
| | 3 Fibrosis or lipodermatosclerosis | | | | | | |
| | 4 Indurated | | | | | | |
| A13. Leg edema location | 0 None | | | | | | |
| | 1 Localized perilucer | | | | | | |
| | 2 Foot, including ankle | | | | | | |
| | 3 To mid calf | | | | | | |
| | 4 To knee | | | | | | |
| A14. Assessment of bioburden | 0 Healed | | | | | | |
| | 1 Lightly colonized | | | | | | |
| | 2 Heavily colonized | | | | | | |
| | 3 Localized infection | | | | | | |
| | 4 Systemic infection | | | | | | |
| Total - (A) CLINICIAN RATED DOMAINS: | | | | | | | |
| (B) PATIENT (PROXY) RATED DOMAINS | | | | | | | |
| B1. Pain amount (as it relates to the leg ulcer) | Numerical rating scale (0-10) | | | | | | |
| | 0 None | | | | | | |
| | 1 >0 - 2 | | | | | | |
| | 2 >2 - 4 | | | | | | |
| | 3 >4 - 7 | | | | | | |
| | 4 >7 | | | | | | |
| B2. Pain frequency (as it relates to the leg ulcer) | 0 None | | | | | | |
| | 1 Occasional | | | | | | |
| | 2 Position dependent | | | | | | |
| | 3 Constant | | | | | | |
| | 4 Disturbs sleep | | | | | | |
| | <i>"Which of the following terms best describes how often you have had pain in the last 24 hours?"</i> | | | | | | |
| B3. Quality of life (as it relates to the leg ulcer) | 0 Delighted | | | | | | |
| | 1 Satisfied | | | | | | |
| | 2 Mixed | | | | | | |
| | 3 Dissatisfied | | | | | | |
| | 4 Terrible | | | | | | |
| | <i>"How do you feel about the quality of your life at the present time?"</i> | | | | | | |
| Total - (B) PATIENT (PROXY) RATED DOMAINS: | | | | | | | |
| Proxy Completed by: | | | | | | | |
| Total LUMT Score: | | | | | | | |

APPENDIX B

CONSENT FORM

PATIENT INFORMATION SHEET

Study Title: Volume Determination of Leg Ulcer using Reverse Engineering Method.

Investigators: Chong Kian Kiong
Dr. Felix Boon Bin

Institution address:

1. Department of Dermatology/Outpatient Department
Hospital Kuala Lumpur
Jalan Pahang
50586 Kuala Lumpur
2. Universiti Teknologi PETRONAS
Bandar Seri Iskandar
31750 Tronoh
Perak Darul Ridzuan

INTRODUCTION

You are invited to participate in a study conducted by the Department of Dermatology Hospital Kuala Lumpur, Outpatient Department Hospital Kuala Lumpur and Universiti Teknologi PETRONAS. This is because you have a condition called chronic leg ulcer. As a potential research subject, you have the right to know the consequences of participating in this study. The following information explains the possible benefits and risks of being in the study to help you make a decision about participation. Your participation in this study is strictly voluntary and you have no obligations to participate whatsoever.

It is important that you read this document thoroughly and discuss any queries with your doctor or anyone else you prefer before agreeing to participate. Your signature, dated, on the consent form is required before the researchers can perform study procedures on you.

PURPOSE OF THE STUDY

Leg ulcer is a chronic disease that is difficult to cure. It is a significant health and socioeconomic issue. It is a difficult condition to treat. It causes considerable discomfort, and limitations in social activities to the patient. Treatment of leg ulcer is time consuming and often not very effective. In this study, we aim to build a new method for doctors to assess your ulcer condition in a more objective way.

WHO WOULD THIS STUDY INVOLVE

This study will involve patients who had been diagnosed to have chronic leg ulcer.

WHAT WILL HAPPEN TO THE PARTICIPANTS AND THE INFORMATION OBTAINED IN THIS STUDY?

Photograph and 3D images of the ulcer on your leg will be taken using special camera and 3D laser scanner. You may be asked to move your leg in a few positions in order to get a good photograph. All medications and other treatment for your ulcer will be continued as usual. The information obtained in this study will be analyzed and the results will help us in the management of patients with leg ulcers in the future.

POTENTIAL BENEFITS OF THE STUDY

The results of this study may be able to help doctors to assess your ulcer condition more objectively. Your participation may contribute to the way doctors assess or examine leg ulcers in the future.

POTENTIAL RISKS OF THE STUDY

This study will involve taking photographs and 3D images of your leg ulcer only. There are no expected risks, discomfort and radiation that could cause long term consequences associated with the study. The procedure and risk for taking the 3D images is the same like taking photographs.

VOLUNTARY PARTICIPATION

Participation in this study is strictly voluntary. If you decide to participate in the study, you are expected to comply with the study requirements. You are allowed to withdraw from the study at any time without penalty or loss of benefits to which you are otherwise entitled. We will be interested to know if the reason for withdrawal is due to adverse events experienced.

CONFIDENTIALITY

All information given by you is confidential. Reports prepared on the study will not include your name or other identification. Information and records may be reviewed by the Institutional Review Board (IRB)/Ethics Committee (EC) and other regulatory authorities to determine the accuracy of the reported data and/or to protect your safety and welfare.

STUDY COSTS/COMPENSATION

This research does not require any payment from you and neither will you get paid or receive any rewards for your participation. The cost of your ulcer treatment will remain the same whether you participate in this research or not. This research does not provide compensation for any problems that may occur.

TREATMENT OF STUDY RELATED INJURY

In the event that you suffer an injury or side effects or complications that is a direct consequence of the study, the attending doctor will be notified and you will be managed appropriately in Hospital Kuala Lumpur.

ETHICAL REVIEW

This study has been reviewed and approved by the Medical Research & Ethics Committee, Ministry of Health Malaysia.

CONTACT NUMBERS

If you have any enquiries regarding the study or experience any side effects of the study, please contact

Dr. Felix Yap Boon Bin

Dermatology Clinic Hospital Kuala Lumpur

03-555259 or 03-5556687

CONSENT FORM

Study Title: Volume Determination of Leg Ulcer using Reverse Engineering Method.

I have read the information on the research project stated above and have been given the explanation by a doctor about the purpose of this document. I understand that I retained the absolute right over the information given and I have the absolute right to withdraw from the study at any time.

I _____ IC Number: _____
have received a copy of the Patient Information Sheet on the above study and agreed to participate in the study.

Patient/Person giving consent

Name : _____

Signature : _____

Identity Card : _____

Date : _____

Tel : _____

Requesting Researcher

Name : _____

Signature : _____

Identity Card : _____

Date : _____

Tel : _____

Requesting Doctor

Name : _____

Signature : _____

Identity Card : _____

Date : _____

Tel : _____

PHOTOGRAPHY REQUEST FORM

Study Title: Volume Determination of Leg Ulcer using Reverse Engineering Method.

I have read the information on the research project stated above and have been given the explanation by a doctor about the purpose of this document. I understand that I retained the absolute right over the information given and I have the absolute right to withdraw from the study at any time.

I _____ IC Number: _____, give my consent for photographs to be taken, as indicated above, of the said patient and for the photographs to be used by the research and academic purposes only.

I understand that the research authorities will, to the best of their ability, protect my identity in the event that the photographs are reproduced in the teaching sessions, academic discussions/meeting and medical/scientific journals.

Patient/Person giving consent

Name : _____

Signature : _____

Identity Card : _____

Date : _____

Tel : _____

Requesting Researcher

Name : _____

Signature : _____

Identity Card : _____

Date : _____

Tel : _____

Requesting Doctor

Name : _____

Signature : _____

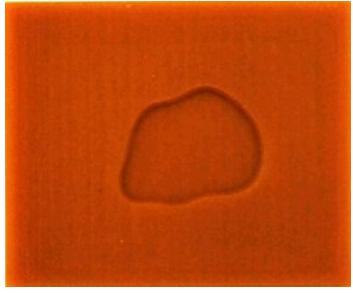
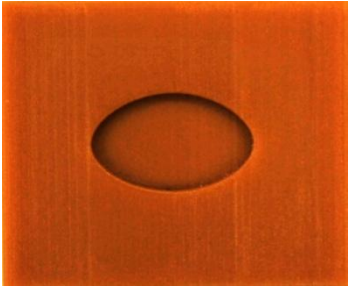
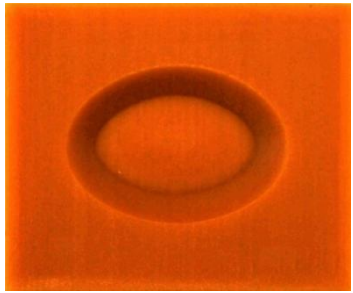
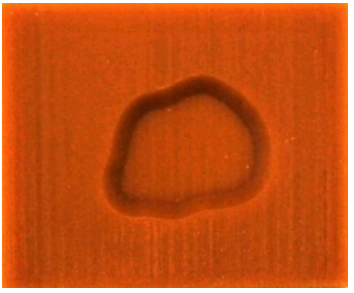
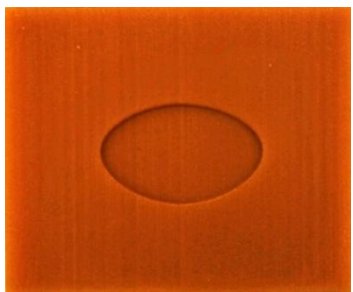
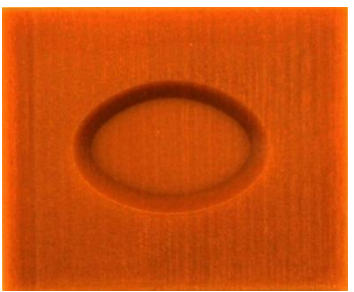
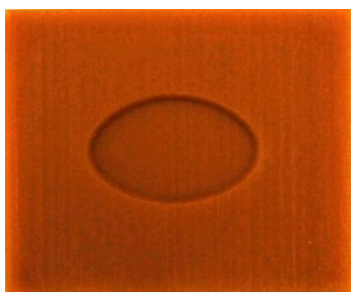
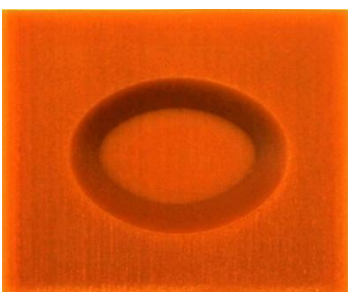
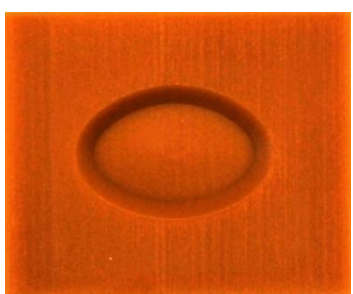
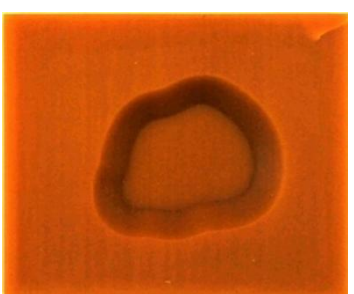
Identity Card : _____

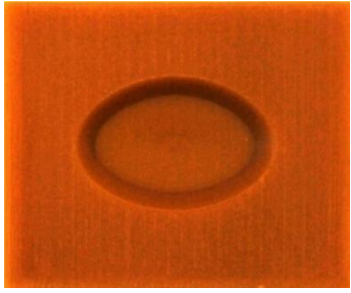
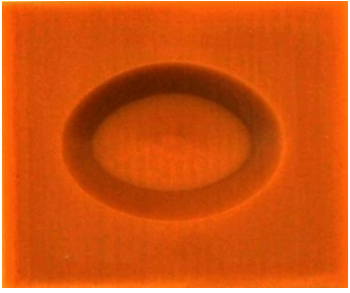
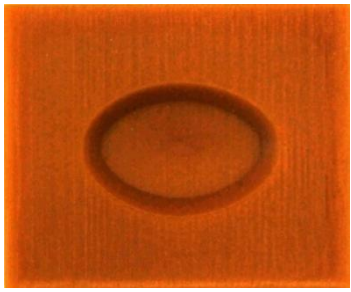
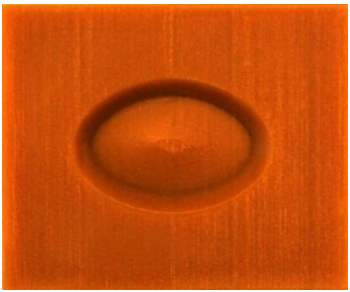
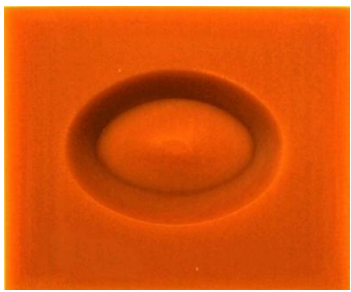
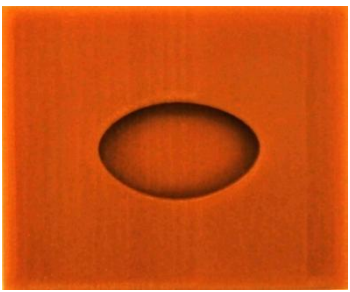
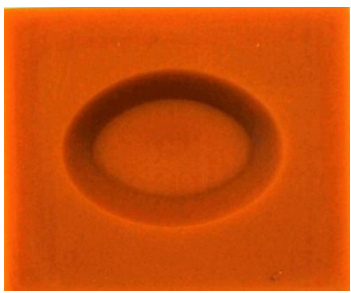
Date : _____

Tel : _____

APPENDIX C


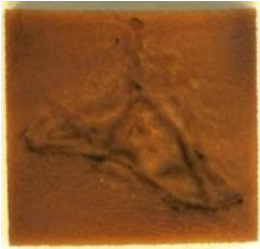

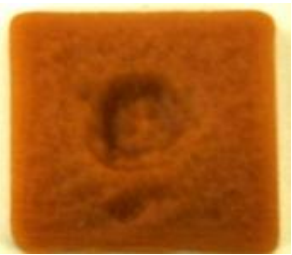
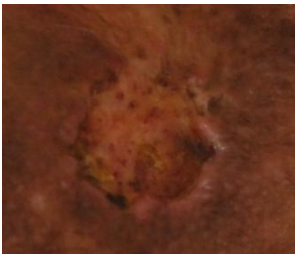

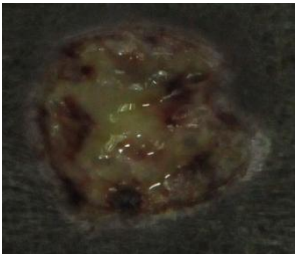

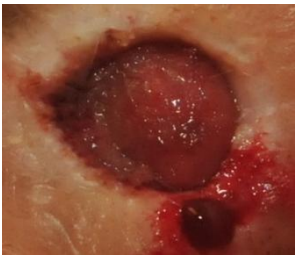

ULCER WOUND ATTRIBUTES PROTOTYPE IMAGE



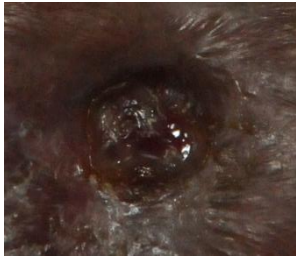

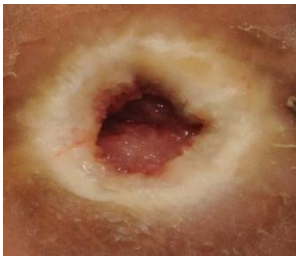



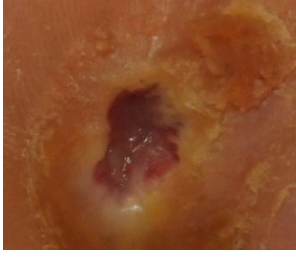

| Model No. | Wound Attributes Prototype | Model No. | Wound Attributes Prototype |
|-----------|---|-----------|--|
| IRSD1H |  | RPO3H |  |
| RSD5E1 |  | IRSD3H |  |
| RPO1H |  | RSD3H |  |
| RSD1H |  | RSD5H |  |
| RSD3E1 |  | IRSD5H |  |

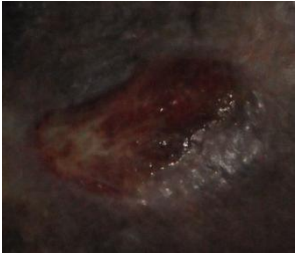


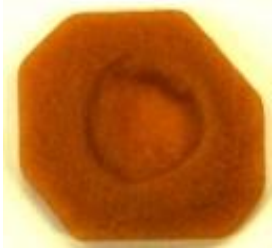




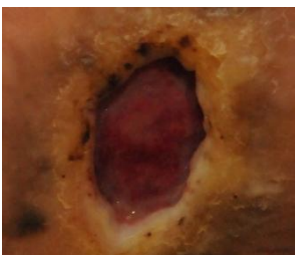

| Model No. | Wound Attributes Prototype | Model No. | Wound Attributes Prototype |
|-----------|---|-----------|---|
| RSD3D1 |  | RSD5D2 |  |
| RSD3D2 |  | RSD3E2 |  |
| RSD5E2 |  | RPO5H |  |
| RSD5D1 |  | | |

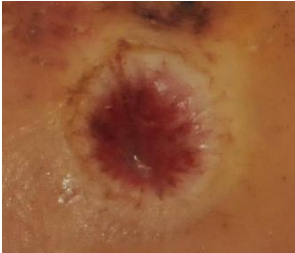

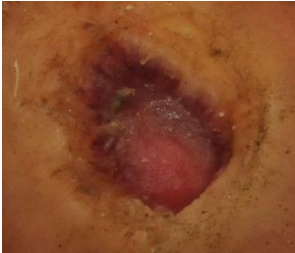

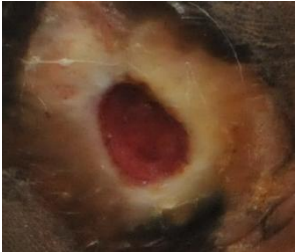



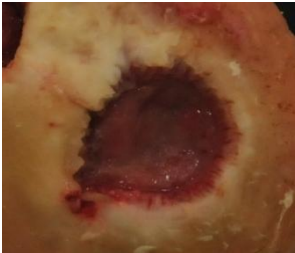

APPENDIX D











ULCER WOUND 2D IMAGES AND PROTOTYPE MODEL

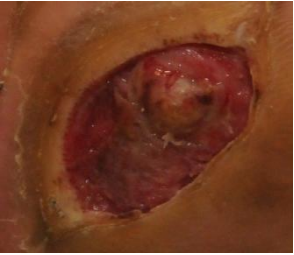

| Ulcer No. | Ulcer 2D Image | Ulcer Wound Model Prototype |
|-----------|---|---|
| Ulcer 01 |  |  |
| Ulcer 02 |  |  |
| Ulcer 03 |  |  |
| Ulcer 04 |  |  |
| Ulcer 05 |  |  |

| Ulcer No. | Ulcer 2D Image | Ulcer Wound Model Prototype |
|-----------|---|--|
| Ulcer 06 |  |  |
| Ulcer 07 |  |  |
| Ulcer 08 |  |  |
| Ulcer 09 |  |  |
| Ulcer 10 |  |  |

| Ulcer No. | Ulcer 2D Image | Ulcer Wound Model Prototype |
|-----------|---|---|
| Ulcer 11 |  |  |
| Ulcer 12 |  |  |
| Ulcer 13 |  |  |
| Ulcer 14 |  |  |
| Ulcer 15 |  |  |

| Ulcer No. | Ulcer 2D Image | Ulcer Wound Model Prototype |
|-----------|---|--|
| Ulcer 16 |  |  |
| Ulcer 17 |  |  |
| Ulcer 18 |  |  |
| Ulcer 19 |  |  |
| Ulcer 20 |  |  |

| Ulcer No. | Ulcer 2D Image | Ulcer Wound Model Prototype |
|-----------|---|---|
| Ulcer 21 |  |  |
| Ulcer 22 |  |  |
| Ulcer 23 |  |  |
| Ulcer 24 |  |  |
| Ulcer 25 |  |  |

| Ulcer No. | Ulcer 2D Image | Ulcer Wound Model Prototype |
|-----------|---|---|
| Ulcer 26 |  A photograph of a circular ulcer on a patient's skin. The ulcer has a dark red, necrotic center surrounded by a lighter red, inflamed border. |  A 3D-printed model of the ulcer, showing a brown, textured surface that replicates the shape and depth of the wound. |

APPENDIX E

R² SAMPLE CALCULATION

| Model | Reference Value, \hat{y} | Measure Value, y_i | SSE | SST |
|--------|----------------------------|----------------------|----------------------------|--------------------------------|
| | | | $(y_i - \hat{y})^2$ | $(y_i - \bar{y})^2$ |
| IRSD1H | 363 | 371 | 64 | 1,937,664 |
| RSD5E1 | 2,673 | 2,683 | 100 | 846,400 |
| RPO1H | 361 | 371 | 100 | 1,937,664 |
| RSD1H | 397 | 408 | 121 | 1,836,025 |
| RSD3E1 | 1,284 | 1,306 | 484 | 208,849 |
| RPO3H | 1,082 | 1,108 | 676 | 429,025 |
| IRSD3H | 1,317 | 1,348 | 961 | 172,225 |
| RSD3H | 1,428 | 1,462 | 1,156 | 90,601 |
| RSD5H | 2,816 | 2,856 | 1,600 | 1,194,649 |
| IRSD5H | 2,618 | 2,666 | 2,304 | 815,409 |
| RSD3D1 | 1,571 | 1,623 | 2,704 | 19,600 |
| RSD3D2 | 1,713 | 1,765 | 2,704 | 4 |
| RSD5E2 | 2,530 | 2,591 | 3,721 | 685,584 |
| RSD5D1 | 2,960 | 3,034 | 5,476 | 1,615,441 |
| RSD5D2 | 3,102 | 3,191 | 7,921 | 2,039,184 |
| RSD3E2 | 1,141 | 1,237 | 9,216 | 276,676 |
| RPO5H | 1,803 | 1,951 | 21,904 | 35,344 |
| | | $\bar{Y} = 1,763$ | $\sum \text{SSE} = 61,212$ | $\sum \text{SST} = 14,140,344$ |

| |
|--|
| $ \begin{aligned} R^2 &= 1 - (\sum \text{SSE} / \sum \text{SST}) \\ &= 1 - (61212 / 14140344) \\ &= 0.995671 \end{aligned} $ |
|--|